KINETIC STUDIES OF HYDROXYL AND HYDROGEN ATOM REACTIONS

Xiaohua Hu, B.S., M.S.

Dissertation Prepared for the Degree of

DOCTOR OF PHILOSOPHY

UNIVERSITY OF NORTH TEXAS

May 2002

APPROVED:

Paul Marshall, Major Professor
Oliver Chyan, Committee Member
Teresa Golden, Committee Member
Richard Timmons, Committee Member
Martin Schwartz, Committee Member and Coordinator of the Graduate Studies Program
Ruthanne D. Thomas, Chair of the Department of Chemistry
C. Neal Tate, Dean of the Robert B. Toulouse School of Graduate Studies

Hu, Xiaohua, Kinetic Studies of Hydroxyl and Hydrogen Atom Reactions. Doctor of Philosophy (Chemistry), May 2002, 173 pp., 33 tables, 32 illustrations, references, 165 titles.

Gas phase kinetics of the reactions involving hydroxyl radical and hydrogen atom were studied using experimental and *ab initio* theoretical techniques.

The rate constant for the H + H_2S reaction has been measured from 298 to 598 K by the laser photolysis / resonance fluorescence (LP-RF) technique. The transition state theory (TST) analysis coupled with the measurements support the suggestion that the reaction shows significant curvature in the Arrhenius plot. Combination with literature data reveals an expression for 190-2237 K is $k_{3.1} = 5.8^{+11.1}_{-3.8} \times 10^{-17}\ T^{1.94 \pm 0.15} \exp[(-455 \pm 67)/T]$ $cm^3\ molecule^{-1}\ s^{-1}$.

The LP-RF technique was also used to measure the rate constant of the H + CH_3Br reaction over the temperature range 400-813 K. TST and density functional theory (DFT) calculations show that the dominant reaction channel is Br-abstraction. Combined the literature data, the flexible TST (FTST) calculations with modified G2//QCISD/6-31G(d,p) barrier height $V^{\dagger}$ = 26.8 kJ mol^{-1} yielded $k_{4.1} = 4.61 \times 10^{-15}\ T^{1.532} \exp(-2631\ K/T)$ $cm^3\ molecule^{-1}\ s^{-1}$ over 298 - 2000 K.

The reaction H + CF_2=CF-CF=CF_2 was first studied by Flash Photolysis / Resonance Fluorescence (FP-RF) Method. The experiments of this work revealed distinctly non-Arrhenius behavior, which was interpreted in terms of a change in mechanism. DFT calculations suggest that the adduct is CF_2H-CF•-CF=CF_2. At lower

temperatures a mixture of this molecule and CF_2•-CFH-CF=CF_2 is likely. The theoretical calculations show that H atom migrates in the fluoroethyl radicals through a bridging intermediate, and the barrier height for this process is lower in the less fluorinated ethyl radical.

High level computations were also employed in studies of the rate constants of OH + chloroethylenes reactions. VTST calculations indicate that, except the reaction of OH + C_2Cl_4, these reactions present a complex behavior. For OH + C_2Cl_4, conventional TST calculation shows a simple positive temperature-dependence behavior.

ACKNOWLEDGMENTS

I wish to express my very sincere gratitude to my Ph.D. advisor, Dr. Paul Marshall, for his kind guidance, great patience, and never-ending encouragement. I am especially grateful to Dr. Marshall for his rich knowledge and great enthusiasm, both of which are benefits that will assist me in my future endeavors.

I would like to thank Dr. Jingping Peng for his extreme help in the experimental and computational works. I am also grateful to Dr. Abdell Goumri for his assistance with some of the experiments. The help from my colleagues, both graduate and undergraduate, is also appreciated.

Finally, I would like to thank the Robert A. Welch Foundation (Grant B-1174), the Environmental Protection Agency and the University of North Texas for financial support in the form of a research assistantship and teaching assistantship.

TABLE OF CONTENTS

LIST OF TABLES

LIST OF ILLUSTRATIONS

CHAPTER 1

INTRODUCTION

Hydroxyl radicals play important roles in both atmospheric chemistry and combustion processes,[1-7] and H atoms are typically the most abundant radicals in flames.[5,6]

In the stratosphere, OH is one of several important catalysts in the chain reaction of ozone loss:[1]

$$OH + O_3 \rightarrow HO_2 + O_2 \quad (1.1)$$

$$HO_2 + O \rightarrow OH + O_2 \quad (1.2)$$

$$\text{Net} \quad O + O_3 \rightarrow 2O_2 \quad (1.3)$$

OH radicals are mainly formed by following reactions at wavelengths less than ~ 310 nm in the troposphere:[1]

$$O_3 + h\nu \rightarrow O^*(^1D) + O_2^*(^1\Delta_g) \quad (1.4)$$

$$O^*(^1D) + H_2O \rightarrow OH + OH \quad (1.5)$$

The reaction

$$OH + NO_2 + M \rightarrow HNO_3 + M \quad (1.6)$$

is the major loss of NO_x in the troposphere. HNO_3 can dissolve in cloud droplets and be removed in the form of rain. The main step in the atmospheric chemistry of methane is the hydrogen abstraction by the OH radical,

$$OH + CH_4 \rightarrow CH_3 + H_2O \quad (1.7)$$

CH_3 is an active radical, and mainly removed by following reactions,

$$CH_3 + O_2 + M \rightarrow CH_3O_2 + H_2O + M \quad (1.8)$$

$$CH_3O_2 + HO_2 \rightarrow CH_3OOH + O_2 \quad (1.9)$$

the formed methyl hydroperoxide can be removed by wet deposition. In fact, the reaction with OH is almost exclusively the tropospheric chemical loss process for alkanes and alkenes.[1] And, attack by OH radical is also the primarily initial step in the atmospheric oxidation of aromatic hydrocarbons,

$$OH + C_6H_5CH_3 \rightarrow C_6H_5(OH)CH_3 \quad (1.10)$$

$$\rightarrow C_6H_5CH_2 + H_2O \quad (1.11)$$

OH radical is important in sulfur chemistry, where it seems to initiate the dominant oxidation route by addition to SO_2,

$$OH + SO_2 + M \rightarrow HOSO_2 + M \quad (1.12)$$

Actually, almost all the oxidizing reactions of the trace gases are initiated by the reaction with OH radical, which in most cases is the rate-determining step.[2] Thus the chemical fates of almost all the trace gases are controlled by OH, which breaks down and converts the emitted gases to water-soluble products that are physically removed from the atmosphere by precipitation.

In the combustion processes, H and OH radicals play key roles too. H atom leads to chain branching through the reaction 1.13, which determines the rate of chain branching in the H_2-O_2 system,

$$H + O_2 \rightarrow OH + O \quad (1.13)$$

$$O + H_2 \rightarrow OH + H \quad (1.14)$$

$$OH + H_2 \rightarrow H + H_2O \quad (1.15)$$

It is found that the higher the temperature is, the larger role the reaction 1.13 acts as in governing the rate of chain reactions.[5] The reactions 1.13 and 1.16

$$OH + CO \rightarrow H + CO_2 \quad (1.16)$$

are the main elementary reactions in the oxidation process of CO, which is an important intermediate in hydrocarbon combustion. In combustion chemistry of ammonia, sulfur compounds and halogen-containing species, H and OH radicals are also involved in the main elementary reactions.[5] In brief, in hydrogen-oxygen flames, reactions with H and OH radicals are important steps in the combustion processes of almost all species.

Sulfur is one of the most abundant elements in the Earth's crust and is one of the essential elements to all life on Earth. In the atmosphere, sulfur impacts regional and global chemistry, climate change, and the health of various living beings. Acid rain has led to a great deal of research on the atmospheric and combustion chemistry of sulfur.[8-15] Hydrogen sulfide (H_2S) is one of the major reduced sulfur gases in the atmospheric sulfur circle. The lifetime for H_2S is usually from a few hours to a few days. The reaction with OH radical is the major step which destroys H_2S,

$$OH + H_2S \rightarrow H_2O + SH \quad (1.17)$$

and has been well studied at low temperatures, where it was found to be fast and to have little or no activation energy.[16] The reaction

$$H + H_2S \rightarrow H_2 + SH \quad (1.18)$$

has been identified by Hynes and Wine as important in sulfur combustion under rich conditions.[17] An earlier review proposed a simple Arrhenius temperature dependence for the rate constant,[18] but the recent measurements of Yoshimura et al. over 1053-2237 K and at 293 K were rationalized in terms of ab initio theoretical calculations and transition state theory (TST) with significant curvature in the Arrhenius plot.[19] To predict the combustion behavior of H_2S accurately, new data for the rate constant of the reaction 1.18 in the intermediate temperature regime are essential. In this research, new measurements of rate constant of this reaction, up to 600 K, were made, the transition state (TS) for this reaction was reexamined at high levels of ab initio theory, and the results were employed in conventional TST. The laser photolysis / resonance fluorescence (LP-RF) technique was applied in this study. A variety of techniques are available for studying radical kinetics in the gas phase. They are discussed in chapter 2.

Combustion can be affected physically, such as changing the pressure. It also can be adjusted by chemical methods, such as adding promoters to accelerate it or inhibitors to slow it. Halogen-containing compounds have been widely used as flame inhibitors. The reactions of these species with H atom are primary reason of the slowing effect on the combustion. H atom reacts faster with halogen-containing compounds than with O_2, especially at low temperatures. For example, the rate constant of

$$H + HCl \rightarrow H_2 + Cl \qquad (1.19)$$

is about 50 times larger than the rate constant of the $H + O_2$ reaction at 1000 K.[5] Thus the chemical basis of the inhibitors is removing H atom from the reaction zone, as a result, the rate of chain branching by $H + O_2 \rightarrow OH + O$ decreases. Bromine-containing species

are considered to be the most effective combustion inhibitors because Br atom is more effective than the other halogen atoms in removing active species from the flame zone. Although different classes of bromine-containing compounds such as Br_2, HBr, CH_3Br, and CF_3Br present slightly different inhibiting effectiveness, the basic mechanism of their influence on combustion is the same: fast decomposition of the inhibitor and subsequent reactions of HBr with radicals in the combustion zone. For CF_3Br, the elementary reactions are

$$H + CF_3Br \rightarrow HBr + CF_3 \quad (1.20)$$

$$H + HBr \rightarrow H_2 + Br \quad (1.21)$$

$$H + Br_2 \rightarrow HBr + Br \quad (1.22)$$

$$Br + Br + M \rightarrow Br_2 + M \quad (1.23)$$

CH_3Br has the similar elementary reactions mainly responsible for suppressing flame propagation. However, the reaction

$$H + CH_3Br \rightarrow CH_3 + HBr \quad (1.24)$$

has not been well studied because of measurement difficulties. In this work, the rate constant of this reaction was measured from 400 K to 813 K; conventional TST and the Flexible TST (FTST) were used in the kinetic modeling to test the agreement between the measurements and the theoretical calculations. The LP-RF technique was employed here too.

The first kinetic studies of the reaction of atomic hydrogen with 1,1,2,3,4,4-hexafluoro-1,3-butadiene or perfluoro-1,3-butadiene (C_4F_6)

$$H + CF_2{=}CF\text{-}CF{=}CF_2 \rightarrow \text{products} \quad (1.25)$$

were also included in this research. The work was motivated by the possible application of C_4F_6 as a non-global warming fluorine precursor for plasma etching and chamber, where reaction 1.25 may be significant when hydrogen species are present. Reaction 1.25 is a likely consumption path if the effluent stream is subject to incineration. C_4F_6 may also serve as a surrogate for perfluoroisobutene, a highly toxic product of incomplete fluorocarbon combustion,[20] in the context of the design of effective incineration processes. Flash photolysis / resonance fluorescence (FP-RF) technique was employed in this study. Chapter 2 will be dedicated to the details of this technique.

Since chlorine-containing compounds are widely found in consumer and industrial wastes, the interest in the treatment of these hazardous chemical materials is growing. In industry, vinyl chloride (CH_2=CHCl) is mainly used for the production of polyvinyl chloride (PVC). The current vinyl chloride production rate is 27 million tons/year worldwide.[21] The dichloroethylenes represent significant organochlorine emissions to the environment. Like vinyl chloride, vinylidene chloride (1,1-$C_2H_2Cl_2$) is used industrially for the production of poly(vinyl dichloroethylene) (PVDC) and 1,1,1-trichloroethane. It was produced at a worldwide rate of 200,000 metric tons in 1985.[22] 1,2-dichloroethylene is not as important as vinylidene chloride industrially. However, it has a significant effect on the environment as a byproduct of chloroethylene manufacture.[22] Trichloroethylene (C_2HCl_3) is a widely used chlorinated solvent with an annual global emission rate of 200,000 metric tons.[23,24] Past and present manufacturing and disposal practices have resulted in the release of tetrachloroethylene into the atmosphere at significant rates. The annual amount of this highly volatile compound

emitted in the US alone was estimated to be about 100,000 metric tons.[25] The Integrated Risk Information System of the EPA [26,27] and the International Agency for Research on Cancer (IARC)[28] have classified chloroethylenes as human carcinogens or possible human carcinogens.

Knowledge of reactions facilitating the breakdown of these toxic compounds is essential to both predict the natural decomposition that is occurring in the atmosphere and determine appropriate disposal practices. The dominant atmospheric chloroethylene loss reaction is expected to be the reaction with OH radical since they do not absorb radiation at wavelengths of > 300 nm (because the atmosphere acts as a filter to cut out short wavelength radiation, only radiation with wavelength > 300 nm remains near the ground), nor do they react significantly with O_3 or NO_3 in the gas phase.[29,30] The standard technology for the complete and permanent disposal of these dangerous compounds is high temperature incineration. The reaction with OH radical is an important process contributing to the initial destruction of halogenated hydrocarbons.[31,32] The reaction mechanism is presumed to be addition to the π electrons associated with the C = C double bond

$$OH + C_2H_{(4-x)}Cl_x \rightarrow \text{adduct} \quad (x=1,2,3,4) \qquad (1.26)$$

Experimentally and theoretically, it is difficult to study radical addition reactions, because they are very fast and present the low-energy barriers, which require a very high theory level to be accurately described.[33-35] Previous studies of the reactions with OH were limited to low temperatures (220-460 K).[22,36-44] To predict the combustion

behavior of these compounds accurately, information on the reaction rate constants and reaction mechanisms over an extended temperature range is necessary. In this work, high level computations were employed in a series of kinetic studies of the reactions of OH radical with ethylene and chloroethylenes. The results were applied for further investigation of the reaction mechanisms by our co-workers.[45-49]

Conventional transition state theory (TST) and its modifications were employed in the kinetic modeling of these works. TST was first introduced in 1935,[50,51] in which reactants pass through a transition state (TS) to become products along the reaction path. The fundamental assumption of the theory is that products can not turn around and recross the TS to reform reactants. For reactions which have big barriers, TST usually provides reasonable estimation of rate constant. However, for reactions which have small or negative barriers, there is a non-zero possibility of the recrossing of products, and TST results will be too high.

An alternative method is to consider different positions for the TS along the reaction path and calculate the rate constant at each position. Then the minimum rate is picked up. This procedure is called variational transition state theory.[52-57] VTST is preferred for reactions without a significant chemical barrier. For bimolecular elementary reactions which have small or negative energy barriers, the simple two-parameter Arrhenius expression

$$k_{VTST} = A\, e^{-Ea/RT} \qquad (1.27)$$

where A is the pre-exponential factor and Ea is the activation energy, is insufficient to describe the temperature dependence of rate coefficients over a broad temperature

range.[58,59] An empirical three-parameter equation is invoked to represent the rate expressions

$$k_{VTST} = B\,T^{n}\,e^{-E/RT} \tag{1.28}$$

where R is the gas constant, B and E ($E \neq E_{\alpha}$) are two variables, and n is the temperature exponent. It yields

$$\ln k_{VTST} = \ln B + n\ln T - E/RT \tag{1.29}$$

By fitting the T and k_{VTST}, B, n and E/R can be obtained.

Flexible transition state theory (FTST) is a specific version of VTST, introduced by Wardlaw and Marcus.[60,61] The further development of the theory has been made by several authors.[62-73] In FTST, the internal modes of motion are divided into two types: 1. conserved modes, which do not change too much between reactants and products, typically vibrations; 2. transitional modes, which are free rotors in the reactants but become vibrations in the products. Thus a free rotor description along the entire reaction coordinate is not appropriate, especially for a low frequency mode, which has a large contribution to the vibrational partition function. Since a realistic representation of the transitional mode potential is included, FTST may accurately describe the contribution of the transitional modes to the TS, especially in the radical recombination reactions.[74]

REFERENCES

(1) Wayne, R. P. *Chemistry of Atmospheres*, 3rd ed.; Oxford University Press Inc.: New York, 2000.

(2) *Atmospheric Chemistry and Global Change*; Brasseur, G. P.; Orlando, J. J.; Tyndall, G. S., Eds.; Oxford University Press: New York, 1999.

(3) Finlayson-Potts, B. J.; Pitts, J. N., Jr. *Atmospheric Chemistry: Fundamentals and Experimental Techniques*; John Wiley & Sons, Inc.: New York, 1986.

(4) Finlayson-Potts, B. J.; Pitts, J. N., Jr. *Chemistry of the Upper and Lower Atmosphere*; Academic Press: San Diego, 2000.

(5) *Gas-Phase Combustion Chemistry*; Gardiner, W. C., Jr., Ed.; Springer-Verlag: New York, 2000.

(6) Glassman, I. *Combustion*, 3rd ed.; Academic Press: San Diego, 1996.

(7) Atkinson, R. *Chem. Rev.* **1985**, *85*, 69.

(8) Andreae, M. O.; Raemdonck, H. *Science* **1983**, *211*, 744.

(9) Astholz, D. C.; Glänzer, K.; Troe, J. *J. Chem. Phys.* **1979**, *70*, 2409.

(10) Charlson, R. J.; Lovelock, J. E.; Andreae, M. O.; Warren, S. G. *Nature* **1987**, *326*, 655.

(11) Kellogg, W. W.; Cadle, R. D.; Allen, E. R.; Lazrus, A. L.; Martell, E. A. *Science* **1972**, *175*, 587.

(12) Kiefer, J. H. *J. Chem. Phys.* **1975**, *62*, 1354.

(13) Lovelock, J. E.; Maggs, R. J.; Rasmussen, R. A. *Nature* **1972**, *237*, 452.

(14) Schwarz, S. E. *Nature* **1988**, *336*, 441.

(15) Stachnik, R. A.; Molina, M. J. *J. Phys. Chem.* **1987**, *91*, 4603.

(16) Westenberg, A. A.; de Haas, N. N. *J. chem. Phys.* **1973**, *59*, 6685.

(17) Hynes, A. J.; Wine, P. H. Combustion Chemistry; 2nd ed.; Gardiner, W. C., Jr., Ed., Chapter 3, in press.

(18) Baulch, D. L.; Drysdale, D. D.; Duxbury, J.; Grant, S. J. *Evaluated Kinetic Data for High-Temperature Reactions*; Butterworth: London, 1976; Vol. 3.

(19) Yoshimura, M.; Koshi, M.; Matsui, H.; Kamiya, K.; Umeyama, H. *Chem. Phys. Lett.* **1992**, *189*, 199.

(20) Tsang, W.; Burgess, D. R., Jr.; Babushok, V. *Combust. Sci. Tech* **1998**, *139*, 385.

(21) Kielhorn, J.; Melber, C.; Wahnschaffe; Aitio, A.; Mangelsdorf, I. *Environ. Health Perspect* **2000**, *108*, 579.

(22) Kirchner, K.; Helf, D.; Ott, P.; Vogt, S. *Ber. Bunsen-Ges. Phys. Chem.* **1990**, *94*, 77.

(23) McCulloch, A.; Midgley, P. M. *Atmos. Environ.* **1996**, *30*, 601.

(24) McCulloch, A.; Aucott, M. L.; Graedel, T. E.; Kleiman, G.; Midgley, P. M.; Li, Y.-F. *J. Geophys. Res.* **1999**, *104*, 8417.

(25) Gillbert, D.; Goyer, M.; Lyman, W.; Magil, G.; Walker, P.; Wallace, A.; Wechsler, A.; Yee, J. An Exposure and Risk Assessment for Tetrachloroethylene; EPA-440/4-85-015:, 1980.

(26) EPA. Clean Air Act of 1990, 42USC.7412, Title I, Part A, Sec. 112, 53; U. S. Environmental Protection Agency:, 1990.

(27) Ramamoorthy, S. *Chlorinated Organic Compounds in the Environment*; Lewis Publishers: New York, 1997.

(28) IARC. Monographs on the Evaluation of the Carcinogenic Risk of Chemicals to Humans; International Agency for Research on Cancer, World Health Organization: Lyon, France, 1979; Vol. 19.

(29) Atkinson, R.; Carter, W. P. L. *Chem. Rev.* **1984**, *84*, 437.

(30) Atkinson, R. *J. Phys. Chem. Ref. Data, Monogr.* **1989**, *1*.

(31) Fairchild, P. W.; Smith, G. P.; Crosley, D. R. 19th Symposium (Int.) on Combustion, 1982.

(32) Warnatz, J.; Bockhorn, H.; Moser, A.; Wenz, H. W. 19th Symposium (Int.) on Combustion, 1982.

(33) Wong, M.; Radom, L. *J. Phys. Chem.* **1995**, *99*, 8582.

(34) Jursic, B. S. *J. Chem. Soc. Perkin Trans.* **1997**, *2*, 637.

(35) Sosa, C.; Schlegel, H. B. *J. Am. Chem. Soc.* **1987**, *109*, 4193.

(36) Zhang, Z.; Liu, R.; Huie, R. E.; Kurylo, M. J. *J. Phys. Chem.* **1991**, *95*, 194.

(37) Abbatt, J. P. D.; Anderson, J. G. *J. Phys. Chem.* **1991**, *95*, 2382.

(38) Edney, E. O.; Kleindienst, T. E.; Corse, E. W. *Int. J. Chem. Kinet.* **1986**, *18*, 1355.

(39) Tuazon, E. C.; Atkinson, R. A.; Aschmann, S. M.; Goodman, M. A.; Winer, A. M. *Int. J.. Chem. Kinet.* **1988**, *20*, 241.

(40) Howard, C. J. *J. Chem. Phys.* **1976**, *65*, 4771.

(41) Chang, J. S.; Kaufman, F. *J. Chem. Phys.* **1977**, *66*, 4989.

(42) Greiner, N. R. *J. Chem. Phys.* **1970**, *53*, 1284.

(43) Liu, A.; Mulac, W. A.; Jonah, C. D. *J. Phys. Chem.* **1989**, *93*, 4092.

(44) Perry, R. A.; Atkinson, R. A.; Pitts, J. N. *J. Chem. Phys.* **1977**, *67*, 458.

(45) Tichenor, L. B.; Lozada-Ruiz, A. J.; Yamada, T.; El-Sinawi, A.; Taylor, P. H., Peng, J.; Hu, X.; Marshall, P. *Proc. Combus. Inst.* **2000**, *28*, 1495.

(46) Tichenor, L. B.; Graham, J. L.; Yamada, T.; Taylor, P. H.; Peng, J.; Hu, X.; Marshall, P. *J. Phys. Chem. A* **2000**, *104*, 1700.

(47) Tichenor, L. B.; El-Sinawi, A.; Yamada, T.; Taylor, P. H.; Peng, J.; Hu, X.; Marshall, P. *Chemosphere* **2001**, *42*, 571.

(48) Yamada, T.; Siraj, M.; Taylor, P. H.; Peng, J.; Hu, X.; Marshall, P. *J. Phys. Chem. A* **2001**, *105*, 9436.

(49) Yamada, T.; El-Sinawi, A.; Siraj, M.; Taylor, P. H.; Peng, J.; Hu, X.; Marshall, P. *J. Phys. Chem. A* **2001**, *105*, 7588.

(50) Eyring, H. *J. Chem. Phys.* **1935**, *3*, 107.

(51) Evans, M. G.; Polyani, M. *Trans. Faraday Soc.* **1935**, *31*, 875.

(52) Bishop, D. M.; Laidler, K. J. *Trans. Faraday Soc.* **1970**, *66*, 1685.

(53) Keck, J. C. *J. Chem. Phys.* **1960**, *32*, 1035.

(54) Keck, J. C. *Adv. Chem. Phys.* **1967**, *13*, 85.

(55) Anderson, J. B. *J. Chem. Phys.* **1973**, *58*, 4684.

(56) Anderson, J. B. *J. Chem. Phys.* **1975**, *62*, 2446.

(57) Chesnavich, W. J.; Su, T.; Bowers, M. T. *J. Chem. Phys.* **1980**, *72*, 2641.

(58) Zellner, R. *J. Phys. Chem.* **1979**, *83*, 18.

(59) Zellner, R. Bimolecular Reaction Rate Coefficients. In *Combustion Chemistry, Chapter 3*; Gardiner, W. C., Jr., Ed.; Springer-Verlag: New York, 1984.

(60) Wardlaw, D. M.; Marcus, R. A. *Chem. Phys. Lett.* **1984**, *110*, 230.

(61) Wardlaw, D. M.; Marcus, R. A. *J. Chem. Phys.* **1985**, *83*, 3462.

(62) Aubanel, E. E.; Wardlaw, D. M. *J. Phys. Chem.* **1989**, *93*, 3117.

(63) Klippenstein, S. J.; Marcus, R. A. *J. Chem. Phys.* **1987**, *87*, 3410.

(64) Klippenstein, S. J.; Marcus, R. A. *J. Phys. Chem.* **1988**, *92*, 3105.

(65) Klippenstein, S. J. *Chem. Phys. Lett.* **1990**, *170*, 71.

(66) Klippenstein, S. J. *J. Chem. Phys.* **1991**, *94*, 6469.

(67) Klippenstein, S. J. *J. Chem. Phys.* **1992**, *96*, 367.

(68) Klippenstein, S. J. *Chem. Phys. Lett.* **1993**, *214*, 418.

(69) Klippenstein, S. J. *J. Phys. Chem.* **1994**, *98*, 11459.

(70) Smith, S. C. *J. Chem. Phys.* **1991**, *95*, 3404.

(71) Smith, S. C. *J. Chem. Phys.* **1992**, *97*, 2406.

(72) Smith, S. C. *J. Phys. Chem.* **1993**, *97*, 7034.

(73) Robertson, S. H.; Wagner, A. F.; Wardlaw, D. M. *J. Chem. Phys.* **1995**, *103*, 2917.

(74) Pesa, M.; Pilling, M. J.; Robertson, S. H.; Wardlaw, D. M. *J. Phys. Chem.* **1998**, *102*, 8526.

CHAPTER 2

EXPERIMENTAL METHODS

A. Flash Photolysis / Resonance Fluorescence (FP-RF) Method

In the late 1940s, Norrish and Porter in Cambridge developed a new kinetic technique, Flash photolysis, which overcame many disadvantages of classical flow systems.[1] In 1967, Braun and Lenzi reported the first absolute rate constants, which were measured by FP-RF technique.[2] Since then, It has become available in several other labs and a good method in studying elementary reactions in a stationary gas.[3-9]

The concept of this technique is simple. In the flash photolysis process, reactants and precursors are mixed and flowed into the reactor. An intense flash, such as UV and visible light is employed, and transient atoms or radical species are produced on a time scale that is short compared to the reaction studied. In the resonance fluorescence process, the generated reactive radicals absorb continuous wave radiation, which is in resonance with a higher electronic state. If the lifetime of the upper electronic state for emission is sufficiently short compared to that for other processes, such as quenching and dissociation, a fraction of the resonance radiation is isotropically scattered. The scattered radiation is detected by single photon counting techniques, and the decay of scattered photons is recorded by a multichannel analyzer. Because the intensity of fluorescence is proportional to the radical concentration, the function between the radical concentration and time is obtained.

A schematic diagram of the apparatus is shown in Fig. 2.1. The reactor consists of a six-way stainless cross. Each arm has an i.d. of 22 mm and is 110 mm long. The intersection region of the side arms defines the reaction zone, which is roughly cubic, about 20 mm each side. Transient species are photolytically generated and detected by resonance fluorescence in the reaction zone. Pulsed radiation enters the reactor through one arm, resonance radiation through another arm at right angles, and fluorescence exists through a third one, which is mutually perpendicular. The other three arms are used as a gas inlet and outlet and as a port to hold a thermocouple. A small fraction of the total flow, about 10 %, is introduced in front of the three optical ports to sweep the gas mixture away from the windows. Full details of the reactor are described in earlier work of our group.[10-12]

For the H + CF_2=CF-CF=CF_2 reaction, the atomic H was produced by pulsed photolysis of NH_3 or H_2O in a large excess of C_4F_6 diluted in Ar bath gas, by radiation from a EG&G Electro-Optics flash lamp system focused through a MgF_2 (λ > 120 nm) lens. The flash lamp was a bulb (special FX 193 with a MgF_2 window) plugged into a Lite-Pac (FY-714) and connected to a power supply (PS-302) with a 10 μF external capacitor. The flash energy was varied from 2.0 to 4.1 J by changing the capacitor voltage between 630 ~ 900 V. N_2 (Air Products, Industrial Grade) was applied to purge the region between the flash lamp and the lens so that the wavelengths of actinic radiation transmitted into the reactor were down to about 120 nm. The relative concentration of H atoms was monitored by time-resolved resonance fluorescence at the Lyman-α wavelength, 121.6 nm, $H(2^2P) \rightarrow H(1^2S)$. The probe radiation was generated by a

microwave-excited discharge lamp with a slow flow of 0.2 % H_2 in Ar at about 0.27 mbar. The lamp was attached to the end of one arm of the reactor, which is perpendicular to the position of the flash lamp. A tuned Evenson cavity was installed at the far end of the lamp body, and connected to the microwave generator (Opthos Instruments, Inc., 2540 MHz). The discharge was initiated with a Tesla coil, and the typical microwave power is 55 W. A jet of air was used to cool the discharge lamp. Fluorescence from the reaction zone was detected with a solar-blind photomultiplier tube (Thorn EMI, RFI-B2F) employed with pulse counting and signal averaging. Typically 100-2000 fluorescence signals were accumulated at each set of conditions, with a repetition rate of 1-2 Hz. The timing of the experiments was controlled by a pulse generator, which provided trigger pulses to the flash lamp and a computer-controlled multichannel scaler (EG&G Ortec ACE-MCS) that was used to collect the resonance fluorescence signal from the PMT via an amplifier / discriminator (Electron Tubes Limited, AD6). Because of a narrow transmittance band of O_2 at the Lyman-α wavelength,[13] a dry air filter was put in front of the PMT to absorb other interfering vacuum UV radiation that was around the neighborhood of the H-atom wavelength. The temperature T of the gas in the reaction zone was monitored with a temperature controller (Omega CN 3910 KC/S), and measured before and after each set of measurements with a sheathed, unshielded thermocouple (Omega, type K, chrome (+) vs. alumel (-)), corrected for radiation errors of up to 10 K, which is expected to be accurate to within ± 2 %.[14] All experiments were carried out in a large excess of Ar bath gas at a total pressure P. The C_4F_6 and H-atom precursor (NH_3 or H_2O) concentrations were derived from P, T, the mole fractions of

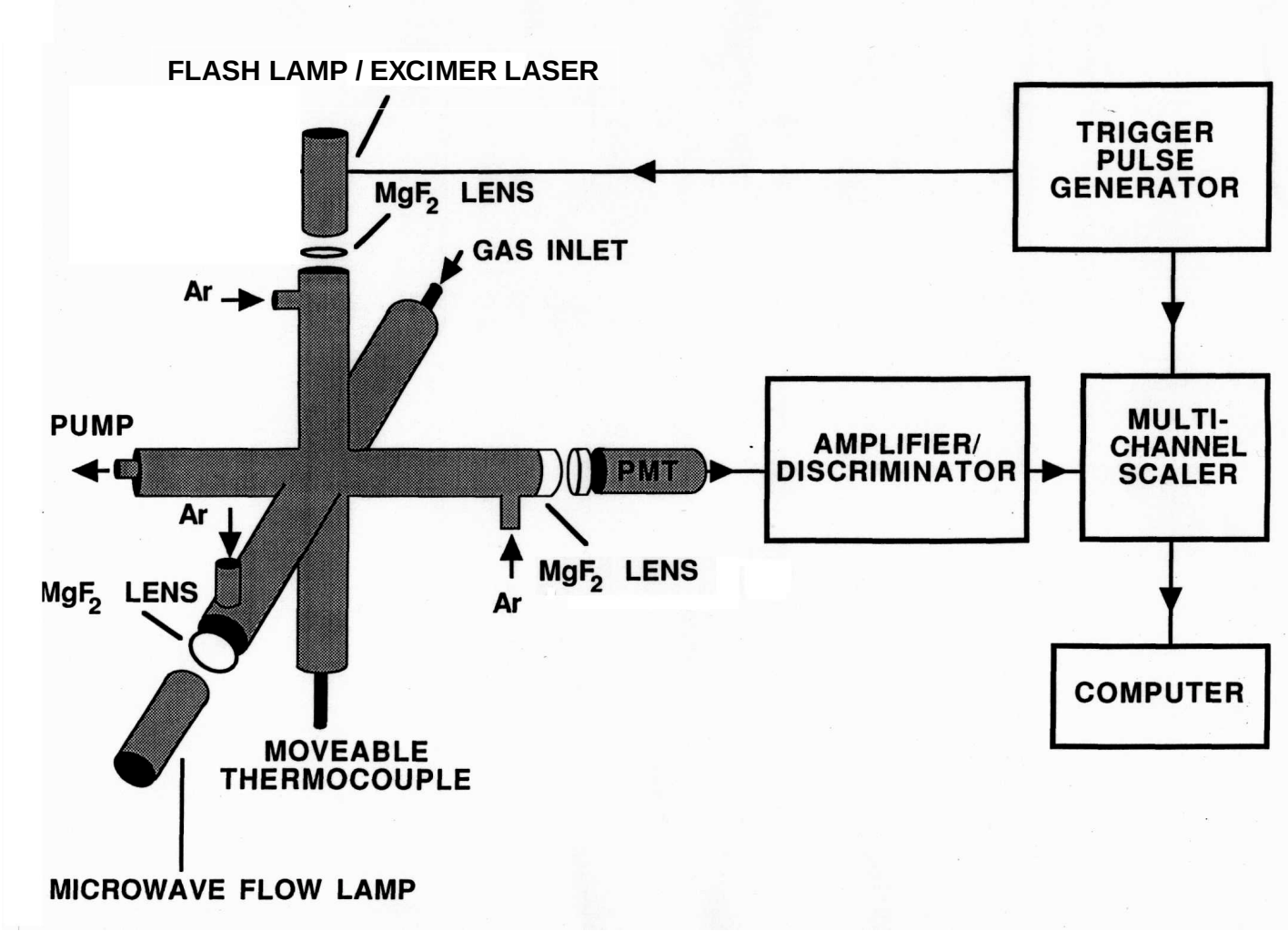

Fig. 2.1. Schematic diagram of the apparatus

these species in Ar mixtures, and the gas flows measured with calibrated mass-flow controllers.

B. Laser Photolysis / Resonance Fluorescence (LP-RF) Method

When an excimer laser is employed as the light source for flash photolysis, FP-RF is called LP-RF, which has many advantages, such as short pulse duration, high repetition rate, and a narrow, well-defined wavelength range. The LP-RF technique was applied to the H + H_2S reaction. In this work, MgF_2 optics was employed. The atomic H was produced by pulsed photolysis of H_2S at 193 nm using a PSX-100 excimer laser (MPB Technologies). The energy of the laser pluses was measured with a pyroelectric detector (Molectron, J25LP). The relative concentration of H atoms was also monitored by time-resolved resonance fluorescence at the Lyman-α wavelength, 121.6 nm. The probing resonant radiation at 121.6 nm was generated by a microwave-excited discharged lamp (0.1 % H_2 in Ar, 0.27 mbar), and the typical microwave power is about 20 W. A four-channel digital delay / pulse generator (Stanford Research Systems, DG35) controlled the experiments' timing. The fluorescence from the reaction zone was detected by a solar-blind PMT (Hamamatsu, R1459) via an amplifier / discriminator (MIT Inc., F-100T), and was also collected by a computer-controlled multi-channel scaler (EG&G Ortec ACE-MCS). The other set up and procedures were similar to that employed for H + C_4F_6.

Kinetic measurements for H + CH_3Br were also made by the LP-RF. The only difference from H + H_2S is that the precursor of H atom is NH_3 for this reaction.

C. Gas Handling

Ar (Big Three, 99.95 %) was used as the bath gas in all the experiments. Ar, N_2 (Liquid Air, Industrial Grade) and air (Big Three, Medical Grade) were used as supplied. H_2S (MG industries, 99.5+ %), CH_3Br (Matheson, 99.5 %), C_4F_6 (Air Liquide, 99.0+ %), NH_3 (MG Industries, 99.99+ %) and H_2 (MG Industries, 99.999 %) were purified by repeated "free-pump-thaw" cycles using a trap cooled to 77 K by a liquid N_2.

Gas mixtures were prepared on a vacuum line that was evacuated to pressures down to 10^{-4} mbar. Glass bulbs were evacuated to the same low pressures before introducing controlled amounts of pure gases into the bulbs.[12] The flow rates were measured with mass-flow controllers (MKS, 1159 series), which were calibrated against a bubble meter (Teledyne-Hastings HBM-1A) and operated by a four-channel readout (MKS, 247C). The bulbs were closed and the vacuum line evacuated again. Then Ar was introduced into the bulbs to prepare known ratios of diluted gas mixtures. In order to have uniform mixtures, each gas mixture was prepared at least two hours prior to running the experiments to make sure good mixing.

D. Experimental Procedure

Before starting kinetic measurements, the reactor was evacuated for at least several hours to remove any impurities stuck on the surface of the reactor. The reactor was assembled with a window-cooling system so that it can be applied for the high temperature measurements. When operating at high temperatures, routine cleaning with acetone or methanol was performed. By using a combination of mechanical and diffusion

pumps, the gas-handling system was also pumped to near vacuum, until the pressure was as low as 10^{-4} mbar. The readout was set to control the flow rates of mixtures, argon bath flow and sweep gas. The reaction pressure was adjusted by a stopcock between the end of gas-handling system and the gas exit of the reactor. When the pressure and temperature reach equilibrium, the microwave fluorescence resonance lamp was initiated, and the power of the generator was adjusted to the value required with 0-1 W reflected power. The flash lamp or laser and the computer-controlled multi-channel scaler were triggered by the digital delay/pulse generator. The dwell time and the pass count for the multi-channel scaler were set according to the reaction speed to get a good exponential decay curve for data analysis.

In the Experiments, a steady slow flow of reactant and precursor mixtures with large excess Ar bath gas was passed to the reactor, and various experimental parameters were changed to check if they influenced the measured rate constants. The flash or laser energy and the initial precursor concentration were altered to check whether any secondary reactions of radicals with photolysis or reaction products affected the rate constant seriously. The gas residence time, τ_{res}, which was the average time that gas flowed from the entrance port of the reactor to the reaction zone, was also changed to see if any thermal reactant decomposition happened during the experiments. For each same condition, five measurements were made from [reactant] = 0 to [reactant] = maximum. A pseudo-first-order rate constant, k_{ps1}, for the reaction was derived from them.

REFERENCES

(1) Pilling, M. J.; Seakins, P. W. *Reaction Kinetics*; Oxford University Press Inc.: New York, 1995.

(2) Braun, W.; Lenzi, M. *Faraday Soc.* **1967**, *44*, 252.

(3) Davenport, J. E.; Ridley, B. A.; Stief, L. J.; Welge, K. H. *J. Chem. Phys.* **1972**, *57*, 520.

(4) Klemm, R. B.; Stief, L. J. *J. Chem. Phys.* **1974**, *61*, 4900.

(5) Kurylo, M. J.; Peterson, N. C.; Braun, W. *J. Chem. Phys.* **1970**, *53*, 2776.

(6) Manning, R. G.; Kurylo, M. J. *J. Phys. Chem.* **1977**, *81*, 291.

(7) Perry, R. A.; Atkinson, R.; Pitts, J. N., Jr. *J. Phys. Chem.* **1977**, *81*, 296.

(8) Stuhl, F.; Niki, H. *J. Chem. Phys.* **1972**, *57*, 3671.

(9) Watson, R. T.; Machado, G.; Fischer, S.; Davis, D. D. *J. Chem. Phys.* **1976**, *65*, 2126.

(10) Goumri, A.; Yuan, W.-J.; Ding, L.; Shi, Y.; Marshall, P. *Chem. Phys.* **1993**, *177*, 233.

(11) Ding, L.; Marshall, P. *J. Phys. Chem.* **1992**, *96*, 2197.

(12) Shi, Y.; Marshall, P. *J. Phys. Chem.* **1991**, *95*, 1654.

(13) Samson, J. A. R. *Techniques of Vacuum Ultraviolet Spectroscopy*; John Wiley & Sons: New York, 1967.

(14) Ding, L.; Marshall, P. *J. Chem. Soc. Faraday Trans.* **1993**, *89*, 419.

CHAPTER 3

REACTION OF H + H_2S

Acting as an important role in sulfur combustion under rich conditions, the reaction

$$H + H_2S \rightarrow H_2 + SH \qquad (3.1)$$

has been studied by many groups since the 1970s.[1-12] In this work, the rate constant k_1 of this reaction in the intermediate temperature range was measured to check whether there is a simple Arrhenius temperature dependence for $k_{3.1}$ of this reaction, as said in an earlier review;[13] or there is a significant curvature in the Arrhenius plot, according to a recent published paper.[1] Dr. Jingping Peng in our group is a coworker of this project.

A. Methodology

Experimental Technique.

The LP-RF technique was used in this study as described in chapter 2. under pseudo-first-order conditions [H] << [H_2S], the H atoms reacted with H_2S:

$$d[H]/dt = -(k_{3.1}[H_2S] + k_{diff3})[H] = -k_{ps3.1}[H] \qquad (3.2)$$

where k_{diff3} accounts for any loss of H atoms out of the reaction zone other than by reaction with H_2S, mainly via diffusion to the reactor walls. Typical values of k_{diff3} were in the range of 100 - 450 s^{-1}. $k_{ps3.1}$ was obtained by fitting the recorded fluorescence intensity I_f versus time profile to an exponential decay (an example is shown as the inset

on Fig. 3.1) over typically at least four lifetimes:

$$I_f = A \exp(-k_{ps3.1}\, t) + B \qquad (3.3)$$

The second-order H + H_2S rate constant k_1 was determined by linear fitting of $k_{ps3.1}$ versus typically five values of [H_2S] (see Fig. 3.1 for an example). In order to verify that pseudo-first-order conditions were maintained, the energy of excimer laser beam was varied to alter the initial radical concentrations by putting different transmission filters in front of the exit of the laser beam. The energy of the photolysis pulse (I_0, 0.1 - 0.6 mJ) was combined with the H_2S absorption cross section of about 8×10^{-18} cm^2 (base e, room temperature) at 193 nm[14] to estimate the initial concentrations $[H]_0$ and $[SH]_0$. Gas mixtures flowed through the reactor slowly compared to the reaction time scale of the H-atoms, so the kinetic conditions were effectively static. The average gas residence time in the heated reactor before photolysis, τ_{res}, was varied by a factor of 2 or more to check for possible pyrolysis of H_2S.

Theoretical Calculations.

The energies and harmonic vibrational frequencies of optimized structures for H, H_2, SH, H_2S, and the activated complex of reaction 3.1 were evaluated using the GAUSSIAN 94 program package[15] at the MP2/6-311G(d,p), QCISD/6-311G(d,p) and QCISD(T)/6-311+G(3df,2p) levels of ab initio molecular orbital theory, and the BHandHLYP/6-311G(d,p) level of density functional theory.

Conventional TST was employed for the kinetic calculations, with the usual assumption of the separability of vibrational and rotational motions of the TS[16]

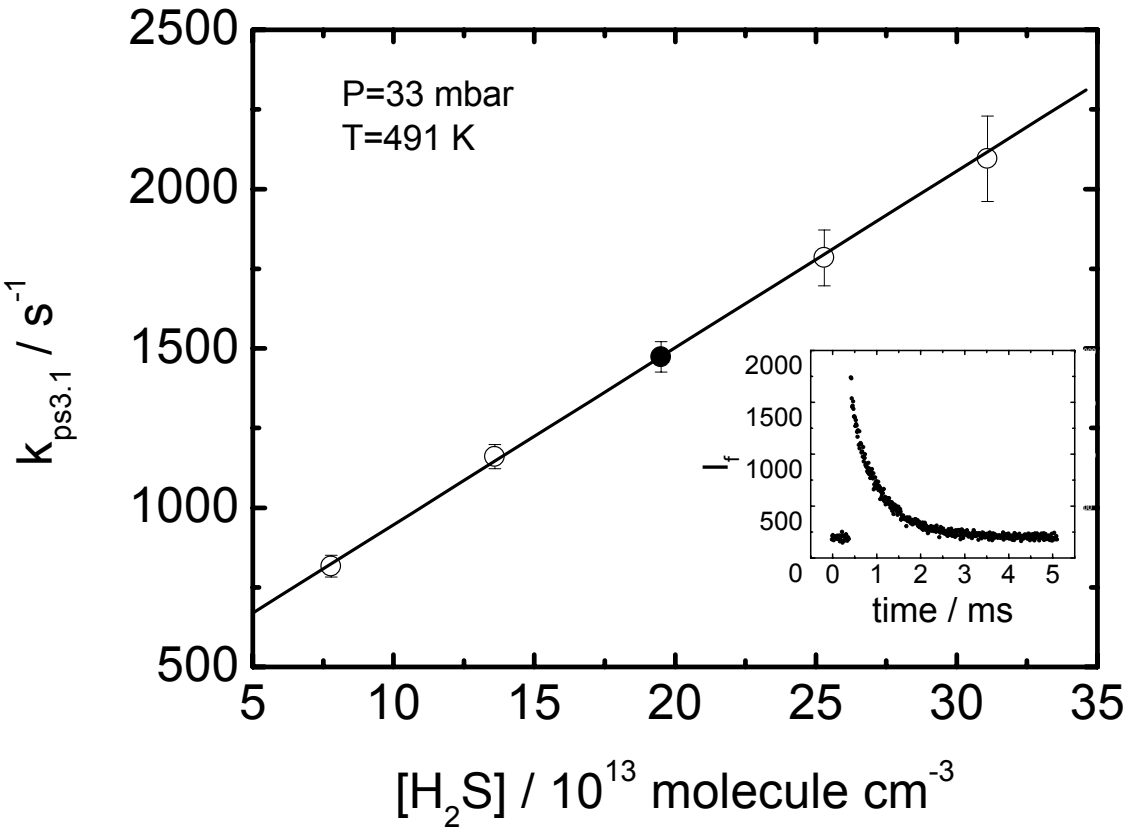

Fig. 3.1. Plot of pseudo-first-order rate constant $k_{ps3.1}$ vs [H_2S] at P = 33 mbar and T = 491 K. The inset shows the decay of time-resolved fluorescence intensity I_f for the solid point. The error bars are $\pm 2\sigma$.

$$k_{TST} = \Gamma \frac{k_B T}{h} \frac{Q_{H_3S^{\neq}}}{Q_H Q_{H_2S}} \exp\left(-\frac{E_0^{\neq}}{RT}\right) \qquad (3.4)$$

where Γ is the Eckart correction factor for quantum-mechanical tunneling.[16] When a particle of energy E moves to a barrier whose height is V, with V > E, according to classical mechanics this particle can not cross the barrier. But in quantum mechanics, if the barrier is thin enough, there is a small but non-zero probability that this particle passes through the barrier. Such leakage by penetration through classically forbidden zones is called tunneling. The optimized geometries and vibrational frequencies at the QCISD(T)/6-311+G(3df,2p) level were used for evaluating Γ, the barrier to reaction including zero point energy $E_0^{\neq}$, and the partition functions Q. To allow for anharmonicity, the ab initio vibrational frequencies were multiplied by a scaling factor of 0.9552, which was obtained by plotting observed fundamentals for H_2S,[17] H_2[18] and SH[19] versus calculated frequencies.

B. Results

The experimental conditions and results for 41 $k_{3.1}$ measurements are summarized in Table 3.1. The listed 1σ uncertainties in $k_{3.1}$ are derived from the precision of slopes of plots such as Fig. 3.1, combined in quadrature with the estimated reproducibility of P, T and the gas flows. Modest values of $\sigma / k_{3.1}$ indicate good linearity in such plots, but the scatter between successive determinations of $k_{3.1}$ was significantly greater than can be accounted for by these σ values alone. At each temperature, the weighted and unweighted means plus the standard deviations of these means were

Table 3.1. Measurements of the rate constants $k_{3.1}$ for the reaction H + H_2S

T, K	P, mbar	τ_{res}, s	I_0, mJ	$[H]_{0, max}$ 10^{11} molecule cm^{-3}	$[H_2S]_{0, max}$[a] 10^{14} molecule cm^{-3}	$k_{3.1} \pm \sigma_{k_{3.1}}$ 10^{-13} cm^3 $molecule^{-1}$ s^{-1}
298	68.5	1.2	0.1	4.6	6.1	8.21 ± 0.14
299	200.4	1.2	0.1	4.6	6.0	8.15 ± 0.26
297	67.8	1.2	0.2	13.2	6.0	7.87 ± 0.17
297	67.0	1.1	0.2	13.1	6.0	7.98 ± 0.26
298	67.2	1.2	0.2	9.7	5.9	7.94 ± 0.20
298						8.05 ± 0.08[b]
337	67.0	2.0	0.2	44.6	20.5	9.93 ± 0.37
337	134.6	4.0	0.1	24.0	22.0	10.6 ± 0.22
338	134.3	2.0	0.1	22.7	20.9	9.57 ± 0.21
337	67.3	2.0	0.1	22.4	20.6	9.68 ± 0.15
337						9.88 ± 0.20[b]
386	67.2	0.8	0.2	9.2	4.2	16.3 ± 0.9
383	201.1	0.8	0.2	9.3	4.3	16.3 ± 0.3
386	66.7	0.8	0.1	4.6	4.2	18.9 ± 0.9
387	68.4	1.8	0.2	6.9	4.2	21.7 ± 0.8
386	69.2	3.6	0.2	9.2	5.6	24.4 ± 0.6
386	134.8	3.5	0.2	9.1	5.6	20.3 ± 1.2
386						18.6 ± 1.2[b]
432	66.3	1.5	0.1	4.6	4.3	27.8 ± 1.3
432	66.8	0.8	0.3	16.8	5.2	24.3 ± 0.9
432	66.8	0.8	0.1	5.6	5.2	20.5 ± 0.7
432	132.6	1.5	0.3	16.8	5.1	24.2 ± 2.1
432						22.9 ± 1.3[b]
490	66.4	2.0	0.3	12.9	4.0	30.5 ± 2.4
491	133.0	2.0	0.3	13.1	4.0	38.3 ± 1.3
491	34.5	2.3	0.2	9.7	4.5	64.6 ± 4.2
491	34.3	1.1	0.2	4.9	2.2	48.0 ± 3.3
491	33.9	2.2	0.2	6.9	3.2	42.4 ± 2.1

Table 3.1. Measurements of the rate constants k_1 for the reaction H + H_2S (contd.)

T, K	P, mbar	τ_{res}, s	I_0, mJ	$[H]_{0,max}$ 10^{11} molecule cm^{-3}	$[H_2S]_{0,max}$[a] 10^{14} molecule cm^{-3}	$k_{3.1} \pm \sigma_{k_{3.1}}$ 10^{-13} cm^3 $molecule^{-1}$ s^{-1}
491	35.2	2.3	0.4	14.3	3.3	61.0 ± 1.3
491	34.1	1.1	0.4	8.1	1.9	48.0 ± 2.6
491	69.9	2.3	0.4	14.8	3.4	48.7 ± 0.8
491	69.8	2.3	0.2	5.6	3.4	50.3 ± 1.5
491	35.9	2.4	0.4	14.6	3.4	55.3 ± 1.1
491	35.9	2.4	0.1	3.6	3.4	58.8 ± 2.1
491						49.8 ± 2.9[b]
601	68.5	1.4	0.4	9.3	2.4	65.7 ± 9.0
598	34.5	1.8	0.6	16.6	2.5	56.6 ± 3.4
598	34.5	1.8	0.2	5.5	2.5	60.9 ± 3.4
598	68.1	1.8	0.6	16.9	2.6	60.2 ± 3.8
597	68.5	3.6	0.6	18.5	2.8	64.1 ± 1.6
598	68.7	1.2	0.6	17.5	2.7	68.6 ± 3.7
597	68.4	3.6	0.6	21.4	3.3	51.4 ± 1.7
598	35.2	1.9	0.5	16.5	3.0	54.5 ± 9.4
598	67.3	3.5	0.5	29.8	5.5	55.5 ± 4.8
599	67.3	1.8	0.5	29.9	5.5	56.7 ± 1.1
599	67.4	1.2	0.5	21.8	4.0	69.5 ± 4.3
598						58.4 ± 1.7[b]

[a] $[H_2S]_{0,max}$ was 2.3 - 6.3 times $[H_2S]_{0,min}$.
[b] Weighted mean value ± rms deviation of the mean.

calculated.[20] The two means at each temperature differ by up to 6 %. The weighted mean and the larger of the two standard deviations at each temperature are reported in Table 3.1. Not all original measurements are included in Table 3.1. Four outlying individual $k_{3.1}$ values were rejected according to Chauvenet's statistical criterion.[21] At 491 K, measurements at short residence times (< 0.75 s) were also made, but as a group they were significantly smaller than the other measurements at 491 K. Therefore they were not included in Table 3.1. At the highest temperature $k_{3.1}$ showed no consistent trend with τ_{res}, which indicates that pyrolysis of H_2S was unimportant at the listed temperatures.

To make an estimate of the extent of interference from secondary chemistry, kinetic modeling was performed using the ACUCHEM program.[22] The following scheme was considered

$H + H_2S \rightarrow H_2 + SH$,	$k_{3.1} = 7.8 \times 10^{-13}$ cm^3 molecule^{-1} s^{-1}
$H + SH \rightarrow H_2 + S$,	$k_{3.2} = 2.2 \times 10^{-11}$ cm^3 molecule^{-1} s^{-1}
$S + SH \rightarrow H + S_2$,	$k_{3.3} = 5.0 \times 10^{-12}$ cm^3 molecule^{-1} s^{-1}
$SH + SH \rightarrow H_2S + S$,	$k_{3.4} = 3.2 \times 10^{-11}$ cm^3 molecule^{-1} s^{-1}
$H \rightarrow$ diffusion,	$k_{diff3} = 250$ s^{-1}

with the worst-case conditions $[H_2S]_0 = 6.0 \times 10^{14}$ molecule cm^{-3} and $[H]_0 = [SH]_0 = 1.3 \times 10^{12}$ molecule cm^{-3}. The value of $k_{3.1}$ was taken from this work and values of $k_{3.2}$, $k_{3.3}$ and $k_{3.4}$ were from Nicholas et al.[7] All are room temperature values. For each modeling of a particular set of k_i values, linear regression was applied to the plot of ln [H] versus time. The resultant slope was $k_{ps3.1}$ and the effective second order rate constant was then

estimated as $k_{eff3} = (k_{ps3.1} - k_{diff3}) / [H_2S]_0$. The relative deviations of k_{eff3} with respect to that without secondary chemistry ($k_{3.2} = k_{3.3} = k_{3.4} = 0$) were 5.4 % for the original k_i values, 8.7 % for $k_{3.3} = k_{3.4} = 0$, and -1.4 % for $k_{3.2} = 0$. This reveals that the reaction H + SH $\rightarrow$ H_2 + S is the main source of interference. $k_{3.1}$ increases more rapidly with increasing temperature than $k_{3.2} - k_{3.4}$, so the primary reaction is more easily separated from any secondary chemistry at elevated temperatures. The energy of the photolyzing laser beam was employed as low as practicable in this work to minimize $[SH]_0$, and the ratio $k_{3.1}[H_2S]_0 / k_{3.2}[SH]_0$ was maintained at 16 or larger.

A weighted Arrhenius fit was performed on the 41 measurements and is shown in Fig. 3.2. It yielded

$$k_{3.1} = (6.6 \pm 0.9) \times 10^{-11} \exp[(-11.2 \pm 0.4) \text{ kJ mol}^{-1} / RT] \text{ cm}^3 \text{ molecule}^{-1} \text{ s}^{-1} \quad (3.5)$$

over the temperature range 298 - 598 K. The quoted errors in this expression are 1σ and are statistical only. Consideration of the covariance leads to a 1σ precision for the fitted $k_{3.1}$ of 3 - 6 %, and allowance for possible systematic errors leads to 95 % confidence intervals of $\pm$ 20 %.

In Table 3.2 are listed optimized geometries, barrier heights, and reaction enthalpies for H + H_2S system calculated at the four different theory levels mentioned previously. The experimental values are listed for comparison also. The harmonic frequencies calculated at the corresponding optimized geometries together with measured harmonics and observed fundamentals are presented in Table 3.3.

The results of the TST calculation are shown in Fig. 3.3. The dotted line represents a TST calculation using the QCISD(T)/6-311+G(3df,2p) barrier height of 16.0

kJ mol^{-1} and the corresponding Eckart corrections. The solid line represents a TST calculation adopting a barrier height of 14.4 kJ mol^{-1}, which was chosen to minimize the rms deviation from our experimental data. The reverse barrier height was varied also by the same amount as the reaction barrier height and the imaginary frequency was unchanged when tunneling correction factors were calculated. The open circles are

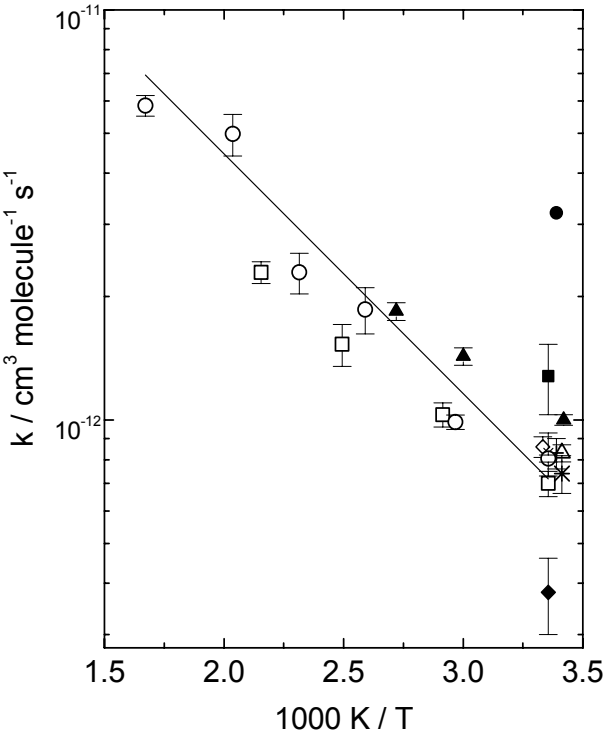

Fig. 3.2. $k_{3.1}$ for the H + H_2S reaction in the range 293 - 600 K. Solid line: Arrhenius fitting of this work; open circle: this work; open square: ref. 5; solid triangle: ref. 6; open triangle: ref. 1; open diamond: ref. 4; solid square: ref. 8; star: ref. 2; cross(×): ref. 12; solid diamond: ref. 10; cross(+): ref. 7; solid circle: ref. 3. The error bars are $\pm 2\sigma$ if σ was given, otherwise, they are ± literature reported errors.

Table 3.2. Geometry, Barrier Height, and Enthalpy for the Reaction H + H_2S

Geometry[a], $E_0^{\neq}$, ΔH_0	BHandHLYP /6-311G(d,p)	MP2 /6-311G(d,p)	QCISD /6-311G(d,p)	QCISD(T) /6-311+G(3df,2p)	Experimental Values[c]
H1 – H2-S-H3 (TS)					
r (H1--H2)	1.2385	1.055	1.1471	1.1613	
r (S-H2)	1.4046	1.4506	1.429	1.428	
r (S-H3)	1.3372	1.3356	1.3394	1.3411	
∠ H1-H2-S	175.26	174.88	175.04	173.79	
∠ H2-S-H3	92.27	90.32	90.78	90.85	
H_2S					
r (S-H)	1.3361	1.3336	1.3377	1.3391	1.328
∠ H-S-H	93.19	92.12	92.20	92.29	92.2
H_2					
r (H-H)	0.7382	0.7384	0.7433	0.7422	0.7414
SH					
r (S-H)	1.3405	1.3381	1.3429	1.3431	1.345
$E_0^{\neq}$, kJ mol^{-1}	10.72	32.26	21.95	16.00	
ΔH_0, kJ mol^{-1}	-67.82	-46.90	-64.99	-59.90	-61.96 ± 5.08 -55.90 ± 3.12[d]
Scaling factor for ZPC[b]	0.9305	0.9244	0.9445	0.9552	

[a] Bond lengths in 10^{-10} m and angles in degree.
[b] Obtained by plotting observed frequencies vs. calculated frequencies.
[c] Taken from ref. 19; [d] Obtained from 23.

Table 3.3. Harmonic frequencies and fundamentals for species of reaction H + H_2S

Modes[a]	BHandHLYP /6-311G(d,p)	MP2 /6-311G(d,p)	QCISD /6-311G(d,p)	QCISD(T) /6-311+G(3df,2p)	Measured harmonics[b]	Fundamentals[b]
Transition state						
A′	918i	1790i	1437i	1398i		
A′	420	516	464	459		
A″	483	596	526	522		
A′	1198	1149	1163	1166		
A′	1677	1391	1439	1455		
A′	2785	2811	2761	2748		
H_2S						
A_1 (ν_2)	1257	1228	1231	1211	1215	1183
A_2 (ν_1)	2784	2817	2765	2711	2722	2615
B_2 (ν_3)	2797	2836	2781	2727	2733	2627
H_2						
σ_g	4522	4533	4423	4411	4401	4159
SH						
σ	2766	2796	2734	2690	2690	2599

[a] Designated in irreducible representations from ab initio calculations and in cm^{-1}.
[b] Taken from ref. 17, 18 and 19.

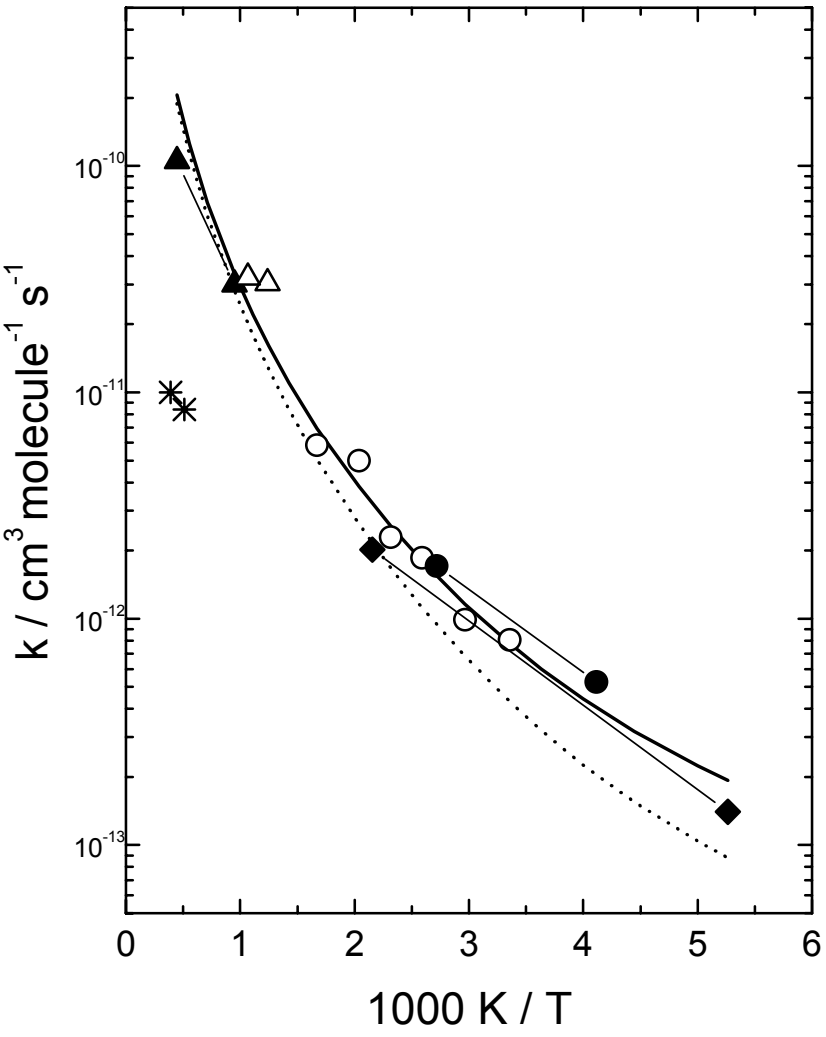

Fig. 3.3. Comparison of k_1 value for the H + H_2S reaction. Open circles: this work; line between solid diamonds: ref. 5; line between solid circles: ref. 6; line between solid triangles: ref. 1; line between stars: ref. 11; line between open triangles: ref. 9; dotted line: TST calculation with $E_0^{\neq}$ = 16.0 kJ/mol; solid line: TST calculation with $E_0^{\neq}$ = 14.4 kJ/mol.

experimental data measured in this work.

Non-linear fitting of the TST data calculated using $E_0^{\neq}$ = 14.4 kJ mol^{-1} over 190 - 2237 K yields

$$k_{3.1} = 1.68 \times 10^{-18} T^{2.44} \exp(-236/T) \text{ cm}^3 \text{ molecule}^{-1} \text{ s}^{-1} \quad (3.6)$$

This expression fits the TST data to within 10 %.

C. Discussion

Fig. 3.2 shows a comparison of the present results with earlier measurements[1-8,10,12] in the temperature range of our investigation. There is good accord with most of the room temperature data, and at higher temperatures our Arrhenius fit lies between the results of Kurylo et al.[5] and Mihelcic et al.[6] Fig. 3.3 shows our results in comparison with two studies of $k_{3.1}(T)$ where T was varied substantially around room temperature,[5,6] together with high temperature measurements.[1,9,11] Clearly, the higher the central temperature of the experiments, the larger the observed activation energy E_a. A fit to the present results (eq. 3.5) together with the fit expressions from ref. 1, 12, 22 and 24, evaluated at 10^{-4} K^{-1} intervals and weighted equally in ln $k_{3.1}$, yields the modified Arrhenius expression

$$k_{3.1} = 5.8^{+11.1}_{-3.8} \times 10^{-17} T^{1.94 \pm 0.15} \exp[(-455 \pm 67)/T] \text{ cm}^3 \text{ molecule}^{-1} \text{ s}^{-1} \quad (3.7)$$

which is a reasonable representation of the combined experimental data set, although it overestimates $k_{3.1}$ at 2237 K by about a factor of 1.5. The parameters of eq. 3.7 agree to within the stated 1σ uncertainties with those of the analogous expression presented by

Yoshimura et al.,[1] which overestimated $k_{3.1}$ at 2237 K by about a factor of 1.7. The common functional form $k = A\ T^n \exp(-B / T)$ may therefore not be the best expression for this rate constant, for which data are available over an unusually wide range of temperature.

Of the ab initio results in Table 3.2, the transition state geometry at MP2/6-311G(d,p) is the closest to the previous calculations by Yoshimura et al.[1] at the HF/6-31G(d,p) and MP2/6-31G(d,p) levels of theory. The QCISD(T)/6-311+G(3df,2p) geometry is probably more accurate, based on the close accord with data for stable species where the bond lengths appear to be good to within about 10^{-12} m and the H_2S angle is in error by less than 0.1°, although the differences from the earlier geometry will have a negligible influence on $k_{3.1}(T)$.

It is noted that the calculated harmonic frequencies at the QCISD(T)/6-311+G(3df,2p) level for the stable species listed in Table 3.3 are in very good agreement with the measured values (relative deviations up to 0.4 % and a rms deviation of 7 cm^{-1}). The real frequencies of the transition state and H_2S do not vary strongly with the level of calculation, although they are generally slightly smaller than the earlier HF/6-31G(d,p) and MP2/6-31G(d,p) results.[1] These differences will have little impact on $k_{3.1}(T)$, but the imaginary frequency ν_i corresponding to motion along the reaction coordinate is important in determining the tunneling correction and is seen to vary significantly with the level of calculation. In particular, the earlier MP2/6-31G(d,p) value of 1890 cm^{-1} is greater than any found here. We would expect overestimation of the barrier height to correlate with overestimation of the curvature at the saddle point and hence ν_i; the close

accord at the QCISD(T)/6-311+G(3df,2p) level between experiment and calculation for E_0^I and ΔH_0 is therefore a necessary condition for an accurate assessment of ν_i.

The tunneling correction factor Γ increases from 1.04 at 2000 K through 4.1 at 298 K to about 27 at 190 K, so the TST results will be especially sensitive to details of the tunneling model at room temperature and below. Nevertheless, as shown in Fig. 3.3, there is rather close accord with the experimental data in this region when the barrier is reduced by only 1.6 kJ mol^{-1} from the ab initio value. It is hard to say to what extent this correction reflects contributions from multidimensional tunneling paths, or simply residual energy errors at the QCISD(T)/6-311+G(3df,2p) level of theory, but in any event it is a modest correction to E_0^I. For comparison, Yoshimura obtained a PMP4/6-311G(d,p) barrier of 17.2 kJ mol^{-1}, adjusted to 13.4 kJ mol^{-1} to match experiment.[1]

Conventional TST calculations match experiment closely up to about 1000 K, but overestimate k_1 above this temperature. For example, $k_{3.1}$ from eq. 3.6 is a factor of 2.0 above the measurements of Yoshimura et al. at 2237 K, while the earlier TST calculations were a factor of 1.7 too large at this temperature.[1] A likely explanation is that variational effects become significant above 1000 K. In this case, that is where the average kinetic energy of the particles, 1.5RT, roughly equals the fitted barrier E_0^I = 14.4 kJ mol^{-1}, but whether this is a general criterion for the need for non-variational TST remains to be explored.

REFERENCES

(1) Yoshimura, M.; Koshi, M.; Matsui, H.; Kamiya, K.; Umeyama, H. *Chem. Phys. Lett.* **1992**, *189*, 199.

(2) Clyne, M. A. A.; Ono, Y. *Chem. Phys. Lett.* **1983**, *94*, 597.

(3) Cupitt, L. T.; Glass, G. P. *Trans. Faraday Soc.* **1970**, *66*, 3007.

(4) Husain, D.; Slater, N. K. H. *J. Chem. Soc., Faraday Trans. 2* **1980**, *76*, 276.

(5) Kurylo, M. J.; Peterson, N. C.; Braun, W. *J. Chem. Phys.* **1970**, *54*, 943.

(6) Mihelcic, D.; Schindler, R. N. *Ber. Bunsen-Ges. Phys. Chem.* **1970**, *74*, 1280.

(7) Nicholas, J. E.; Amodio, C. A.; Baker, M. J. *J. Chem. Soc., Faraday Trans. 1* **1979**, *75*, 1868.

(8) Perner, D.; Franken, T. *Ber. Bunsen-Ges. Phys. Chem.* **1969**, *73*, 897.

(9) Pratt, G.; Rogers, D. *J. Chem. Soc., Faraday Trans. 1* **1977**, *73*, 54.

(10) Rommel, H.; Schiff, H. I. *Int. J. Chem. Kinet.* **1972**, *4*, 547.

(11) Roth, P.; Lohr, R.; Barner, U. *Combust. Flame* **1982**, *45*, 273.

(12) Bradley, J. N.; Trueman, S. P.; Whytock, D. A.; Zaleski, T. A. *J. Chem. Soc., Faraday Trans. 1* **1973**, *69*, 416.

(13) Baulch, D. L.; Drysdale, D. D.; Duxbury, J.; Grant, S. J. *Evaluated Kinetic Data for High-Temperature Reactions*; Butterworth: London, 1976; Vol. 3.

(14) Okabe, H. *Photochemistry of Small Molecules*; John Wiley: New York, 1978.

(15) Frisch, M. J.; Trucks, G. W.; Schlegel, H. B.; Gill, P. M. W.; Johnson, B. G.; Robb, M. A.; Cheeseman, J. R.; Keith, T. A.; Petersson, G. A.; Montgomery, J. A.; Raghavachari, K.; Al-Laham, M. A.; Zakrzewski, V. G.; Ortiz, J. V.; Foresman, J. B.; Cioslowski, J.; Stefanov, B.; Nanayakkara, A.; Challacombe, M.; Peng, C. Y.; Ayala, P. Y.; Chen, W.; Wong, W.; Andres, J. L.; Replogle, E. S.; Gomperts, R.; Martin, R. L.; Fox, D. J.; Binkley, J. S.; Defrees, D. J.; Baker, J.; Stewart, J. P.; Head-Gordon, M.; Gonzalez, C.; Pople, J. A. Gaussian 94 (Revision D.2); Gaussian, Inc.: Pittsburgh, PA, 1995.

(16) Johnston, H. S. *Gas-Phase Reaction Rate Theory*; Ronald: New York, 1966.

(17) Allen, H. C.; Plyler, E. K. *J. Chem. Phys.* **1956**, *25*, 1132.

(18) Huber, K. P.; Herzberg, G. *Constants of Diatomic Molecules*; Van Nostrand Reinhold: New York, 1979; Vol. 4.

(19) Chase, M. W. J.; Davies, C. A.; Downey, J. R. J.; Frurip, D. J.; McDonald, R. A.; Syverud, A. N. *J. Phys. Chem. Ref. Data* **1985**, *14*, Suppl. 1.

(20) Massey, B. S. *Measures in Science and Engineering: Their Expression, Relation and Interpretation*; John Wiley: New York, 1986.

(21) Pugh, E. M., Jr.; Winslow, G. H. *The Analysis of Physical Measurements*; Addison-Wesley: Reading, 1966.

(22) Braun, W.; Herron, J. T.; Kahaner, D. K. *Int. J. Chem. Kinet.* **1988**, *22*, 51.

(23) Nicovich, J. M.; Kreutter, K. D.; van Dijk, C. A.; Wine, P. H. *J. Phys. Chem.* **1992**, *96*, 2518.

(24) Kleinbaum, D. G.; Kupper, L. L.; Muller, K. E.; Nizam, A. *Applied Regression Analysis and Other Multivariable Methods*; Duxbury Press: Pacific Grove, 1998.

CHAPTER 4

REACTION OF H + CH_3Br

As one of the inhibitors of flame propagation in some cases, few reports about the reaction of CH_3Br with atomic hydrogen have been published since it was first studied in 1933,[1] in which the reaction 4.1 was argued to be the primary reaction.

$$H + CH_3Br \rightarrow CH_3 + HBr \quad (4.1)$$

In this work, the Arrhenius factor and the activation energy were investigated by kinetic measurements over a wider temperature range and compared with the previously published results.[2-4] Then, the density functional theory (DFT) and the conventional transition state theory (TST) were applied to pick up the right reaction channel. Also, the TST and the Flexible TST (FTST)[5,6] were used in the kinetic modeling, which was employed to test if there is a good agreement between the measurements and the theoretical calculations. Dr. Jingping Peng is a coworker on this project.

A. Methodology

Experimental Technique.

The LP-RF technique was also used in this work. The detail of this technique was described in chapter 2. The H atom precursor in here was NH_3. Under pseudo-first-order conditions $[H] << [CH_3Br]$, the H atoms reacted with CH_3Br:

$$d[H]/dt = -(k_{4.1}[CH_3Br] + k_{diff4})[H] = -k_{ps4.1}[H] \quad (4.2)$$

where k_{diff4} accounts for any loss of H atoms out of the reaction zone other than by reaction with CH_3Br, mainly via diffusion to the reactor walls. Typical values of k_{diff4} were in the range of 65 - 545 s^{-1}. $k_{ps4.1}$ was obtained by fitting the recorded fluorescence intensity I_f versus time profile to an exponential decay (an example is shown as the inset on Fig. 3.1 in chapter 3) over typically at least four lifetimes:

$$I_f = A \exp(-k_{ps4.1}\, t) + B \qquad (4.3)$$

The second-order H + CH_3Br rate constant k_1 was determined by linear fitting of $k_{ps4.1}$ versus typically five values of $[CH_3Br]$. In order to verify that pseudo-first-order conditions were maintained, the energy of excimer laser beam was varied to alter the initial radical concentrations, by putting different neutral density filters in front of the exit of the laser beam. The energy of the photolysis pulse (I_0, 0.2 - 0.6 mJ) was combined with the NH_3 absorption cross section of about 1.1×10^{-17} cm^2 $molecule^{-1}$ (base e, 0 ^oC) at 193 nm[7] to estimate the initial concentrations $[H]_0$ and $[NH_2]_0$, and with the CH_3Br absorption cross section of about 8.0×10^{-19} cm^2 $molecule^{-1}$ (base e, room temperature) at 193 nm[7] to estimate the initial $[CH_3]_0$ and $[Br]_0$. Gas mixtures flowed through the reactor slowly compared to the reaction time scale of the H-atoms, so the kinetic conditions were effectively static. The average gas residence time in the heated reactor before photolysis, τ_{res}, was varied by a factor of 2 or more to check for possible pyrolysis of CH_3Br.

Theoretical Calculations.

All the ab initio calculations were performed using the GAUSSIAN 94 program package.[8] The DFT calculations were contributed by Timothy O'Hara. The structures of

species HBr, CH_3, CH_3Br, and transition state of reaction H + $CH_3Br \rightarrow CH_3$ + HBr were optimized at HF/6-31G(d), MP2(FULL)/6-31G(d), MP2/6-311G(d,p), and QCISD/6-31G(d,p) levels of ab initio theory. The harmonic vibrational frequencies of optimized structures at HF/6-31G(d), MP2/6-311G(d,p), and QCISD/6-31G(d,p) levels were calculated. The G2 energies were calculated based on the geometries optimized at the MP2(FULL)/6-31G(d), MP2/6-311G(d,p), and QCISD/6-31G(d,p) levels, respectively. As a preliminary investigation, three channels of reaction H + CH_3Br were considered: Br-abstraction (k_1), H-abstraction (k_2) and Br-substitution (k_3) (see Figure 4.1). They were studied at BHandH/6-311G(d,p) level of density functional theory and G2 energies of the system were calculated based on the geometries optimized at this level.

Conventional TST was employed for the kinetic calculations, with the usual assumption of the separability of vibrational and rotational motions of the TS[9]

$$k_{TST} = \Gamma \frac{k_B T}{h} \frac{Q_{CH_4Br^{\neq}}}{Q_{HBr} Q_{CH_3}} \exp\left(-\frac{E_0^{\neq}}{RT}\right) \qquad (4.4)$$

where Γ is the Eckart correction factor for quantum-mechanical tunneling.[9] The barrier height $E_0^{\neq}$ (including zero point energy correction) were calculated at G2, modified G2//MP2/6-311G(d,p), and modified G2//QCISD/6-31G(d,p) levels, respectively. The frequencies at HF/6-31G(d) level scaled by 0.8929 were used to calculate the vibrational partition functions of the species for the G2 rate constant. The frequencies at MP2/6-311G(d,p) level scaled by 0.9473 and at QCISD/6-31G(d) level scaled by 0.9407 were used to calculate the vibrational partition functions of the species for the rate constants at

these two levels, respectively. The later two scaling factors were obtained by plotting observed fundamentals of HBr,[10] CH_3[11] and CH_3Br[11] versus the calculated frequencies.

The Flexible TST treatment was performed at the QCISD/6-31G(d,p) level and the separation R between H and the center of mass (c.m.) of CH_3Br was fixed at the value of the transition state in order to take into account of the hindered rotor effect. Since this is an atom + non-linear-top system, only two internal angles, which were the angle θ formed by the intersection of the line joining the c.m.s of the two fragments and the principle axis of CH_3Br (passes through Br and C atoms) at the c.m. of CH_3Br and the dihedral angle ϕ of the plane containing CH bond with respect to the same plane at equilibrium structure (see Figure 4.2), were needed to define the potential energy function of the transitional/external-rotation modes. The rate expression for this FTST[12] treatment is

$$k(T) = g_e \frac{k_B T}{h} \frac{\sigma}{\sigma^\dagger} \frac{e^{-\frac{V^\dagger}{RT}}}{Q_{trans}(T)} \left(\frac{Q_c^\dagger}{Q_{vib,CH_3Br}(T)} \right) \left(\frac{Q_{pd}^\dagger(T) Q_{fr,CH_3Br}^\dagger(T)}{Q_{fr,CH_3Br}(T)} \right) \Gamma^\dagger(T) \qquad (4.5)$$

where g_e is the ratio of electronic degeneracy factors for the reactants and transition state and $\sigma/\sigma^\dagger$ is the ratio of reactant and transition state symmetry factors; $V^\dagger$ is the barrier height for the reaction including zero point energy correction (ZPC); $Q_{trans}(T)$ is the translational partition function of the system which takes the reduced mass μ; $Q_c^\dagger(T)$ is the conserved mode partition function, which was calculated as the product of vibrational partition functions of all modes except the two lowest frequencies (doubly degenerated) and the imaginary frequency; $Q_{fr,CH_3Br}^\dagger(T)$ is the partition function for the free rotation of

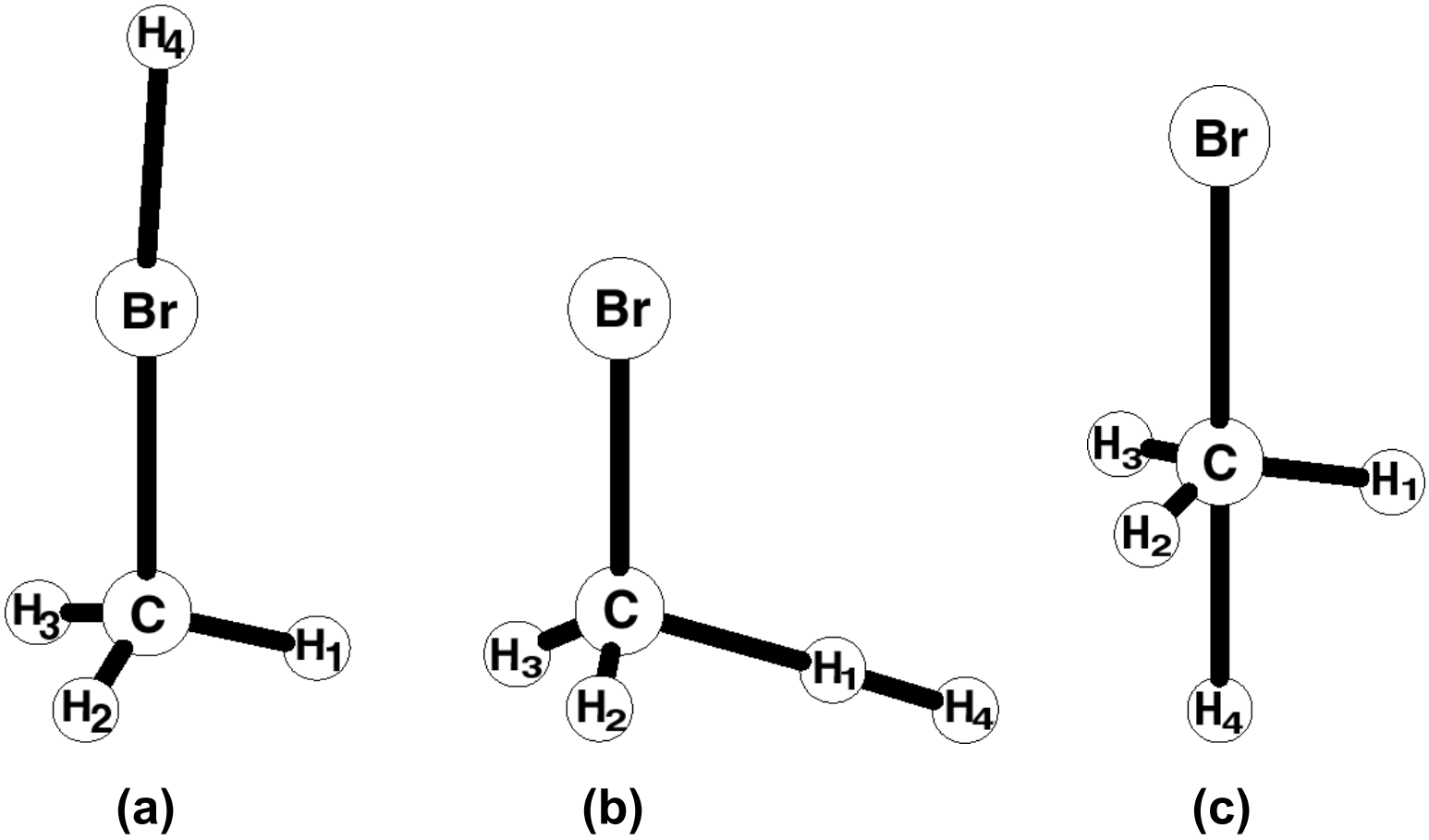

Fig. 4.1. Geometries of transition states for reaction H + CH_3Br optimized at BHandH/6-311G(d,p) level: (a) Br-abstraction; (b) H-abstraction; (c) Br-substitution.

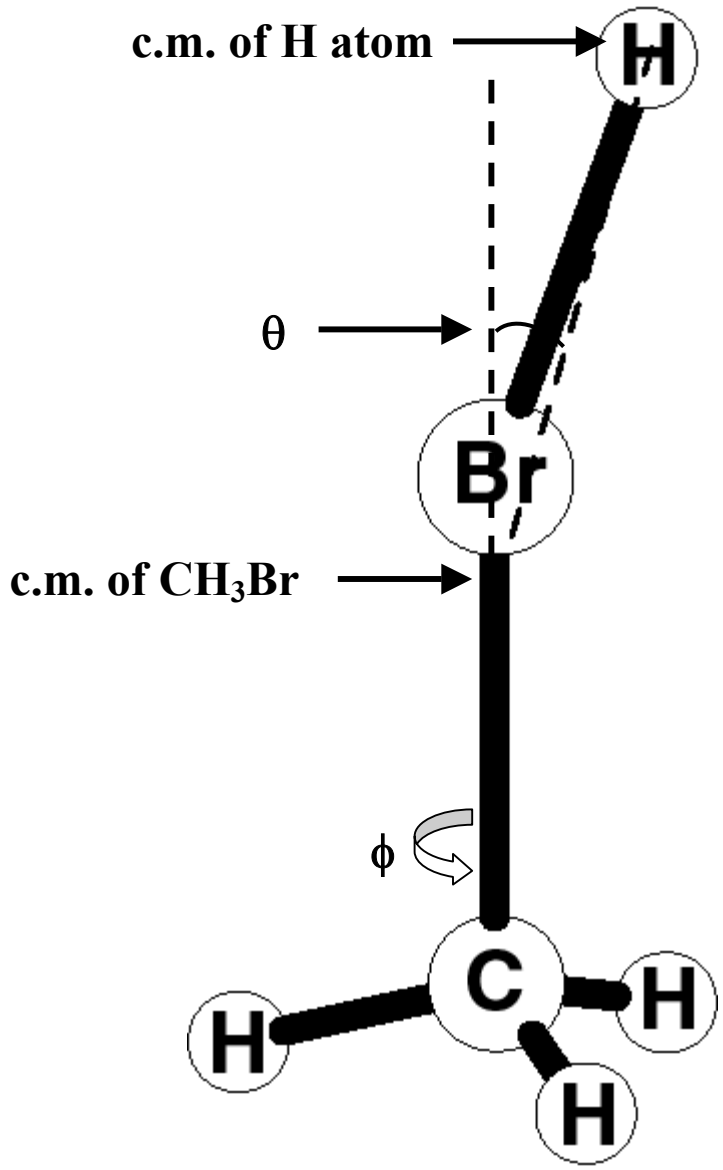

Fig. 4.2. Diagram of two internal angles in TS: (1) θ, formed by the intersection of the line joining the c.m.s of two fragments and the principle axis of CH_3Br; (2) ϕ, formed by the plane containing CH bond with respect to the same plane at equilibrium structure. ϕ = 0 corresponds to the left-hand CH bond lying trans to the HBr bond.

fragment CH_3Br in the transition state; $Q^{\dagger}_{pd}(T)$ is the partition function for the pseudodiatomic formed from the c.m.s of the two fragments H and CH_3Br; $\Gamma^{\dagger}(T)$ is a hindering function in the form of the configuration integral:

$$\Gamma^{\dagger}(T) = (4\pi)^{-1} \int_0^{\pi} d\theta \sin\theta \int_0^{2\pi} d\phi \, e^{-\frac{V_{tr}}{RT}} \qquad (4.6)$$

It was evaluated in the following way. First, a relaxed scan at the QCISD/6-31G(d,p) level starting at the transition state on angle θ with the range 0^o – 136^o and step-size 8^o, and on ϕ with the range 0^o – 60^o and step-size 6^o was performed; next, the $\Gamma^{\dagger}(T)$ was evaluated at each temperature approximately as the summation of the volumes of column with bottom area $\Delta\theta \times \Delta\phi$ and height $\sin\theta \times \exp(-V_{tr}/RT)$, where the height was the average at the center of each area and the unit of angles was radian. As a test of this kind of numerical integration, the above procedure were applied to evaluate the double integral of $\sin 2\phi \, e^{-\theta}$ on the range $0 - 120\pi/180$ for ϕ and $0 - 136\pi/180$ for θ. The result is within 0.1 % of the analytically calculated value. The Eckart correction factors (about 2 at room temperature) were also included in the reported FTST rate constants.

B. Results and Discussion

The experimental conditions and results for 26 $k_{4.1}$ measurements are summarized in Table 4.1. The listed 1σ uncertainties in $k_{4.1}$ are derived from the precision of slopes of plots such as Figure 4.3, combined in quadrature with the estimated reproducibility of P, T. Modest values of $\sigma / k_{4.1}$ indicate good linearity in such plots. At each temperature, the weighted and unweighted means plus the standard deviations of these means[13] were

calculated. The two means at each temperature differ by up to 6 %. The weighted mean and the larger one of the two standard deviations at each temperature are reported in Table 4.1. Not all our original measurements are included in Table 4.1. Two outlying individual $k_{4.1}$ measurements were rejected according to Chauvenet's statistical criterion.[14] At the highest temperature $k_{4.1}$ showed no consistent trend with τ_{res}, which indicates that pyrolysis of CH_3Br was unimportant at the listed temperatures.

To make an estimate of the extent of interference from secondary chemistry, kinetic modeling was performed using the ACUCHEM program.[15] The following scheme was considered

$$H + CH_3Br \rightarrow CH_3 + HBr, \quad (4.1)$$

$$H \rightarrow \text{diffusion}, \quad (4.7)$$

$$H + CH_3\ (+Ar) \rightarrow CH_4\ (+Ar), \quad (4.8)$$

$$H + NH_2\ (+Ar) \rightarrow NH_3\ (+Ar), \quad (4.9)$$

$$CH_3 + CH_3 \rightarrow C_2H_6, \quad (4.10)$$

$$CH_3 + NH_2 \rightarrow CH_3NH_2, \quad (4.11)$$

$$NH_2 + NH_2 \rightarrow N_2H_4, \quad (4.12)$$

$$H + HBr \rightarrow H_2 + Br, \quad (4.13)$$

$$CH_3 + HBr \rightarrow CH_4 + Br. \quad (4.14)$$

The reaction

$$CH_3 + Br\ (+Ar) \rightarrow CH_3Br\ (+Ar) \quad (4.15)$$

was not included in this scheme, according to tests at 400 K and 813 K, which showed

Table 4.1. Rate constant measurements of the reaction H + CH_3Br and the gas flows

T, K	P, mbar	τ_{res} s	I_0, mJ	$[H]_{0,max}$ 10^{12} molecule cm^{-3}	$[CH_3Br]_{0,max}$ 10^{15} molecule cm^{-3}	$f_{modeling}$	$k_{4.1} \pm \sigma_{k_{4.1}}$ $10^{-13} cm^3$ $molec.^{-1}$ s^{-1}
400	68.2	2.7	0.5	7.3	6.1	0.6957	0.800 ± 0.018
400	68.4	1.3	0.5	7.3	5.9	0.6857	0.720 ± 0.030
400	134.5	2.6	0.5	7.4	6.3	0.6957	0.800 ± 0.020
400	134.2	2.6	0.2	3.7	6.3	0.8073	0.880 ± 0.021
400							0.810 ± 0.028
443	68.6	1.2	0.6	5.1	5.2	0.8235	1.40 ± 0.05
443	68.6	1.2	0.2	2.2	5.2	0.8988	1.51 ± 0.05
443	133.8	2.4	0.6	5.2	5.6	0.8295	1.46 ± 0.04
443							1.46 ± 0.03 [b]
498	67.8	2.1	0.5	7.6	2.5	0.8460	3.46 ± 0.08
498	68.1	2.2	0.3	3.8	2.5	0.8992	3.30 ± 0.11
498	67.4	4.3	0.5	7.5	2.4	0.8541	3.63 ± 0.17
498	34.8	2.2	0.5	7.3	2.4	0.8375	3.04 ± 0.11
498	34.9	2.2	0.3	3.7	2.4	0.9041	3.49 ± 0.13
498	34.1	4.3	0.5	7.2	2.4	0.8477	3.45 ± 0.24
498	71.8	4.5	0.4	4.9	3.6	0.9026	3.43 ± 0.18
498	72.0	4.5	0.2	2.4	3.6	0.9470	3.75 ± 0.14
498							3.41 ± 0.07 [b]
571	136.9	3.8	0.6	10.7	1.8	0.8756	6.83 ± 0.28
571	69.2	3.8	0.6	10.3	1.7	0.8766	6.89 ± 0.24
571	69.4	3.8	0.3	5.1	1.7	0.9281	7.62 ± 0.26
571							7.11 ± 0.21 [b]
670	68.6	3.2	0.5	7.3	84.6	0.9337	16.9 ± 1.4
670	69.4	3.3	0.3	3.7	84.9	0.9560	15.2 ± 1.1
670	68.8	1.6	0.5	7.4	77.3	0.9294	15.8 ± 0.5
670	135.4	3.2	0.5	7.5	86.1	0.9257	13.7 ± 0.3
670							14.4 ± 0.6 [b]
813	70.0	2.7	0.6	13.3	36.4	0.9322	37.1 ± 3.9
813	71.8	1.4	0.6	13.7	34.0	0.9457	47.0 ± 5.4
813	70.9	1.4	0.3	6.8	33.6	0.9652	44.4 ± 4.0
813	139.0	2.7	0.6	13.5	37.4	0.9368	40.0 ± 2.5
813							41.0 ± 1.9 [b]

[a] $[CH_3Br]_{0,max}$ was 5-17 times of $[CH_3Br]_{0.min}$; [b] Mean value.

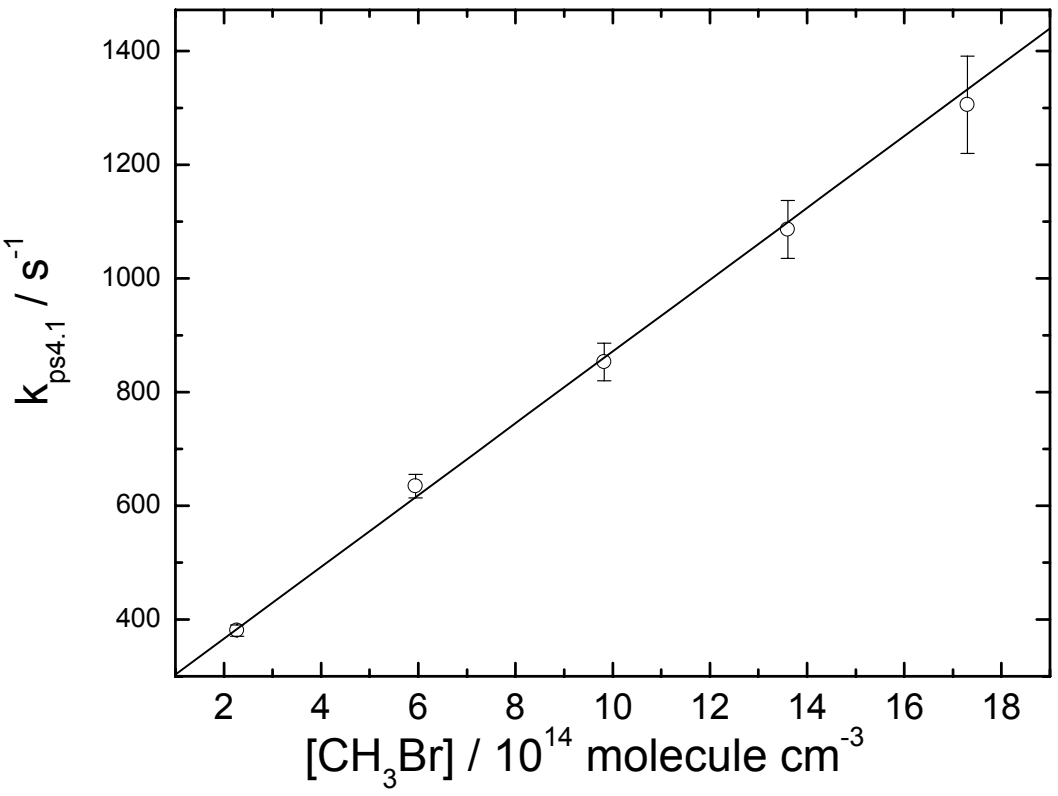

Fig. 4.3. Plot of pseudo-first-order rate constant $k_{ps4.1}$ vs [CH_3Br] at P = 67 mbar and T = 571 K. The points are with 2σ error bar.

the relative deviations of [H] from modeling are less than 0.5 % when this reaction was included. Therefore, the reaction 4.15 could be ignored. The modeling was performed on each individual set of measurement. For each modeling, $k_{4.1}$ was taken as the measured one in this work; $k_{4.7}$ was fixed as 150 s^{-1}; $k_{4.8}$ was evaluated using the expression preferred by Baulch et al.,[16] $k = 6.0 \times 10^{-29} \times (T/298)^{-1.8}$ cm^6 $molecule^{-2}$ s^{-1} at 67 mbar pressure; $k_{4.9}$ was estimated as $k_{4.8}$; $k_{4.11}$ and $k_{4.12}$ were taken as the same as $k_{4.10} = 4.1 \times 10^{-11} \times \exp(137\ K/T)$ cm^3 $molecule^{-1}$ s^{-1};[17] $k_{4.13}$ was set equal to 1×10^{-11} cm^3 $molecule^{-1}$ s^{-1},[18] and $k_{4.14} = 8.92 \times 10^{-12} \times \exp(-810\ K/T)$ cm^3 $molecule^{-1}$ s^{-1}.[19] The initial concentrations of species H, NH_3, CH_3, CH_3Br in modeling were those used in each set of measurement. A linear regression was applied to the plot of ln [H] from modeling versus time. The resultant slope was $k_{ps4.1}$ and the effective second order rate constant was then estimated as $k_{eff4} = (k_{ps4.1} - k_{diff4}) / [CH_3Br]_0$, where k_{diff4} was the slope of linear fit of ln [H] from modeling with $[CH_3Br]_0 = [CH_3]_0 = 0$ molecule cm^{-3} versus time. The relative deviations of k_{eff4} with respect to the input $k_{4.1}$ range from about +30 % at 400 K to about +7 % at 813 K. This implies that the $k_{4.1}$ measured under the experimental conditions in this work was overestimated to some extent due to the secondary chemistry. Therefore, a particular correction factor from the modeling was applied to each set of measurement as shown in Table 4.1 under the heading of $f_{modeling}$. A weighted Arrhenius fit was performed on the 26 measurements and is shown in Figure 4.4. It yielded

$$k_{4.1} = (1.23 \pm 0.12) \times 10^{-10} \exp[(-(22.4 \pm 0.4)\ kJ\ mol^{-1} / RT]\ cm^3\ molecule^{-1}\ s^{-1} \quad (4.16)$$

over the temperature range 400 - 813 K. The quoted errors in this expression are 1σ and are statistical only. Consideration of the covariance leads to a 1σ precision for the fitted

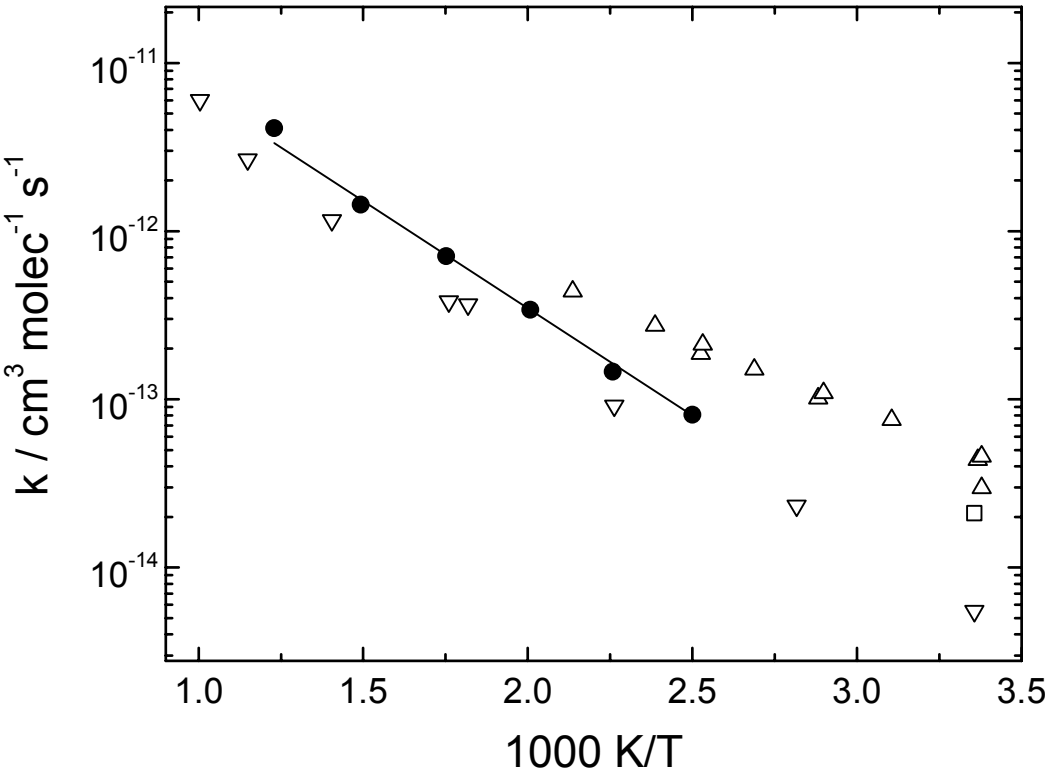

Fig. 4.4. $k_{4.1}$ of H + CH_3Br reaction in the range of 296 - 996K. Solid line: Arrhenius fitting of this work; solid circles: this work; open square: Ref. 2; open uptriangles: Ref. 4; open downtriangles: Ref. 3.

$k_{4.1}$ of 2 - 4 %, and allowance for possible systematic errors leads to 95 % confidence intervals of ± 13 %. Three sets of directly measured $k_{4.1}$ values from literature are included in Fig. 4.4. At 298 K the $k_{4.1}$ measured by Westenberg et al.[3] is about 8 times smaller than that measured by Aders et al.,[4] although these authors claimed relative errors of less than 10 % in both sets of measurements. At about 450 K the measurement by Aders et al. is about 5 times larger than Westenberg's measurement.

The geometries, barrier heights and vibrational frequencies of the transition states for the three channels of reaction H + CH_3Br calculated at the BHandH/6-311G(d,p) level are summarized in Figure 4.1, Table 4.2 and Table 4.3. The preliminary calculation for transition state of Br-abstraction showed a symmetry-breaking problem. The expected C_{3v} symmetry was broken to C_1 or C_s symmetry. From C_{3v} to C_1 or C_s symmetry, r_{CBr} increased by 0.00003 Å; r_{HBr} decreased by 0.00036 Å; the maximum change in r_{CH} was 0.00009Å, and the maximum change in $\angle_{HCBr}$ was 0.13°. The ZPCs for G2 energies and frequencies for TST calculations were scaled by 0.9478. The ratios of k_n (n = 2 and 3) over k_1 from TST calculations (without any tunneling correction) versus 1000 K/T are presented in Figure 4.5. It shows that the channels 2 and 3 are negligible even at flame temperatures. This result supports the analysis of Chadwell and Titani in 1933.[1]

The optimized geometries, barrier heights and reaction enthalpies at three different G2 levels for H + $CH_3Br \rightarrow CH_3$ + HBr are listed in Table 4.4. The experimental values are also listed for comparison. The calculated frequencies, which were scaled by a corresponding factor and the observed fundamentals, are presented in Table 4.5.

Table 4.2. Transition state geometries and barrier heights for the reaction H + CH_3Br

Geometry[a], $E_0^{\neq}$	Br-abstraction (C_1 or C_s symmetry)	H-abstraction (C_s symmetry)	Br-substitution (C_{3v} symmetry)
r_{BrH4}	1.8047		
r_{CBr}	2.0322	1.8682	2.0981
r_{CH1}	1.0822	1.4139	1.0804
r_{CH2}	1.0823	1.0818	1.0804
r_{CH3}	1.0824	1.0818	1.0804
r_{CH4}			1.6028
r_{H1H4}		0.8861	
$\angle_{H1CBr}$	105.90	108.09	98.79
$\angle_{H2CBr}$	105.75	112.70	98.79
$\angle_{H3CBr}$	105.68	112.70	98.79
$\angle_{H4BrC}$	177.23		
$\angle_{H4CBr}$			180.0
$\angle_{CH1H4}$		178.66	
$D_{H2CBrH1}$	120.03	112.97	120.00
$D_{H3CBrH1}$	-120.01	-112.97	-120.00
$D_{H4BrCH1}$	-16.74		
$D_{H4H1CBr}$		180.0	
$E_0^{\neq}$, kJ mol^{-1} (G2 method)	27.58	51.19	63.28
Scaling factor for ZPC [b]	0.9478	0.9478	0.9478

[a] Refer to Fig. 4.1.; calculated at the BHandH/6-311G(d,p) level; bond lengths in angstrom and angle in degree.

[b] Obtained by plotting observed frequencies vs. calculated frequencies.

Table 4.3. Calculated frequencies of transition states for reaction H + CH_3Br

Br-abstraction‡ (cm^{-1})	H-abstraction‡ (cm^{-1})	Br-substitution‡ (cm^{-1})
669i	1193i	1193i
27	278	431
41	516	431
700	701	540
862	946	1097
865	990	1097
1259	1128	1231
1466	1134	1421
1467	1419	1421
3148	2008	3148
3288	3185	3319
3288	3308	3319

‡ Geometry refers to Fig. 4.1.; calculated at the BHandH/6-311G(d,p) level.

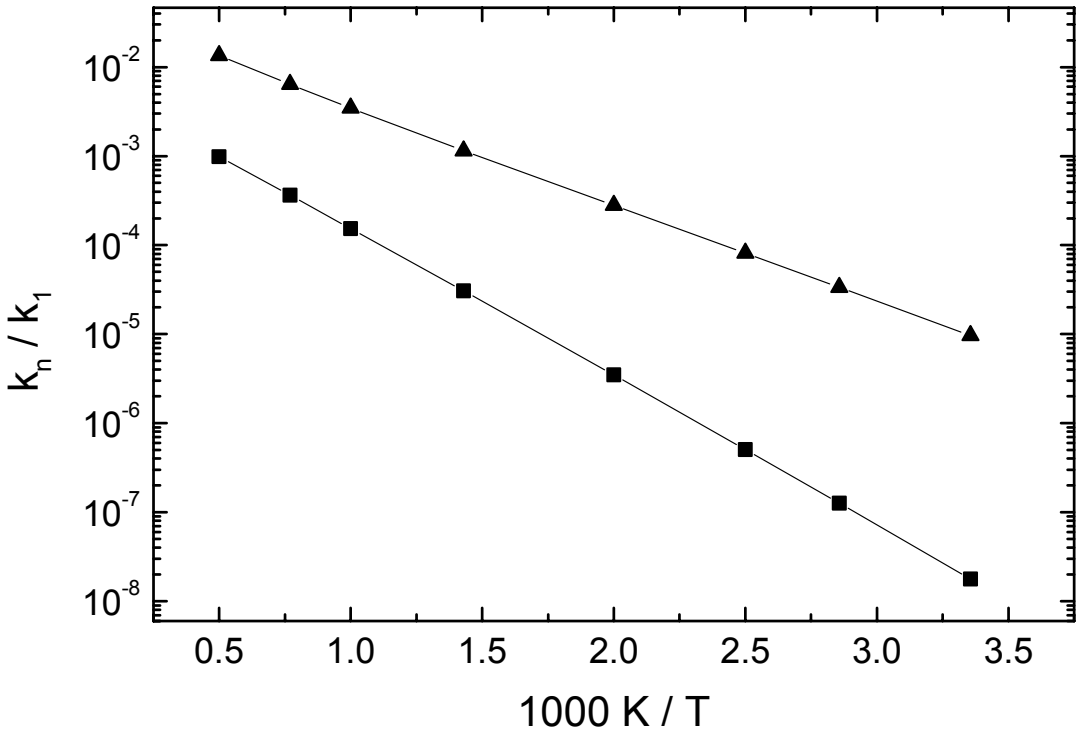

Fig. 4.5. Ratio of rate constants vs. temperature for reaction H + CH_3Br. The triangles: k_2 / k_1 (H-abs / Br-abs); the squares: k_3 / k_1 (Br-sub / Br-abs).

Table 4.4. Geometry, barrier height and enthalpy for the reaction H + $CH_3Br \rightarrow$ CH_3 + HBr

Geometry[a], $E_0^{\neq}$, ΔH_0	MP2(FULL) /6-31G(d)	MP2 /6-311G(d,p)	QCISD /6-31G(d,p)	Experimental Values
CH_3Br--H (TS)[b]				
r_{HBr}	1.7101	1.7226	1.8330	
r_{CBr}	2.1201	2.0791	2.0865	
r_{CH}	1.0845	1.0860	1.0826	
$\angle_{HCH}$	104.55	105.55	105.21	
CH_3Br[b]				
r_{CBr}	1.9476	1.9350	1.9581	1.939[f], 1.939[h]
r_{CH}	1.0867	1.0877	1.0839	1.113[f], 1.096[h]
$\angle_{HCBr}$	107.86	108.39	107.72	111.23[f], 107.93[h]
CH_3[c]				
r_{CH}	1.0783	1.0792	1.0774	1.079[g]
HBr				
r_{HBr}	1.4356	1.4126	1.4100	1.4144[g]
$E_0^{\neq}$, kJ mol^{-1} (G2 method)	30.51	26.95	28.72	
ΔH_0, kJ mol^{-1} (G2 method)	-73.07	-70.72	-71.21	$-(74.60 \pm 0.98)$[g,h]
Scaling factor for ZPC	0.8929[d]	0.9473[e]	0.9407[e]	

[a] Bond lengths in angstrom and angle in degree.

[b] C_{3v} symmetry.

[c] D_{3h} symmetry.

[d] ZPC at the HF/6-31G(d) level.

[e] Obtained by plotting observed frequencies vs. calculated frequencies.

[f] Taken from Ref. 2.

[g] Taken from Ref. 10.

[h] $\Delta H_{f,0K}$ of CH_3Br was taken from Ref. 11.

Table 4.5. Harmonic frequencies and fundamentals for species of reaction $H + CH_3Br \rightarrow CH_3 + HBr$

Modes[a]	HF /6-31G(d) [b]	MP2 /6-311G(d,p) [c]	QCISD /6-31G(d,p) [d]	Fundamentals
Transition state				
A_1	1014i	1083i	810i	
E (2)	261	85	132	
A_1	476	655	585	
E (2)	748	794	802	
A_1	1148	1189	1194	
E (2)	1417	1395	1422	
A_1	2935	2963	2978	
E (2)	3065	3102	3112	
CH_3Br				
A_1 (ν_3)	570	614	578	611[e]
E (ν_6, 2)	946	938	937	955[e]
A_1 (ν_2)	1324	1308	1308	1306[e]
E (ν_5, 2)	1451	1417	1445	1443[e]
A_1 (ν_1)	2926	2957	2973	2973[e]
E (ν_4, 2)	3028	3066	3085	3056[e]
CH_3				
A_2" (ν_2)	275	396	395	607[e], 580[f]
E' (ν_4, 2)	1375	1371	1387	1398[e], 1383[f]
A_1" (ν_1)	2933	3006	3006	3000[e], 3002[f]
E' (ν_3, 2)	3090	3189	3182	3162[e], 3184[f]
HBr				
σ_g	2501	2593	2547	2559[f]

[a] Designated in irreducible representations from ab initio calculations and in cm^{-1}; Number in parentheses is degeneracy. [b] Scaled by 0.8929. [c] Scaled by 0.9473. [d] Scaled by 0.9407. [e] Taken from Ref. 2. [f] Taken from Ref. 10.

The potential energy of the transitional / external-rotation modes is shown in Figure 4.6. When ϕ equals to zero degree, one H atom in the CH_3 group is in the same plane containing the CBr bond and the added H atom, but opposite to the added H atom. It is a gauche conformation, and the barrier heights lie in the minimum. Then the barrier heights increase as the rotation of the CH_3 group. When ϕ equals to 60 degree, an eclips conformation is formed, and barrier heights arrive at the maximum. After that, the barrier heights decrease. When another gauche conformation is formed at 120 degree, the barrier heights become the minimum again. Therefore, there are 3 minimums and 3 maximums in a 360 degree circle of ϕ, except when θ equals to zero degree. Figure 4.6 shows that the CH_3 rotor is a free rotor, and the barrier height is zero, when θ equals to zero degree. Since the barrier heights at $\theta = 136^o$ are greater than 140 kJ mol^{-1}, and exp $(-V_{tr}/RT)$ is very small, the contributions of $\theta > 136^o$ to the integral of the hindering function $\Gamma^{\dagger}(T)$ were ignored.

The rate constants from conventional TST and FTST calculations were fitted to the measured $k_{4.1}$ in this work by adjusting the corresponding barrier heights to minimize the rms deviations. The Eckart factors were recalculated at each adjusted barrier height. For the conventional TST calculation (all modes treated as vibrations) with original G2 barrier and scaled HF/6-31G(d) frequencies, the barrier height was adjusted down by 10.3 kJ mol^{-1} and the relative errors to the measured $k_{4.1}$ are 6 % - 24 %. For the TST calculation with the modified G2//QCISD/6-31G(d,p) barrier height and scaled QCISD/6-31G(d,p) frequencies, the barrier height was adjusted down by 5.6 kJ mol^{-1} and the relative errors to the measured $k_{4.1}$ are 2 % - 22 %. For the TST calculation with modified

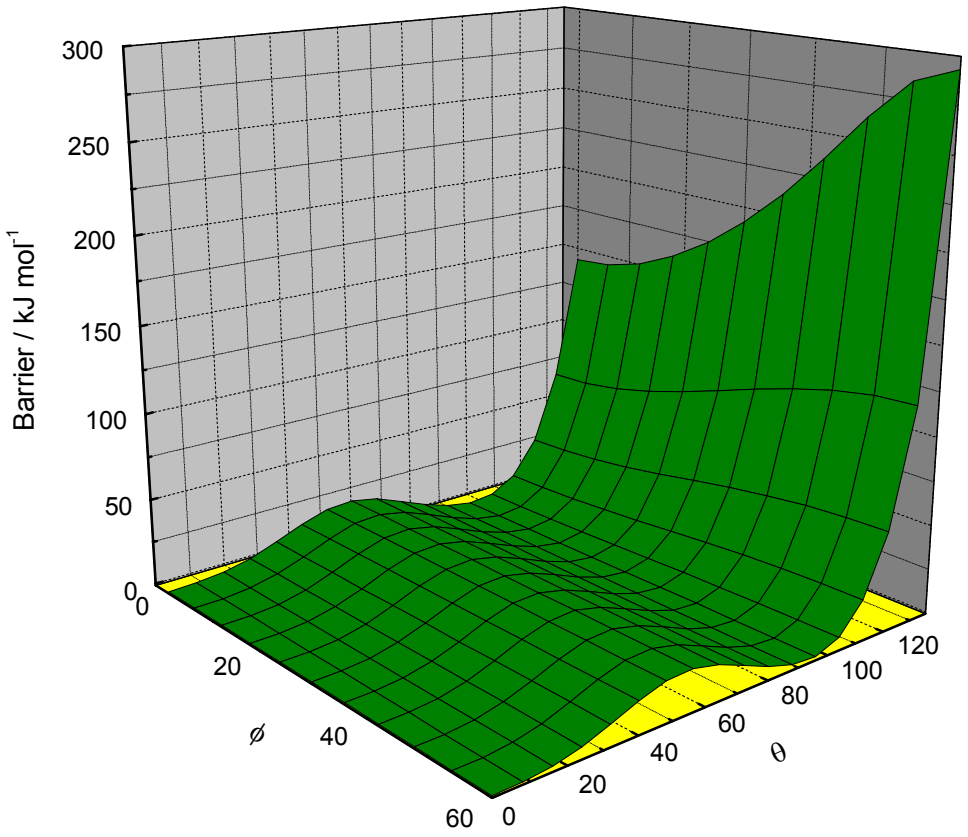

Fig. 4.6. Barrier height of the transitional / external-rotation modes of the TS relative to H + CH_3Br at the QCISD/6-31G(d,p) level of theory

G2//MP2/6-311G(d,p) barrier height and scaled MP2/6-311G(d,p) frequencies, no barrier height adjustment was needed and the relative errors to the measured $k_{4.1}$ are 8 % - 50 %. The lowest (double degenerate) frequencies of the TS at the MP2/6-311G(d,p) level are 85 cm^{-1} (see Table 4.5). Since a lower frequency has more contribution to the vibrational partition function, a more realistic treatment of the two low frequency modes should give more accurate values for $k_{4.1}$. The G2//QCISD/6-31G(d,p) barrier height of FTST calculation at QCISD/6-31G(d,p) level was adjusted down by only 1.9 kJ mol^{-1} and the relative errors to the measured $k_{4.1}$ are between 6 % and 37 %.

A non-linear fitting procedure was applied to the adjusted results of the calculations. The non-linear fitting of the TST data calculated with original G2 barrier height $E_0^{\neq}$ = 20.2 kJ mol^{-1} over 298 - 2000 K yielded

$$k_{4.1} = 9.86 \times 10^{-18}\, T^{2.165} \exp(-1516\ K/T)\ \ cm^3\ molecule^{-1}\ s^{-1} \qquad (4.17)$$

This expression fits the TST data to within 5 %. The non-linear fitting of the TST data calculated with modified G2//MP2/6-311G(d,p) barrier height $E_0^{\neq}$ = 27.0 kJ mol^{-1} over 298 - 2000 K yielded

$$k_{4.1} = 4.31 \times 10^{-17}\, T^{2.199} \exp(-2360\ K/T)\ \ cm^3\ molecule^{-1}\ s^{-1} \qquad (4.18)$$

This expression fits the TST data to within 7 %. The non-linear fitting of the TST data calculated with modified G2//QCISD/6-31G(d,p) barrier height $E_0^{\neq}$ = 23.1 kJ mol^{-1} over 298 - 2000 K yielded

$$k_{4.1} = 1.51 \times 10^{-16}\, T^{1.940} \exp(-2189\ K/T)\ \ cm^3\ molecule^{-1}\ s^{-1} \qquad (4.19)$$

This expression fits the TST data to within 4 %. The non-linear fitting of the FTST data calculated with modified G2//QCISD/6-31G(d,p) barrier height $V^{\dagger}$ = 26.8 kJ mol^{-1} over 298 - 2000 K yielded

$$k_{4.1} = 4.61 \times 10^{-15} T^{1.532} \exp(-2631\ K/T)\ \ cm^3\ molecule^{-1}\ s^{-1} \qquad (4.20)$$

This expression fits the FTST data to within 5 %. The adjusted results of FTST calculations and TST calculations at MP2/6-311G(d,p) and QCISD/6-31G(d,p) levels together with the experimental data are shown in Figure 4.7. It is noted that all the three models fit the experimental data well and are too close to be separated clearly, but combination with the measurements by Westenberg et al.,[3] the FTST model is considered to be the most reasonable representation.

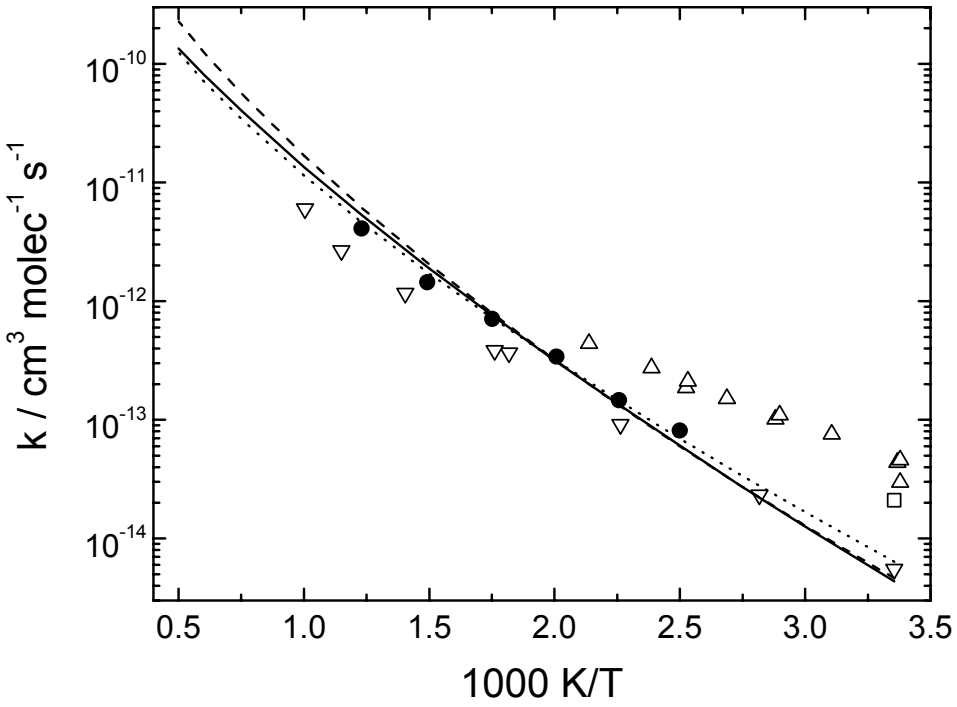

Fig. 4.7. Comparison of $k_{4.1}$ of H + CH_3Br reaction. Solid line: FTST calculation with $V^{\dagger}$ = 26.8 kJ mol^{-1} over 298 - 2000 K; dashed line: TST calculation with $E_0^{\neq}$ = 27.0 kJ/mol^{-1} over 298 – 2000 K; dotted line: TST calculation with $E_0^{\neq}$ = 23.1 kJ/mol^{-1} over 298 – 2000 K; solid circles: this work; open square: Ref. 2; open uptriangles: Ref. 4; open downtriangles: Ref. 3.

REFERENCES

(1) Chadwell, H. M.; Titani, T. *J. Am. Chem. Soc.* **1933**, *55*, 1363.

(2) Townes, C. H.; Schawlow, A. L. *Microwave Spectroscopy*; McGraw-Hill: New York, 1955.

(3) Westenberg, A. A.; deHaas, N. *J. Chem. Phys.* **1975**, *62*, 3321.

(4) Aders, W.-K.; Pangritz, D.; Wagner, H. G. *Ber. Bunsenges. Phys. Chem.* **1975**, *79*, 90.

(5) Wardlaw, D. M.; Marcus, R. A. *J. Chem. Phys.* **1985**, *83*, 3462.

(6) Wardlaw, D. M.; Marcus, R. A. *Chem. Phys. Lett.* **1984**, *110*, 230.

(7) Okabe, H. *Photochemistry of Small Molecules*; John Wiley: New York, 1978.

(8) Frisch, M. J.; Trucks, G. W.; Schlegel, H. B.; Gill, P. M. W.; Johnson, B. G.; Robb, M. A.; Cheeseman, J. R.; Keith, T. A.; Petersson, G. A.; Montgomery, J. A.; Raghavachari, K.; Al-Laham, M. A.; Zakrzewski, V. G.; Ortiz, J. V.; Foresman, J. B.; Cioslowski, J.; Stefanov, B.; Nanayakkara, A.; Challacombe, M.; Peng, C. Y.; Ayala, P. Y.; Chen, W.; Wong, W.; Andres, J. L.; Replogle, E. S.; Gomperts, R.; Martin, R. L.; Fox, D. J.; Binkley, J. S.; Defrees, D. J.; Baker, J.; Stewart, J. P.; Head-Gordon, M.; Gonzalez, C.; Pople, J. A. Gaussian 94 (Revision D.2); Gaussian, Inc.: Pittsburgh, PA, 1995.

(9) Johnston, H. S. *Gas-Phase Reaction Rate Theory*; Ronald: New York, 1966.

(10) *NIST-JANAF Thermochemical Tables*; 4 ed.; Chase, M. W. J., Ed.; the American Chemical Society and the American Institute of Physics: Woodbury, N. Y., 1998.

(11) *Thermodynamic Properties of Individual Substances*; 4 ed.; Gurvich, L. V.; Veyts, I. V.; Alcock, C. B.; Iorish, V. S., Eds.; Hemisphere: New York, 1992; Vol. 2.

(12) Robertson, S. H.; Wagner, A. F.; Wardlaw, D. M. *J. Chem. Phys.* **1995**, *103*, 2917.

(13) Massey, B. S. *Measures in Science and Engineering: Their Expression, Relation and Interpretation*; John Wiley: New York, 1986.

(14) Pugh, E. M., Jr.; Winslow, G. H. *The Analysis of Physical Measurements*; Addison-Wesley: Reading, 1966.

(15) Braun, W.; Herron, J. T.; Kahaner, D. K. *Int. J. Chem. Kinet.* **1988**, *22*, 51.

(16) Baulch, D. L.; Cobos, C. J.; Cox, R. A.; Esser, C.; Frank, P.; Just, T.; Kerr, J. A.; Pilling, M. J.; Troe, J.; Walker, R. W.; Warnatz, J. *J. Phys. Chem. Ref. Data* **1992**, *21*, 411.

(17) MacPherson, M. T.; Pilling, M. J.; Smith, M. J. C. *J. Phys. Chem.* **1985**, *89*, 2268.

(18) Seakins, P. W.; Pilling, M. J. *J. Phys. Chem.* **1991**, *95*, 9878.

(19) Baulch, D. L.; Duxbury, J.; Grant, S. J.; Montague, D. C. *J. Phys. Chem. Ref. Data* **1981**, *10*.

CHAPTER 5

REACTION OF H + C_4F_6

The reaction of atomic hydrogen with perfluoro-1,3-butadiene,

$$H + CF_2{=}CF\text{-}CF{=}CF_2 \rightarrow \text{products} \qquad (5.1)$$

was studied for the first time here. The experiments reveal distinctly non-Arrhenius behavior which is used to interpret in terms of a change of mechanism. At low temperatures addition of H atoms may create a substituted butenyl radical, a process which reaches equilibrium at higher temperatures so that the thermochemistry can be assessed. At even higher temperatures it is speculated that an observed increase in the overall rate constant reflects fragmentation of the adduct to further products

A. Experimental Method

The utilization of the FP-RF technique in this study was described in the previous chapter. H atom was generated by photolysis of NH_3 or H_2O. The C_4F_6 reacted with H atoms under pseudo-first-order conditions, $[H] << [C_4F_6]$, which implies an exponential decay of [H]:

$$d[H]/dt = -(k_{5.1}[C_4F_6] + k_{diff5})[H] = -k_{ps5.1}[H]$$

$$[H] = [H]_0 \exp(-k_{ps5.1}\, t) \qquad (5.2)$$

where k_{diff5} accounts for any loss of H atoms out of the reaction zone other than by reaction with C_4F_6, mainly via diffusion to the reactor walls, and at high temperatures, by

reaction with the H-atom precursor. $k_{ps5.1}$ was obtained by fitting the recorded fluorescence intensity I_f versus time t profile to an exponential decay over typically at least four lifetimes:

$$I_f = A\,[H] + B \qquad (5.3)$$

where A reflects the proportionality between [H] and the extent of resonance fluorescence, and B represents the constant contribution from scattered light in the system. The second-order H + C_4F_6 rate constant $k_{5.1}$ was determined at a given set of conditions by linear fitting of $k_{ps5.1}$ versus typically five values of [C_4F_6]. In order to verify that pseudo-first-order conditions were attained, the flash energy and precursor concentrations were varied to alter the initial radical concentrations, so that each flash lamp pulse photolyzed a fresh reaction mixture, the reactants flowed through the reactor. The rate of sweeping gas through the reaction zone was slow compared to the reaction time scale of the H-atoms, so the kinetic conditions were effectively static. The average gas residence time in the heated reactor before photolysis, τ_{res}, was varied to check for possible pyrolysis of C_4F_6. Dr. Abdell Goumri is a coworker of these experiments.

B. Results

A typical exponential decay of fluorescence is shown in Figure.5.1, as are representative plots of $k_{ps5.1}$ vs. [C_4F_6] over the temperature range studied, 290-1010 K. The linear fits to these plots passed close to the k_{diff5} measurement obtained with zero reactant concentration, which ranged from about 80 s^{-1} at low temperatures and up to 870 s^{-1} at the highest temperature. The slopes of 48 of these plots yield the $k_{5.1}$ values listed in

Table 5.1, together with the statistical uncertainties. Good linearity in these plots leads to small σ/k values. Also shown are the experimental parameters T, P, τ_{res}, the energy discharged in the flash lamp E, and the concentrations employed. As may be seen from Table 5.1, there is no significant variation of $k_{5.1}$ with E (typically varied by a factor of 2),

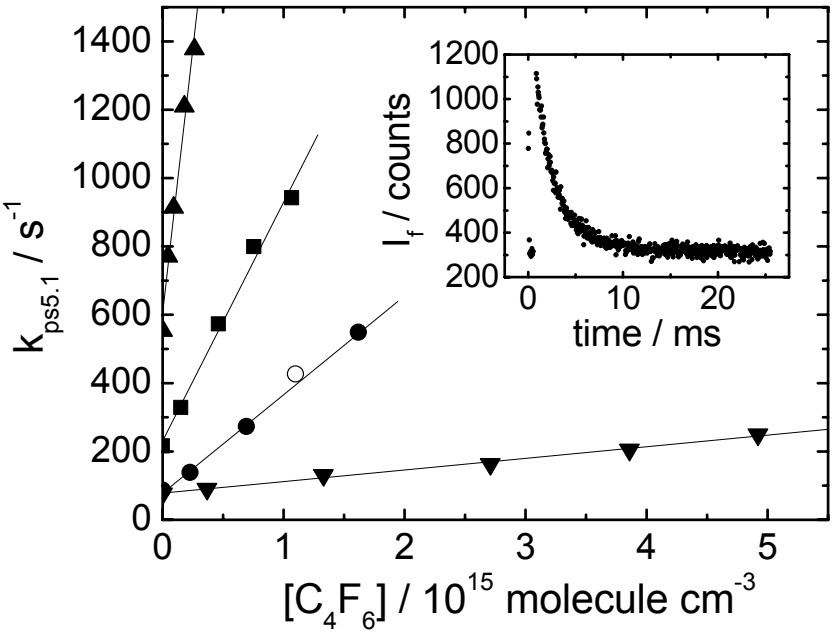

Fig. 5.1. Plots of pseudo-first-order rate constant $k_{ps5.1}$ vs. $[C_4F_6]$. Downward triangles: 291 K; circles: 406 K; squares: 518 K; upward triangles: 1006 K. The insert shows the fluorescence decay corresponding to the open circle.

Table 5.1. Rate constant measurements of the reaction H + C_4F_6

T, K	P, Mbar	τ_{res}, s	E, J	[precursor],[a] 10^{15} molecule cm^{-3}	[C_4F_6], 10^{14} molecule cm^{-3}	$k_{5.1} \pm \sigma_{k_{5.1}}$, 10^{-13} cm^3 $molecule^{-1}$ s^{-1}
290	69	6.4	3.6	2.6	3.63 - 46.8	0.363 ± 0.020
290	69	6.4	3.6	0.88	3.63 - 47.3	0.366 ± 0.020
291	136	6.6	2.0	1.8	3.68 - 49.1	0.342 ± 0.013
291	136	6.6	4.1	1.8	3.68 - 49.1	0.366 ± 0.030
330	141	5.9	4.1	1.4	3.43 - 21.1	0.635 ± 0.015
330	73	3.0	4.1	1.4	3.15 - 21.8	0.748 ± 0.023
383	71	2.6	4.1	0.60	2.78 - 18.4	1.41 ± 0.04
386	71	5.2	4.1	0.60	2.73 - 18.6	1.43 ± 0.07
406	133	4.5	4.1	1.1 [b]	2.33 - 16.5	2.79 ± 0.07
406	68	2.2	4.1	1.1 [b]	2.35 - 16.0	2.74 ± 0.03
439	68	2.1	4.1	0.49	2.23 - 15.4	3.58 ± 0.12
439	68	4.3	4.1	0.49	2.23 - 15.3	3.68 ± 0.06
518	56	1.5	2.0	0.67	1.53 - 10.7	7.33 ± 0.26
519	27	0.70	4.1	0.16	0.749 - 4.99	7.14 ± 0.18
519	27	0.70	2.0	0.16	0.749 - 4.99	6.40 ± 0.09
588	136	3.2	4.1	0.61 [b]	1.67 - 11.4	11.5 ± 0.1
588	68	1.5	4.1	0.60 [b]	1.64 - 11.2	11.9 ± 0.6
615	136	0.77	4.1	0.18	0.785 - 5.50	11.9 ± 0.7
617	68	1.6	4.1	0.18	0.816 - 5.66	12.7 ± 0.3
663	33	0.68	4.1	0.16	0.673 - 4.91	11.1 ± 0.2
663	71	1.5	4.1	0.17	0.869 - 5.37	10.8 ± 0.3
674	132	2.7	4.1	0.65 [b]	1.45 - 9.77	7.78 ± 0.42
674	65	1.3	4.1	0.62 [b]	1.34 - 9.30	8.75 ± 0.39
683	72	1.4	4.1	0.33	1.44 - 10.1	7.10 ± 0.39
683	33	1.3	4.1	0.16	0.715 - 4.99	6.58 ± 0.28
683	69	1.4	4.1	0.32	1.35 - 10.7	7.37 ± 0.22
740	67	1.3	4.1	0.15	0.733 - 4.63	7.48 ± 0.44
740	35	0.64	4.1	0.15	0.687 - 4.54	7.98 ± 0.38
786	35	0.60	4.1	0.14	0.646 - 4.28	9.34 ± 0.40
786	68	1.2	4.1	0.14	0.640 - 4.35	9.53 ± 0.09
800	136	2.4	4.1	0.28	1.38 - 8.71	12.3 ± 0.3
800	65	1.1	4.1	0.25	1.11 - 8.13	11.9 ± 0.2
834	136	2.2	4.1	0.52	1.17 - 8.42	15.6 ± 0.4

Table 5.1. Rate constant measurements of the reaction H + C_4F_6 (contd.)

T, K	P, Mbar	τ_{res}, s	E, J	[precursor],[a] 10^{15} molecule cm^{-3}	[C_4F_6], 10^{14} molecule cm^{-3}	$k_{5.1} \pm \sigma_{k_{5.1}}$, 10^{-13} cm^3 $molecule^{-1}$ s^{-1}
834	65	1.1	4.1	0.50	1.14 - 7.84	14.8 ± 0.2
885	68	1.0	4.1	0.28	1.86 - 7.64	14.8 ± 0.4
885	69	2.1	4.1	0.29	1.97 - 8.23	14.7 ± 0.3
885	35	0.53	2.0	0.29	0.815 - 3.88	13.9 ± 0.5
885	35	0.53	4.1	0.29	0.815 - 3.88	14.8 ± 0.1
911	69	1.0	4.1	0.47	1.03 - 7.50	20.2 ± 1.0
911	133	2.0	4.1	0.47	1.16 - 7.47	22.1 ± 0.4
949	68	1.0	4.1	0.12	0.583 - 3.63	26.1 ± 0.8
949	132	1.9	4.1	0.45	1.01 - 6.93	25.6 ± 1.3
949	69	1.0	4.1	0.46	1.04 - 7.28	23.6 ± 1.1
1006	33	0.50	4.1	0.21	0.481 - 1.94	33.8 ± 3.0
1006	67	0.90	4.1	0.21	0.537 - 2.92	29.5 ± 3.5
1006	129	1.8	4.1	0.83	0.470 - 2.72	34.0 ± 2.2
1006	65	1.8	4.1	0.80	0.454 - 2.63	36.0 ± 1.6
1011	53	0.94	4.1	0.58[b]	0.545 - 3.33	31.8 ± 1.8

[a] Unless noted, the H-atom precursor is NH_3

[b] H_2O used as H-atom source

pseudo-first order conditions were attained, and that reaction 5.1 was successfully isolated from secondary chemistry involving photolytically or chemically produced species and any interaction between a precursor and C_4F_6. The independence of $k_{5.1}$ from τ_{res}, varied by a factor of 2-4, especially at the higher temperatures, shows that pyrolysis of C_4F_6 did not interfere.

There are clearly three regimes in Fig. 5.2. A weighted Arrhenius fit to the data at T < 620 K yields

$$k_{5.1}(T) = (3.40 \pm 0.34) \times 10^{-11} \exp[(-16.7 \pm 0.4) \text{ kJ mol}^{-1}/RT] \text{ cm}^3 \text{ molecule}^{-1} \text{ s}^{-1}$$

$$(290 \text{ K} < T < 620 \text{ K}) \qquad (5.4)$$

The quoted errors are 1σ and are statistical only. Consideration of the covariance leads to a 1σ precision for the fitted $k_{5.1}(T)$ of 3-6%, and allowance for possible systematic errors leads to a 95% confidence interval of ± 16%.

A similar analysis of the high temperature regime at T > 700 K leads to

$$k_{5.1}(T) = (1.83 \pm 0.53) \times 10^{-10} \exp[(-34.1 \pm 2.1) \text{ kJ mol}^{-1}/RT] \text{ cm}^3 \text{ molecule}^{-1} \text{ s}^{-1}$$

$$(700 \text{ K} < T < 1010 \text{ K}) \qquad (5.5)$$

with a 1σ precision of 3-6% for $k_{5.1}(T)$ and a 95% confidence interval, allowing for possible systematic errors, of ± 16%. In the intermediate regime, 620 K < T < 700 K, fluorescence decays remained exponential and $k_{5.1}$ dropped rapidly with temperature, with an effective activation energy of about –84 kJ mol^{-1}.

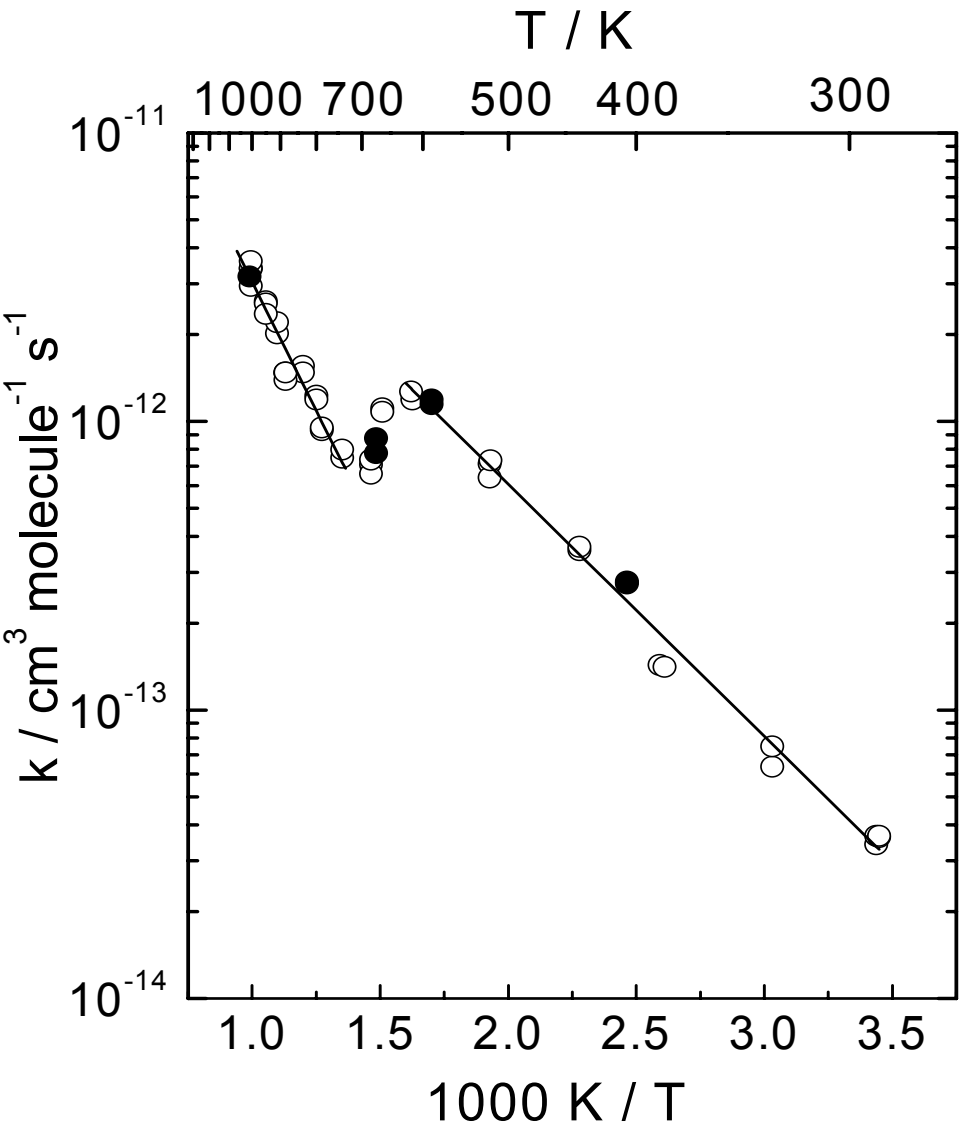

Fig. 5.2. Arrhenius plot for the H + C_4F_6 reaction, showing 48 measurements made with NH_3 (open circles) and H_2O (solid circles) as H-atom precursors, and fits to the low and high temperature data (solid lines).

C. Discussion

Low temperature regime, T < 620 K

C-F bonds are essentially inert to H-atom attack[1] under our conditions and a plausible path for reaction in the low temperature regime is addition to a π bond followed by collisional stabilization. Two initial adduct are possible, corresponding to addition to a terminal or central carbon atom:

$$H + CF_2=CF\text{-}CF=CF_2\ (+Ar) \rightarrow CF_2H\text{-}CF\bullet\text{-}CF=CF_2\ (+Ar) \qquad (5.1a)$$

$$H + CF_2=CF\text{-}CF=CF_2\ (+Ar) \rightarrow CF_2\bullet\text{-}CFH\text{-}CF=CF_2\ (+Ar) \qquad (5.1b)$$

In order to make a qualitative assessment of which adduct is more likely, Dr. Marshall has derived the geometries, vibrational frequencies and energies of the reactants, transition states and adducts at the HF/6-31G(d) level of ab initio molecular orbital theory.[2] Energies at the HF/6-31G(d) geometries were recalculated using density functional theory with a larger basis set, denoted B3LYP/6-311G(2df,p). Figure 5.3 is the geometries for C_4F_6, five C_4F_6H isomers and two transition states for H + C_4F_6 addition. The calculation results show that the adduct in 5.1a is more stable than the adduct in 5.1b, in line with an argument that the radicals are electron deficient and so the more substituted radical center is stabilized inductively by the substituents, and there is a somewhat smaller barrier to addition. These differences are not large, and it is speculated that over much of the temperature range 290-620 K a mixture of both adducts may be formed.

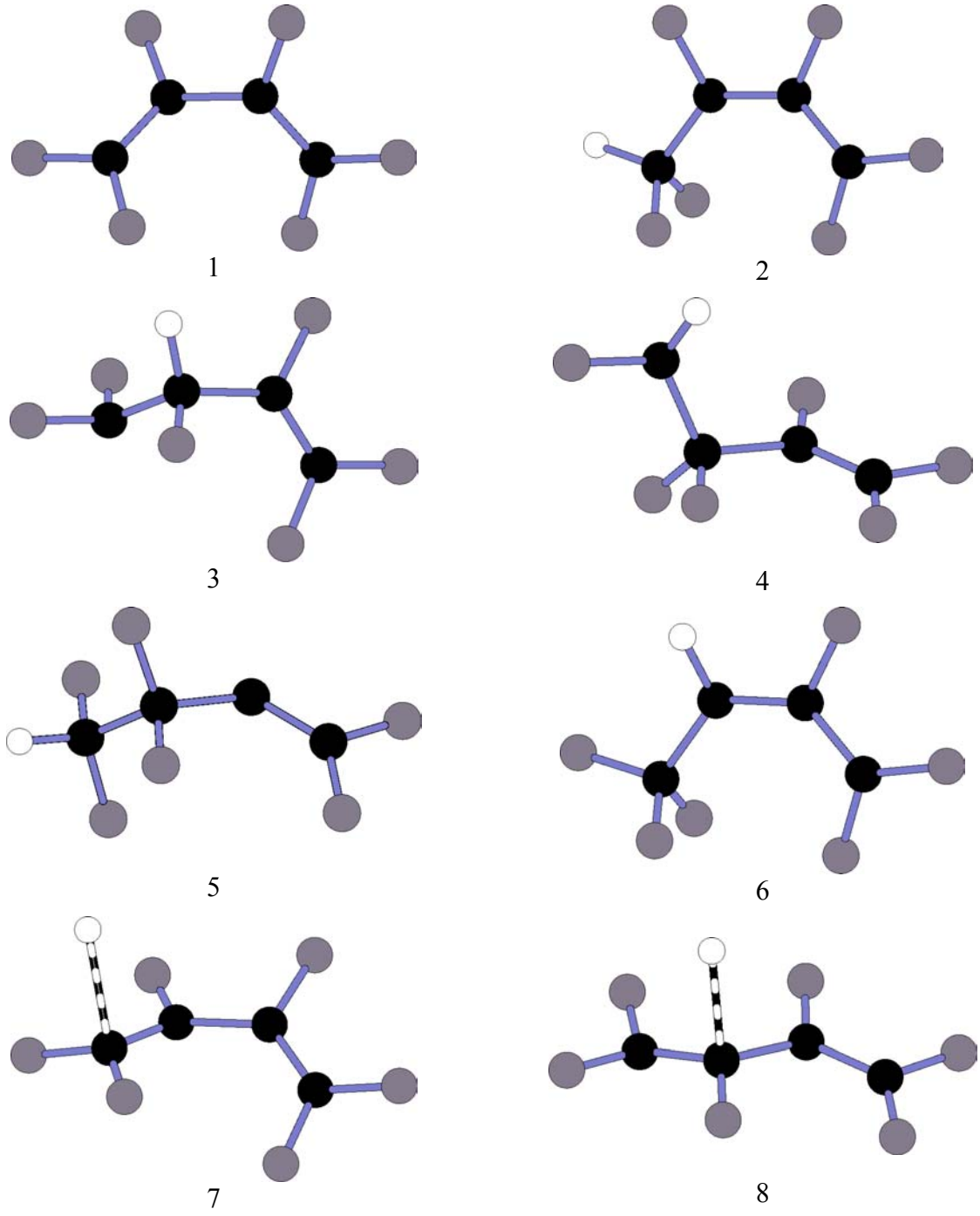

Fig. 5.3. Geometries for C_4F_6, five C_4F_6H isomers and two transition states for H + C_4F_6 addition, calculated at the HF/6-31G(d) level of theory. **1** C_4F_6; **2** CF_2H-CF•-$CF=CF_2$; **3** •CF_2-CFH-$CF=CF_2$; **4** •CFH-CF_2-$CF=CF_2$; **5** CF_2H-CF_2-C•=CF_2; **6** CF_3-CH•-$CF=CF_2$; **7** H…CF_2-CF•-$CF=CF_2$ TS; **8** •CF_2-CF(…H)-$CF=CF_2$ TS

High temperature regime, T > 700 K

As noted in the previous section, direct attack by H on a C-F bond seems unlikely. It is speculated that an addition-fragmentation mechanism may operate at high temperatures:

$$H + C_4F_6 \rightleftarrows \text{adduct} \rightarrow \text{fragments} \qquad (5.6)$$

where the overall observed rate constant, summarized by eq. 5.5, is the product of the concentration equilibrium constant for adduct formation K_c, equal to the ratio of forward and reverse rate constants, and the rate constant for adduct fragmentation, defined here as k_6. The nature of the fragments is unknown. It is noted that fission of the central C-C bond of the adduct in 5.1b would lead to the perfluorovinyl radical C_2F_3 and the stable trifluoroethylene molecule, C_2F_3H. Similarly, the adduct in 5.1a could lead to the same products if C-C fission is concerted with a 1,2 hydrogen atom shift. Combination of $\Delta_f H_{298}$ for these two fragments, -220[3] and –474 ± 8.4 kJ mol^{-1},[4] respectively, with $\Delta_f H_{298}(H)$ = 218 kJ mol^{-1} and $\Delta_f H_{298}(C_4F_6)$ = -942 kJ mol^{-1}, [4] yields an overall reaction enthalpy for reaction 5.6 of ΔH_{298} = 30 kJ mol^{-1}. This endothermicity compares well with the measured activation energy of 34 kJ mol^{-1}, although there is considerable uncertainty in ΔH_{298}, which is guessed to be at least 20 kJ mol^{-1}. The accord does not mean the fragments are uniquely identified, but indicates that the general scheme of eq. 5.6 is plausible. Analogous products, with F replaced by H, were proposed for the high-temperature reaction of H with butadiene by Benson and Haugh.[5]

Intermediate temperature regime, 620 K < T < 700 K

We suggest that the abrupt drop in the overall rate constant $k_{5.1}$ is caused by adduct formation coming to equilibrium. As the temperature is raised close to the point where H-atom addition becomes thermodynamically unfavorable, only the most stable adduct in 5.1a will be formed. Isomer in 5.1b will dissociate more quickly and not contribute to net loss of H atoms here. The rate constant k_{-1a} for the endothermic dissociation of the adduct in 5.1a has a large activation energy, so that at slightly higher temperatures the reverse of 1a becomes significantly faster and H is no longer consumed via channel 5.1a. Over a narrow temperature range both adduct formation and dissociation are comparable. Over this range it is considered the following mechanism quantitatively:

$H + CF_2{=}CF\text{-}CF{=}CF_2 \rightarrow$ adduct	k_{1a}
adduct $\rightarrow H + CF_2{=}CF\text{-}CF{=}CF_2$	k_{-1a}
adduct $\rightarrow$ products (excluding H)	k_6
$H \rightarrow$ loss	k_{diff5}

Solution of the rate equations via the Laplace transform method[6] yields

$$[H] = [H]_0 \frac{(k_{-1a} + k_6 + \lambda_1)e^{\lambda_1 t} - (k_{-1a} + k_6 + \lambda_2)e^{\lambda_2 t}}{\lambda_1 - \lambda_2} \qquad (5.7)$$

where

$$\lambda_{1,2} = \frac{-(k_{1a}[C_4F_6] + k_{-1a} + k_6 + k_{diff5}) \pm \sqrt{(k_{1a}[C_4F_6] + k_{diff5} - k_{-1a} - k_6)^2 + 4k_{1a}k_{-1a}[C_4F_6]}}{2} \qquad (5.8)$$

Fluorescence decays were again fit to the form of eq. 5.3, where now [H] is described by eq. 5.7-5.9. There are only three variables to be adjusted in this fitting: A, B and k_{-1a}, and

these were varied directly to minimize the root mean square deviations between observed decays and eq. 5.7. An example is shown as the inset of Fig. 5.4, and we were intrigued to see how an apparently exponential decay could be equally well represented as a biexponential, eq. 5.7. The other parameters were found as follows. k_{1a} was obtained via

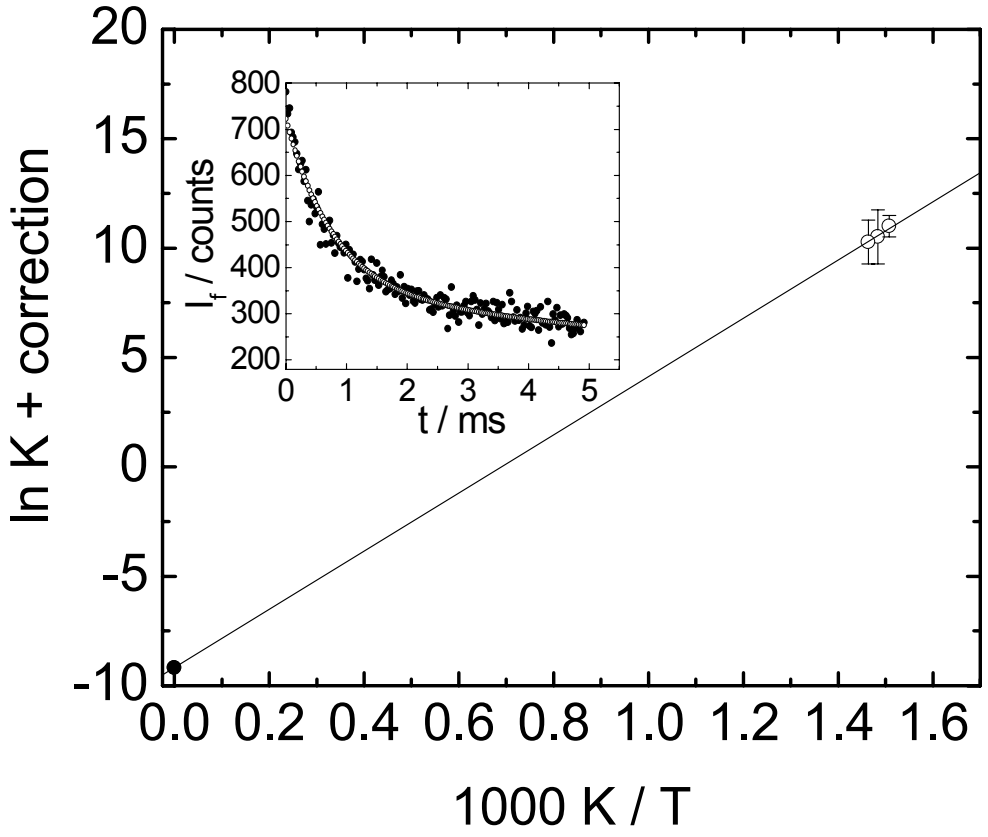

Fig. 5.4. Van't Hoff plot for addition of H to C_4F_6. The intercept is constrained to the statistical mechanical value of $\Delta S_{298}/R$ (see text). The inset shows a typical fluorescence decay obtained at 674 K together with a biexponential fit (see text, eq. 5.7).

a short upward extrapolation of eq. 5.4 while k_6 was derived from a short downward extrapolation of eq. 5.5, coupled with application of the scheme shown in eq. 5.6, i.e., $k_{5.1}$(T) for T > 700 K $= K_c k_6$, so that

$$k_6 = \frac{k_{5.1}(T; T > 700\text{K}) k_{-1a}}{k_{1a}} \tag{5.9}$$

k_{diff5} was obtained from decays with zero reactant concentration.

The results of this kinetic analysis are summarized in Table 5.3. The concentration equilibrium constant for adduct formation K_c equals k_{1a}/k_{-1a}, and from this we calculated the equilibrium constant K, which is dimensionless and is defined relative to a standard state of unit activity for 10^5 Pa. The temperature variation of K contains thermochemical information. Because of the short temperature range we employ a "third-law" analysis, illustrated in Fig. 5.4. This is a van't Hoff plot where the intercept is fixed at the statistical mechanical value of ΔS_{298}/R for channel 5.1a. Statistical mechanics were also employed to derive the temperature variation of ΔS and ΔH, to obtain the correction added to ln K in Fig. 5.4, equal to about 0.4:

$$\ln K + \text{correction} = \Delta S_{298}/\text{R} - \Delta H_{298}/\text{RT} \tag{5.10}$$

where

$$\text{correction} = -(\Delta S_T - \Delta S_{298})/\text{R} + (\Delta H_T - \Delta H_{298})/\text{RT} \tag{5.11}$$

The slope of Fig. 5.4 yields ΔH_{298} = -111 kJ mol^{-1} for reaction 5.1a, with an estimated uncertainty of ± 7 kJ mol^{-1} based on the 2σ error bars for ln K. This is minus the bond dissociation enthalpy (BDE_{298}) for the adduct and, for comparison, the BDE_{298} in the ethyl radical is 150.2 ± 0.9 kJ mol^{-1}.[7] Apparently the electronegative substituents in the

perfluorobutadiene system destabilize the radical adduct and/or the limited conjugation between the two π bonds in the reactant is lost upon addition of an H atom. The conjugation in C_4F_6 is only partial because the lowest energy configuration is non-planar: steric repulsions between the terminal CF_2 groups lead to a dihedral angle along the carbon backbone of 53º rather than zero.

Table 5.2. Thermochemical information for adduct formation between H and C_4F_6

T, K	Number of decays	K_c[a] ± $\sigma_{Kc,}$ 10^{-15} cm^3 $molecule^{-1}$	Ln K[b] ± $\sigma_{ln\ K,}$ 10^4
663	8	3.85 ± 0.84	10.62 ± 0.24
674	8	2.77 ± 1.44	10.13 ± 0.62
683	12	2.10 ± 1.11	9.88 ± 0.50

[a]Mean and standard deviation of K_c

[b]Mean and standard deviation of ln K

It should be stressed that the above analysis depends on the correctness of the assumed mechanism. Sato and coworkers have drawn attention to the facile 1,2 migration of F atoms in chemically activated fluoroethyl radicals.[8,9] If such processes occur in the present system then three further isomers of C_4F_6H would be accessible, and geometries of **4**, **5**, and **6** are shown in Fig. 5.3. According to the results of theoretical calculation,[2] **4** and **5** are less stable than **2** and **3** and therefore are not important, and that isomer **6** is the most stable of all. The greater density of states in the larger systems studied here will tend to make such isomerization less important, but we cannot rule it out completely.

D. 1,2-H Atom Migration in Fluorinated Ethyl Radicals

1,2-halogen atom migration in β-substituted ethyl radicals has been the subject of extensive experimental[10-14] and theoretical[15-23] studies, and led to a good understanding of structure and activation energy. However, 1.2-hydrogen atom migration in halogenoethyl radicals is known little. In the Sato and coworkers' work about 1,2-Fluorine atom migration in 1,2-difluoroethyl and 1,1,2-trifluoroethyl radicals,[9] they mentioned that hydrogen atom migrated through a hydrogen atom bridging intermediate, and more easily in the less fluorinated ethyl radical. Since their results were obtained by the INDO (Intermediate Neglect of Differential Overlap, a semi-empirical computational method) calculations, the absolute barrier value was not reliable, as they already pointed out in the paper. Also they did not prove that the hydrogen atom bridging intermediate was a true transition state in their work. An additional investigation, 1,2-H atom migration in ethyl radical and fluorinated ethyl radicals was made using ab initio quantum mechanics here.

All calculations were performed using the GAUSSIAN 94 program package.[24] Initial geometries of open and bridged structures of ethyl radical and fluorinated ethyl radicals were obtained by the semi-empirical computational methods, AM1 (Austin Model 1) and PM3 (Parametric Model 3). They were optimized at the HF/3-21G(d), HF/6-31G(d), HF/6-31G(d,p) and MP2/6-31G(d,p) levels of theory. The single point energies and harmonic vibrational frequencies of optimized structures were evaluated at the same levels. The bridged structures of the radicals were optimized as transition states. At each level, to examine whether the obtained transition state was the right one or not,

the normal modes of the vibrational frequencies were checked by the GaussView program.[25] And, both directions' IRC jobs were performed at HF/6-31G(d), HF/6-31G(d,p) and MP2/6-31G(d,p) levels of theory corresponding to each optimized transition state structure.

Table 5.3 shows the open and bridged structures of ethyl and fluorinated ethyl radicals ($C_2H_{(5-n)}F_n\bullet$, n=1,2,3,4). The open structure of the CH_2F-$CHF\bullet$ radical has a gauche conformation. However, the bridged structure of the CH_2F-$CHF\bullet$ radical has trans- and cis- conformations. The optimized geometries calculated at the four different theoretical levels mentioned previously and the harmonic frequencies calculated at the corresponding optimized geometries are presented in Appendix Table 8.2. Only one imaginary frequency was found for each transition state (bridged structure). When checked by GaussView, the H atom shifted between two carbon atoms, and the IRC job produced two structures of the corresponding radicals. For example, for TS $(CH_2...H...CHF)\bullet$, the IRC job gave the structure of CH_3-$CHF\bullet$ radical at one direction of the reaction path, and the structure of CH_2F-$CH_2\bullet$ radical at the other direction of the reaction path. These calculations confirm that the bridging intermediate through which H atom migrates in the fluoroethyl radicals is a reliable transition state.

The calculated total energies of each radical and barrier height at various theory levels are presented in Table 5.4. All methods give somewhat similar overall descriptions of the various fluoroethyl radicals: the barrier of 1,2-H atom migration is higher in the more fluorinated ethyl radical. This result agrees with the expectation of Sato et al. For the substituted ethyl radicals which have same fluorine atoms number, the ones in which

more fluorine atoms are connected to the unsaturated carbon have lower total energies than others in which more hydrogen atoms are connected to the unsaturated carbon. To explain this, more investigations are needed. An accurate result should be carried out by some higher level calculations. A G3 or G3 (MP2) calculation will be preferred in the future work.

Table 5.3. Structures of ethyl radical, fluoroethyl radicals, and transition states for the 1,2-hydrogen atom migration [a]

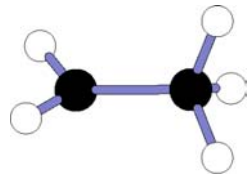	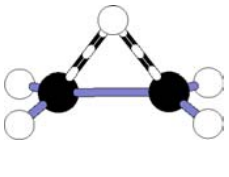	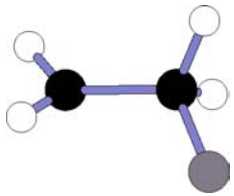	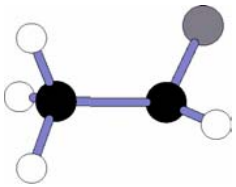	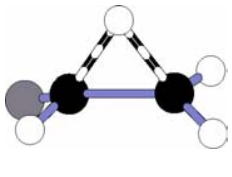	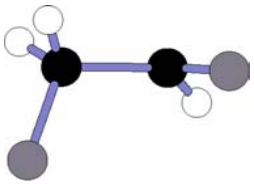
CH_3-CH_2•	TS (CH_2...H...CH_2)•	CH_2F-CH_2•	CH_3-CHF•	TS (CH_2...H...CHF)•	CH_2F-CHF•
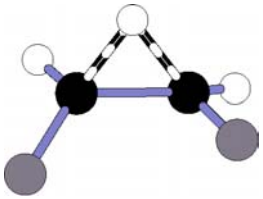	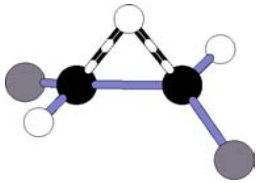	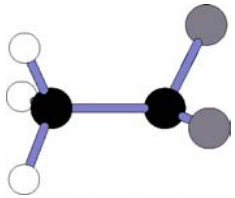	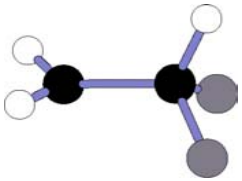	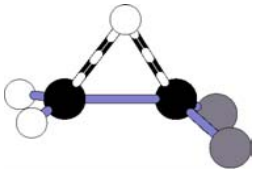	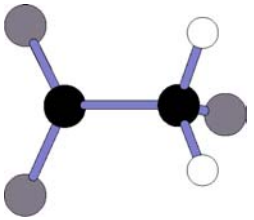
TS cis-(CHF...H...CHF)•	TS trans-(CHF...H...CHF)•	CH_3-CF_2•	CHF_2-CH_2•	TS (CH_2...H...CF_2)•	CH_2F-CF_2•
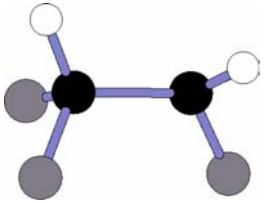	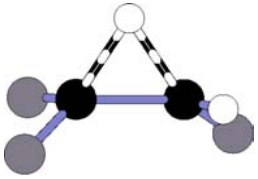	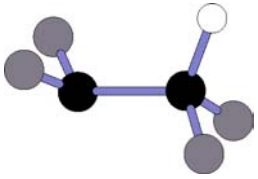	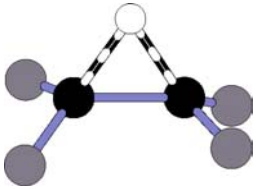		
CF_2H-CHF•	TS (CF_2...H...CHF)•	CF_2-CF_2•	TS (CF_2...H...CF_2)•		

[a] Black circle: carbon atom; gray circle: fluorine atom; empty circle: hydrogen atom

Table 5.4. Total energy of ethyl radical, fluoroethyl radicals and TSs, and barrier heights for the 1,2-hydrogen atom migration at various levels of theory [a]

Ethyl Radical

Method	TS (CH_2...H...CH_2)•	CH_3-CH_2•	ΔE
HF/3-21G(d)	-78.0658723	-78.1636468	256.7
HF/6-31G(d)	-78.505312	-78.5971488	241.1
HF/6-31G(d, p)	-78.516597	-78.6055251	233.5
MP2/6-31G(d, p)	-78.800573	-78.8758875	197.7

Monofluoroethyl Radical

Method	TS (CH_2...H...CHF)•	CH_2F-CH_2•	CH_3-CHF•	ΔE
HF/3-21G(d)	-176.3748227	-176.47583	-176.4819556	265.1
HF/6-31G(d)	-177.3466167	-177.44315	-177.4478771	253.5
HF/6-31G(d, p)	-177.3566815	-177.45018	-177.4547363	245.5
MP2/6-31G(d, p)	-177.800995	-177.87866	-177.8866668	203.9

1,1-Difluoroethyl Radical

Method	TS (CH_2...H...CF_2)•	CHF_2-CH_2•	CH_3-CF_2•	ΔE
HF/3-21G(d)	-274.6993933	-274.80731	-274.8143992	283.3
HF/6-31G(d)	-276.2032209	-276.30802	-276.312752	275.2
HF/6-31G(d, p)	-276.2113433	-276.31339	-276.3177472	267.9
MP2/6-31G(d, p)	-276.8159811	-276.90212	-276.9115141	226.2

1,2-Difluoroethyl Radical

Method	TS cis-(CHF...H...CHF)•	CH_2F-CHF•	ΔE
HF/3-21G(d)	-274.6729903	-274.7899193	307.0
HF/6-31G(d)	-276.1795284	-276.2907903	292.1
HF/6-31G(d, p)	-276.1883419	-276.2962018	283.2
MP2/6-31G(d, p)	-276.7930724	-276.8871306	247.0

Table 5.4. Total energy of ethyl radical, fluoroethyl radicals and TSs, and barrier heights for the 1,2-hydrogen atom migration at various levels of theory [a] (contd.)

Method	TS trans-(CHF...H...CHF)•	CH_2F-CHF•	ΔE
HF/3-21G(d)	-274.6830115	-274.7899193	280.7
HF/6-31G(d)	-276.1870726	-276.2907903	272.3
HF/6-31G(d, p)	-276.1957294	-276.2962018	263.8
MP2/6-31G(d, p)	-276.8020452	-276.8871306	223.4

Trifluoroethyl Radical

Method	TS (CF_2...H...CHF)•	CF_2H-CHF•	CH_2F-CF_2•	ΔE
HF/3-21G(d)	-372.9977185	-373.1135145	-373.11545	304.0
HF/6-31G(d)	-375.0360591	-375.150333	-375.15097	300.0
HF/6-31G(d, p)	-375.0428169	-375.1540725	-375.15444	292.1
MP2/6-31G(d, p)	-375.8088692	-375.9055415	-375.90733	253.8

Tetrafluoroethyl Radical

Method	TS (CF_2...H...CF_2)•	CF_2-CF_2•	ΔE
HF/3-21G(d)	-471.43881	-471.3100683	338.0
HF/6-31G(d)	-474.0109866	-473.8840779	333.2
HF/6-31G(d, p)	-474.0127594	-473.8887631	325.6
MP2/6-31G(d, p)	-474.9257307	-474.8138933	293.6

[a] Total energy in hartree and barrier height in kJ/mol

REFERENCE

(1) Berry, R. J.; Ehlers, C. J.; Burgess, D. R., Jr.; Zachariah, M. R.; Marshall, P. *Chem. Phys. Lett.* **1997**, *269*, 107.

(2) Hu, X.; Goumri, A.; Marshall, P. *J. Phys. Chem.* **2001**, *in press*.

(3) Haworth, N. L.; Smith, M. H.; B., b. G.; Mackie, J. C. *J. Phys. Chem. A* **2000**, *104*, 7600.

(4) Afeefy, H. Y.; Liebman, J. F.; Stein, S. E. Neutral Thermochemical Dara. In *NIST Chemistry WebBook, NIST Standard Reference Datrabase Number 69*; Mallard, W. G., Linstrom, P. J., Eds.; NIST: Gaithersburg, MD, 2000.

(5) Benson, S. W.; Haugen, G. R. *J. Phys. Chem.* **1967**, *71*, 1735.

(6) Steinfeld, J. I.; Francisco, J. S.; Hase., W. L. *Chemical Kinetics and Dynamics*; Prentice Hall: Englewood Cliffs, NJ, 1989.

(7) Brouard, M.; Lightfoot, P. D.; Pilling, M. J. *J. Phys. Chem.* **1986**, *90*, 445.

(8) Kohida, T.; Kotaka, M.; Sato, S.; Ishida, T.; Yamamoto, K.; Yamazaki, T.; Kitazume, T. *Bull. Chem. Soc. Jpn.* **1987**, *60*, 3131.

(9) Kotaka, M. S., S. Shimokoshi, K. *J. Fluorine Chem.* **1987**, *37*, 387.

(10) Chen, K. S.; Elson, I. H.; Kochi, J. K. *J. Am. Chem. Soc.* **1973**, *95*, 5341.

(11) Edge, D. J.; Kochi, J. K. *J. Am. Chem. Soc.* **1972**, *94*, 6485.

(12) Farrar, J. M.; Lee, Y. T. *J. Chem. Phys.* **1976**, *65*, 1414.

(13) Jacox, M. E. *Chem. Phys.* **1981**, *58*, 289.

(14) Kawamura, T.; Edge, D. J.; Kochi, J. K. *J. Am. Chem. Soc.* **1972**, *94*, 1752.

(15) Hoffmann, R.; Radom, L.; Pople, J. A.; Schleyer, P. V. R.; Hehre, W. J.; Salem, L. *J. Am. Chem. Soc.* **1972**, *94*, 6221.

(16) Schlegel, H. B. *J. Phys. Chem.* **1982**, *86*, 4678.

(17) Schlegel, H. B.; Sosa, C. *J. Phys. Chem.* **1984**, *88*, 1141.

(18) Hoz, T.; Sprecher, M.; Basch, H. *J. Phys. Chem.* **1985**, *89*, 1664.

(19) Guerra, M. *J. Am. Chem. Soc.* **1992**, *114*, 2077.

(20) Engel, B.; Peyerimhoff, D. D. *J. Phys. Chem.* **1989**, *93*, 4462.

(21) Kato, S.; Morokuma, K. *J. Chem. Phys.* **1980**, *72*, 206.

(22) Chen, Y.; Rauk, A.; Tschuikow-Roux, E. *J. Chem. Phys.* **1990**, *93*, 6620.

(23) Ihee, H.; Zewail, A. H.; Goddard III, W. A. *J. Phys. Chem. A* **1999**, *103*, 6638.

(24) Frisch, M. J.; Trucks, G. W.; Schlegel, H. B.; Gill, P. M. W.; Johnson, B. G.; Robb, M. A.; Cheeseman, J. R.; Keith, T. A.; Petersson, G. A.; Montgomer, J. A.; Raghavachari, K.; Al-Laham, M. A.; Zakrzewski, V. G.; Ortiz, J. V.; Foresman, J. B.; Cioslowski, J.; Stefanov, B. B.; Nanayakkara, A.; Challacombe, M.; Peng, C. Y.; Ayala, P. Y.; Chen, W.; Wong, W.; Andres, J. L.; Replogle, E. S.; Gomperts, R.; Martin, R. L.; Fox, D. J.; Binkley, J. S.; Defrees, D. J.; Baker, J.; Stewart, J. P.; Head-Gordon, M.; Gonzalez, C.; Pople, J. A. Gaussina 94 (Revision D.2); Gaussian, Inc.: Pittsburgh, PA, 1995.

(25) GaussView; 2.0 ed.; Gaussian, Inc.: Pittsburgh, PA, 1998.

CHAPTER 6

COMPUTATIONAL STUDIES OF OH + CHLOROETHYLENES

As stated in Chapter One, the wide use of chloroethylenes in industry results in the release of these hazardous compounds into the atmosphere at significant rates. High-temperature incineration is considered to be the best available technology for the complete and permanent disposal of these toxic materials. The reaction with hydroxyl radicals is an important process contributing to the initial destruction halogenated hydrocarbons under both atmospheric and combustion conditions.[1,2]

Since the importance of the reaction of OH radicals with chloroethylenes both in natural and planned decomposition, the knowledge of the reaction rate constants and mechanisms over an extended temperature range is necessary. However, previous measurements were limited to low temperatures.[3-11] and few theoretical studies were reported.[12,13]

In 1997, Villà and González-Lafont developed an approach for theoretically studying the fast addition reaction of hydroxyl radical with ethylene.[14] In their work, the reaction coordinate for addition of OH to the C = C bond was defined as a distinguished coordinate pathway (DCP) at the MP4sdq(fc)/6-311+G(d,p) level, since it had been found the C – O bond was the most significant varying parameter along the reaction path in the transition state region. The DCP was defined as the sequence of minimum energy structures at various fixed C – O separations, which were optimized also at the

MP4sdq(fc)/6-311+G(d,p) level. At each of these geometries, the frequencies at the MP2(full)/6-311+G(d,p) were calculated. Then the energy of system was computed at the spin-projected PMP4sdtq/6-311+G(d,p) level of theory. They found this approach provided a very good agreement with experiment measurements. However, there were two mistakes found in this work: 1. a wrong degeneracy of reaction path was used in the calculation; 2. the computational results are based on the assumption that the reaction is high-pressure-limit, in which the rate constant is independent of the pressure. In fact, at high temperatures, this is a pressure-dependent reaction.[15] Nevertheless, their work provided an example of the application of the variational transition state theory (VTST) to a fast radical addition reaction to π bonds. These kinds of reactions, in general, present low or negative activation energies (see Fig. 6.1-b). In contrast to the reactions with positive activation energies, the rate constants of the reactions with negative barriers present a negative temperature dependence.

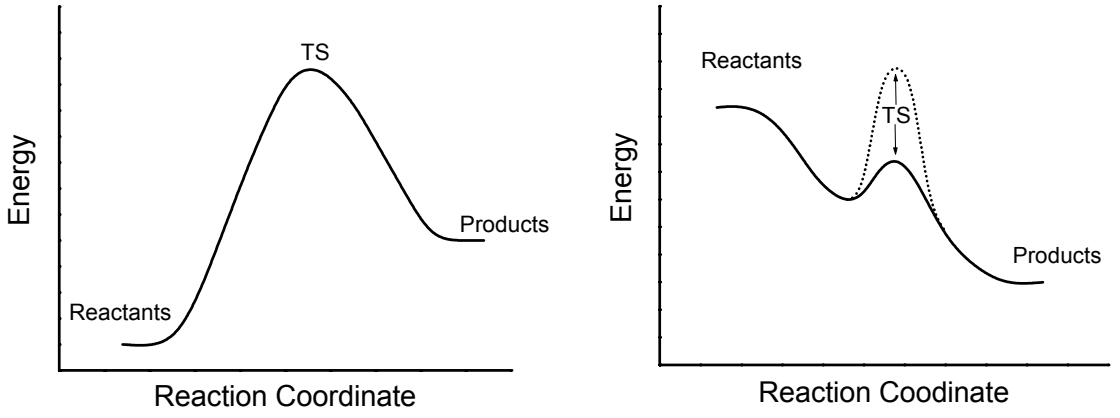

a b

Fig. 6.1. Schematic diagram of the potential energy surface of the reactions with: a. positive barrier; b. negative barrier

The purpose of current study is to modify the Villà and González-Lafont's approach in order to decrease the cost for obtaining initial information, such as optimized geometries and frequencies, so as to apply it to theoretical calculations of the whole set of reactions of OH with chloroethylenes for further investigation of reaction mechanisms.

A. Computational Methodology

All the ab initio calculations were performed using the GAUSSIAN 94 program package.[16] VTST was employed for the kinetic calculations. Part of ab initio and VTST calculations for C_2H_4, C_2Cl_4 and C_2HCl_3 were contributed by Dr. Jingping Peng. The VTST calculations were carried out as follows. First the reaction path was defined. The geometry of each point along with the reaction path was optimized, and frequencies were obtained at the same level. Then energies were calculated at a spin-projected level, relative to reactants. (In open shell unrestricted calculations, the wave functions are not the eigenfunctions of the operators for S^2 and S_z. If they are expanded in terms of pure spin wave functions, contamination from higher spin states is included besides the desired spin state. Normally the spin contamination is small enough to be ignored. However, when a single bond is stretched toward breaking, or a π bond is twisted to a perpendicular conformation, the spin contamination will be large so that the shape of the potential energy surface can be distorted. Since transition states are likely to have elongated bonds, twisted π systems, or delocalized unpaired electrons, they are easy to have a big spin contamination. Spin contamination can be eliminated by the treatment of spin projection. In this work, the transition states have significant large contamination.

For example, at the HF/6-31G(d,p) level of theory, S^2 values of CH_2-CHCl...OH, CCl_2-CHCl...OH and CH_2-CH_2...OH are 1.0505, 1.0868 and 1.0101, respectively. They are obviously larger than the standard value 0.75. Thus, the spin projection is necessary to be applied in this work.) These energies, geometries and frequencies were used to derive conventional TST rate constants as a function of position along the reaction path by using POLYRATE 8.0 program package.[17] At each temperature, the VTST result was obtained by interpolation to find the minimum rate constant. Temperatures were up to 1000 K.

OH + C_2H_4

The structure of transition state (TS) of OH + C_2H_4 reaction was optimized at the HF/3-21G(d), HF/6-31G(d,p), HF/6-311G(d,p), MP2/6-31G(d,p), MP2/6-311G(d,p) and QCISD/6-31G(d,p) levels. The harmonic vibrational frequencies of optimized TS structures were calculated at same levels. The reaction path was defined by the intrinsic reaction coordinate (IRC) based on the optimized TS geometry at each level. IRC is a method used in the GAUSSIAN 94 program, which requests that a reaction path be followed.[18,19] The TS geometry is used as the initial geometry, and from that point, one or both directions can be followed. At each point along the reaction path, the geometry is optimized.

OH + $C_2H_{(4-X)}Cl_x$ (x=1, 2, 3)

The structures of species OH, $C_2H_{(4-X)}Cl_x$ (x=1, 2, 3) and TS of reaction of OH + $C_2H_{(4-X)}Cl_x$(x=1, 2, 3) were optimized at the HF/6-31G(d,p) level. The harmonic

vibrational frequencies of optimized structures were calculated at the same level scaled by 0.9011, which was obtained by plotting observed fundamental of OH,[20] C_2H_4[20] and C_2Cl_4[20] versus the calculated frequencies. The reaction path was defined by IRC based on the optimized TS geometry using HF/6-31G(d,p). The projected frequencies (the imaginary frequency was projected by using special keyword, IOP(7/45=1), in the GAUSSIAN 94 job) of each point along the reaction path were computed by the same level and scaled by 0.9011 too. The reaction barrier height at each point $E_0^{\neq}$ (excluding zero point energy correction) was evaluated at the PMP4/6-311+G(d,p) level based on the optimized geometry obtained by IRC, relative to reactants.

OH + C_2Cl_4

Conventional TST calculations was used for this reaction because of the presence of a small but distinct barrier to the initial addition of OH to the C=C bond. The structures of species OH, C_2Cl_4 and the TS of reaction of OH + C_2Cl_4 were optimized at the HF/6-31G(d) level. The vibrational frequencies of optimized structures were calculated at the same level scaled by 0.8929.[21] The energies were evaluated using G3[22] and G3(mp2)[23] theories. Energy calculations were estimated using the reactants as the basis for the relative total energy difference. Both G3 and G3(mp2) methods use the HF/6-31G(d) level to calculate frequencies and the MP2(full)/6-31G(d) level to optimize the geometry. The G3 method then uses the total energy calculated by QCISD(T)/6-31G(d), MP4/6-31G(d), MP4/6-31+G(d), MP4/6-31G(2df,p) and MP2(full)/G3large for the higher energy correction. G3(mp2) uses QCISD(T)/6-31G(d) and

MP2(fc)/G3MP2large for the higher energy correction. The G3large basis set is a modified 6-311+G(3df,2p) basis set and has a better balance of polarization functions than the original 6-311+G(3df,2p) basis set. It also includes core polarization functions. G3MP2large basis set is the same as the G3large basis set, except that core polarization functions are not included.[23]

B. Results and Discussion

OH + C_2H_4

Figure 6.2 is the comparison of two methods defining the reaction path, IRC and DCP, at HF/6-31G(d,p), MP2/6-31G(d,p), MP4sdq(fc)/6-311+G(d,p) and QCISD/6-31G(d,p) levels. In the range of the C – O distance between 1.95 and 2.24 Å, which is in the transition state region, there is no significant difference between IRC and DCP. Figure 6.3 is the results of IRC at HF/3-21G(d), HF/6-31G(d,p), HF/6-311G(d,p), MP2/6-31G(d,p), MP2/6-311G(d,p), QCISD/6-31G(d,p) levels and DCP at MP4sdq(fc)/6-311+G(d,p) level used by Villà and González-Lafont. Clearly, in the transition state region, at the highest level, QCISD/6-31g(d,p), C – C distance is closer and closer to the corresponding value in ethylene as the C – O distance increases. It is accurate but expensive too. The results of MP2 jobs evidently deviate from the results of QCISD job and DCP job. They are not good to be used to modify Villà and González-Lafont's approach. The HF jobs almost repeat the path of QCISD, their results are closer to the result of DCP compared with those at the QCISD and MP2 levels, and they are much cheaper. Therefore, the HF/6-31G(d,p) level was used in the geometry optimization and

frequency calculation in the following studies as a replacement in the Villà and González-Lafont's approach (except in the reaction OH + C_2Cl_4). Table 6.1 is the optimized geometrical parameters of reactants and TS of the reaction OH + C_2H_4 at the HF/6-31G(d,p) level. Figure 6.4 is the optimized TS structure at the same level.

OH + C_2H_3Cl

There have been several experimental investigations of the rate coefficient and the mechanism of this reaction since 1976.[3,4,24-26] The following reactions can be used to describe the mechanism for the initial stages of this reaction:

$$OH + CH_2{=}CHCl \rightarrow HOC_2H_3Cl\bullet \quad (6.1)$$

$$HOC_2H_3Cl\bullet \rightarrow OH + CH_2{=}CHCl \quad (6.2)$$

$$HOC_2H_3Cl\bullet + M \rightarrow HOC_2H_3Cl + M \quad (6.3)$$

The reaction of the elimination of a Cl atom can compete with the reaction 6.2:

$$HOC_2H_3Cl\bullet \rightarrow CH_2{=}CHOH + Cl \quad (6.4)$$

These prior measurements and modeling observations suggested that at room temperature and moderate pressures, the reactions 6.1, 6.2 and 6.3 were dominant, and Cl elimination was but a minor component. For explaining this behavior, two possible mechanisms were suggested.[4,25,27] One is that the OH radical addition only occurs at the CH_2 end (β site) and the rate-determining step is OH 1,2-migration. The other is that the OH addition occurs at both ends (α and β sites), but β site is main position, and the OH 1,2-migration is slow enough to be negligible. The elimination plays a minor role in this reaction because only when the OH adds at α site, it can directly proceed. High level theoretical

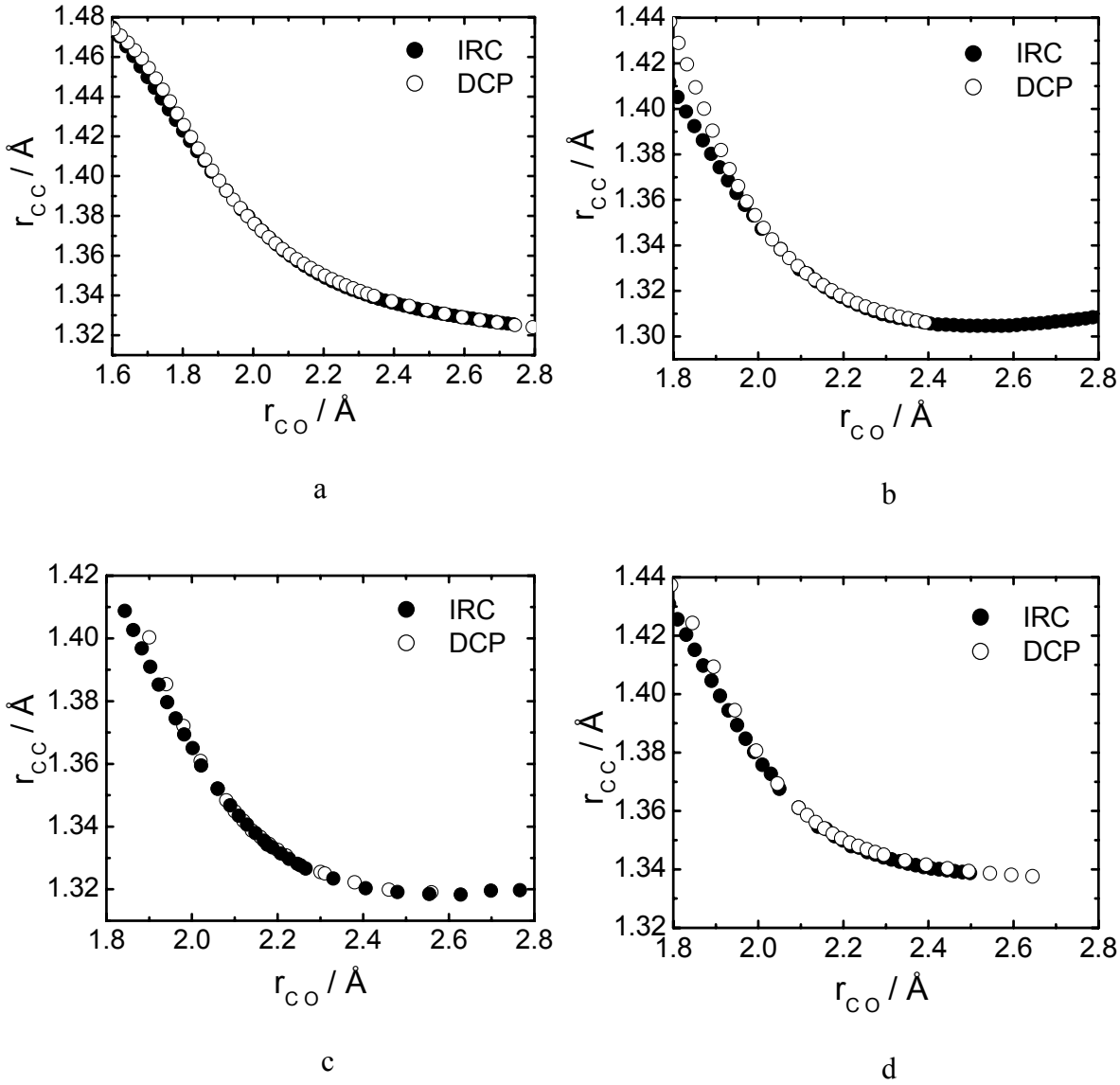

Fig. 6.2. Comparison between IRC and DCP of the reaction OH with C_2H_4 at different theory levels: a. HF/6-31G(d,p); b. MP2/6-31G(d,p); c. MP4sdq(fc)/6-311+G(d,p); d. QCISD/6-31G(d,p).

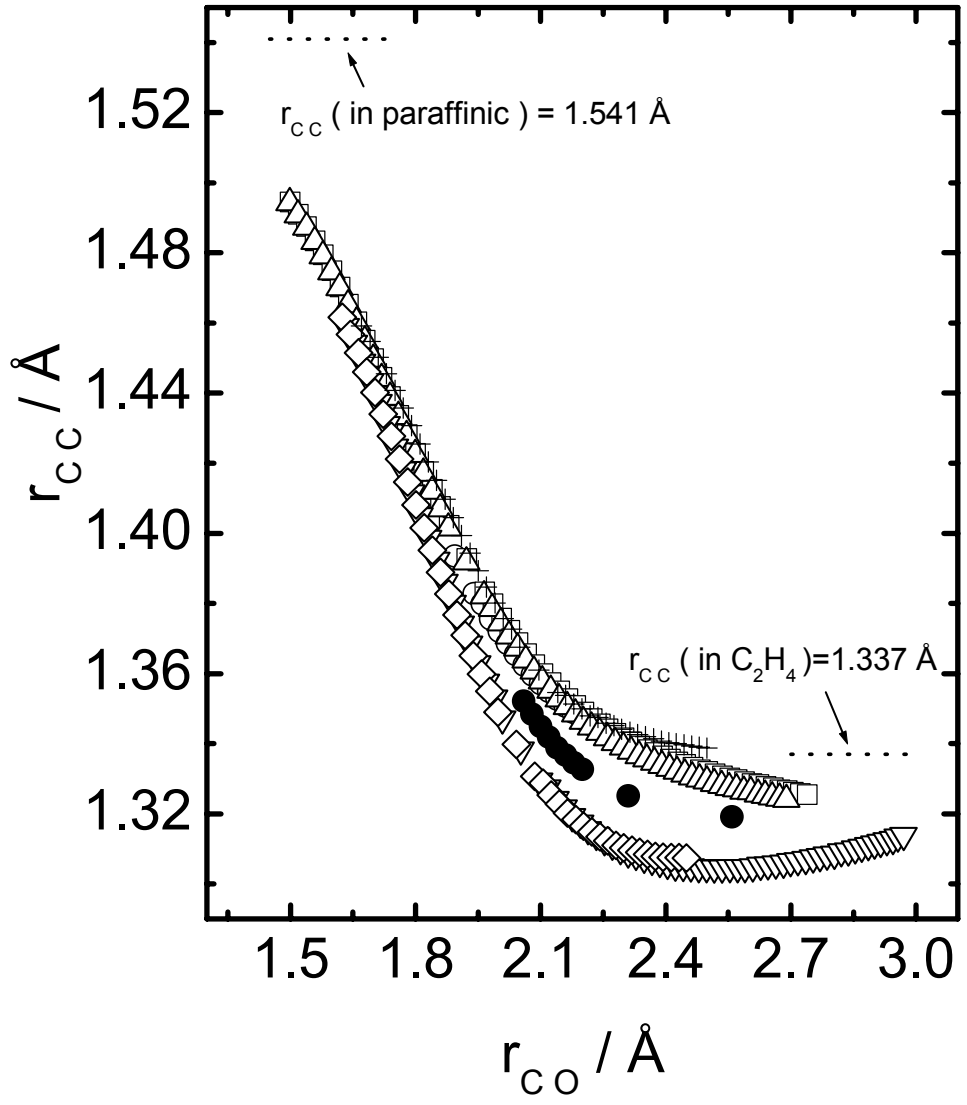

Fig. 6.3. Results of IRC at different levels and DCP at Mp4sdq(fc)/6-311+G(d,p) level (•) for the OH + C_2H_4 reaction. (O) HF/3-21G(d); (□) HF/6-31G(d,p); (Δ) HF/6-311G(d,p); (∇) MP2/6-31G(d,p); (◊) MP2/6-311G(d,p); (+) QCISD/6-31G(d,p); (**…**) experimental data, reference 28.

Fig. 6.4. Optimized TS structure of the reaction OH + C_2H_4 at the HF/6-31G(d,p) level.

Table 6.1. Optimized geometrical parameters[a] for reactants and transition state of the reaction OH + C_2H_4 at the HF/6-31G(d,p) level.

	a	b	c	d	e	f	g
OH			0.9549				
C_2H_4	1.317			1.077		1.077	
TS	1.393	1.924	0.9507	1.073	1.073	1.076	1.076

	ba	da	ea	fa	ga	cb
OH						
C_2H_4				121.8		
TS	106.0	119.1	119.1	121.1	121.1	100.7

	dab	eab	fab	gab	cba	daf
OH						
C_2H_4						180.0
TS	105.0	-103.9	86.07	-87.59	6.369	

[a] Refer to Figure 6.4 for definition of parameters: e.g. a = bond length (Å), ba = bond angle (degree), cba = dihedral angle (degree) between the plane containing bonds c, b and the plane containing bonds b, a

calculations are provided in present work for further verification of the reaction mechanism.[26]

The theoretical approach was described as above. The optimized geometries of reactants and TSs are shown in Fig. 6.5 and Table 6.2. As maybe seen from Fig. 6.6, for vinyl chloride, the barrier for β addition lies below the reactants' energy, whereas α addition requires overcoming a positive barrier.

The derived VTST rate constants are plotted in Fig. 6.7. The α channel has a simple positive temperature dependence. The β channel is more important at all temperatures and has a more complex behavior. The negative relative transition state energy implies a negative temperature dependence for the rate constant, an effect that dominates at low temperatures, whereas increases in temperature more rapidly increase the partition function of the loose TS as compared to the reactants, leading to a positive activation energy at higher temperatures. The calculated rate constants for OH addition to vinyl chloride are listed in Table 6.3.

OH + $C_2H_2Cl_2$

The reaction mechanism of OH + 1,1-dichloroethylene and 1,2-dichloroethylene is presumed to be addition to the π electrons associated with the C=C double bond, according to previous studies.[5-9] These prior measurements confirmed that secondary reaction involving Cl atoms was important for both substrates.[6,7] The chlorine atom deactivated the carbon, which it was attached on, toward OH attack while activating the

α site β site

Fig. 6.5. Optimized TS structures of the reaction OH + C_2H_3Cl at the HF/6-31G(d,p) level.

Table 6.2. Optimized geometrical parameters[a] for reactants and transition states of the reaction OH + C_2H_3Cl at the HF/6-31G(d,p) level.

	a	b	c	d	e	f	g
OH			0.9549				
C_2H_3Cl	1.311			1.737	1.072	1.075	1.074
TS 1 [b]	1.390	1.938	0.9517	1.756	1.070	1.074	1.074
TS 2 [c]	1.387	1.931	0.9513	1.733	1.071	1.073	1.073

	ba	da	ea	fa	ga	cb
OH						
C_2H_3Cl		123.3	123.9	119.5	122.4	
TS 1 [b]	103.5	117.6	121.8	119.2	121.3	98.27
TS 2 [c]	106.3	121.4	123.8	117.4	119.2	99.46

	dab	eab	fab	gab	cba	daf	eag	dag	eaf
OH									
C_2H_3Cl						180.0	180.0	0.0	0.0
TS 1 [b]	107.8	-107.8	85.48	-85.48	52.34				
TS 2 [c]	84.91	-84.91	104.9	-104.9	-42.79				

[a] Refer to Figure 6.5 for definition of parameters: e.g. a = bond length (Å), ba = bond angle (degree), cba = dihedral angle (degree) between the plane containing bonds c, b and the plane containing bonds b, a

[b] OH added at CHCl end (α site)

[c] OH added at CH_2 end (β site)

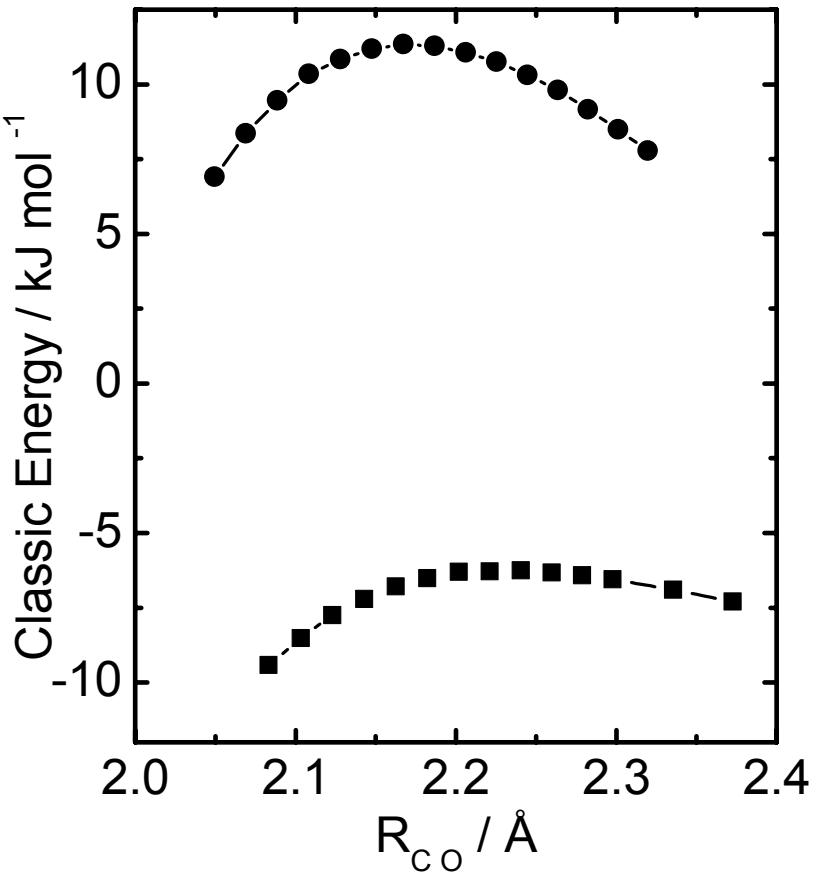

Fig. 6.6. Classical energies (no ZPE) relative to OH + CH_2=CHCl for addition of OH at the CH_2 end (β site, squares) and the CHCl end (α site, circles), calculated at the PMP4/6-311+G(d,p)//HF/6-31G(d,p) level of theory.

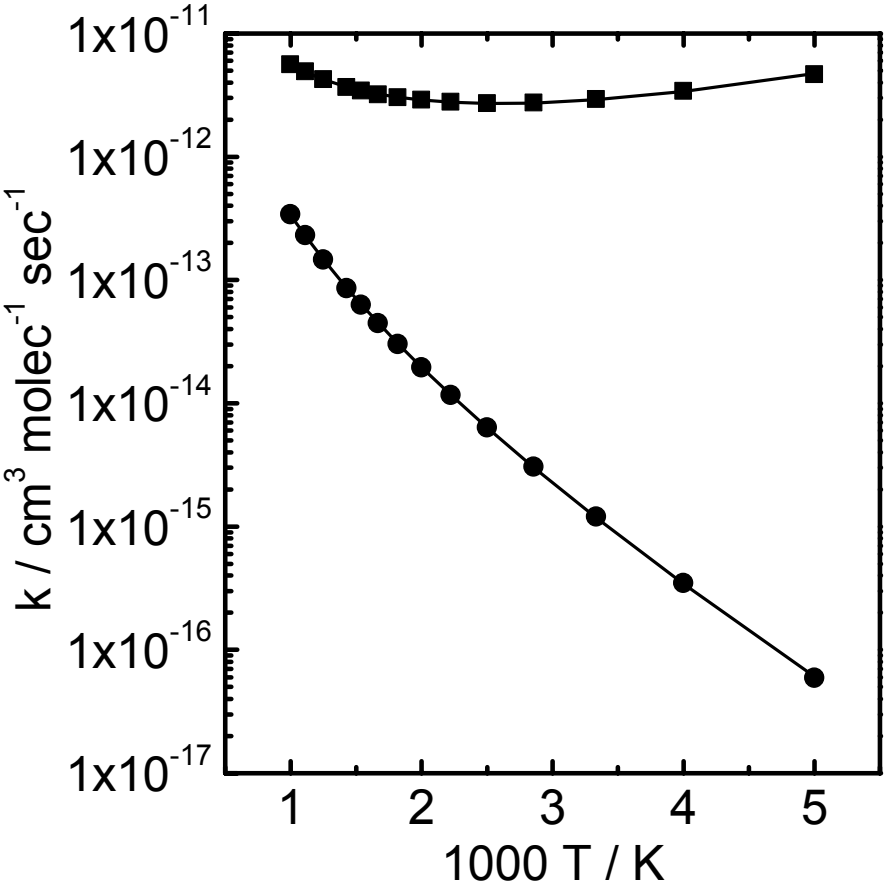

Fig. 6.7. Ab initio high-pressure limit rate constants for OH addition to CH_2=CHCl: square, β channel; circle, α channel).

Table 6.3. Rate constants for OH addition to vinyl chloride

	$k_{VTST} = B\ T^n\ e^{-E/RT}$ (cm^3 $molecule^{-1}$ s^{-1})
TS 1 (α site)	$1.00 \times 10^{-19}\ T^{2.350}\ \exp(-1209/T)$
TS 2 (β site)	$1.25 \times 10^{-18}\ T^{2.099}\ \exp(805/T)$

other one.[8] For the reaction of OH with 1,1-dichloroethylene at low temperatures, Cl elimination was insignificant compared with OH addition to the CH_2 side of the substrate.[5] And, it had been observed that the reactivity of the chloroethylenes was quite less than that of unsubstituted olefinic hydrocarbons.[9] This is reasonable when considered the fact that the highest occupied molecular orbital is composed of carbon-carbon π bonding and Cl atom lone-pair electrons contributions. There are greater nonbonding interactions in the transition state occurred in the OH with chloroethylene reactions than it does in the OH with alkene reactions, where the HOMO is pure carbon-carbon π bonding. The relative importance of the adduct stabilization, Cl elimination, and H abstraction of dichloroethylene is particularly interesting. The current work is to estimate thermodynamic properties of these reactions for further investigation in this field.[29]

VTST was performed to calculate the rate constant for OH addition to 1,1- and 1,2-dichloroethylene. The calculations were carried out as described as before. These VTST results correspond to the high-pressure limit for OH addition, where the initially formed excited adduct is always stabilized by collisions. At limited pressures, the observed rate constant is possibly smaller than the calculated one, because some fraction of the excited adducts can dissociate back to reactants before collisional stabilization or fragmentation. Under a given pressure, at elevated temperatures, this effect will be more noticeable, as the reaction moves further from the high-pressure limit.

Figure 6.8 and Table 6.4 present the optimized TS structures and geometrical parameters of reactants and TS at HF/6-31G(d,p) theory level. The classical energies

along the IRC at PMP4/6-311+G(d,p) level are shown in Figure 6.9 and 6.10. The variationally located TSs lie at C – O separations around 0.05 Å smaller than the local energy maxima along the IRCs. For 1,1-dichloroethylene, β addition (at CH_2 end) presents a negative barrier of -7 kJ mol^{-1}, whereas α addition (at CCl_2 end) requires a positive barrier of approximately +10 kJ mol^{-1}. For OH addition to 1,2-$C_2H_2Cl_2$, the energy curves of cis- and trans- structures are very similar, and both have a significant positive barrier.

The derived VTST rate constants are shown in Figure 6.11 and Table 6.5. For 1,1-dichloroethylene, as similar as the reactions of OH with vinyl chloride, the α channel has a simple positive temperature dependence. The β channel is more important at all temperatures and has a more complex behavior. At low temperatures, the negative relative TS energy contributes to a negative temperature dependence for the rate constant, whereas at high temperatures, a positive temperature dependence has been yielded, because the partition function of the loose TS more rapidly increase as temperature increasing, compared to the reactants.

OH + C_2HCl_3

The reaction mechanism of OH + trichloroethylenes was presumed to be the same as the one for OH + dichloroethylenes. Previous studies[5,11] reported that the rate coefficients were independent of pressure, thus the addition complex was rapidly thermalized by collisions with the buffer gas or that a decomposition pathway was available. Ab initio calculations were performed in current work to estimate

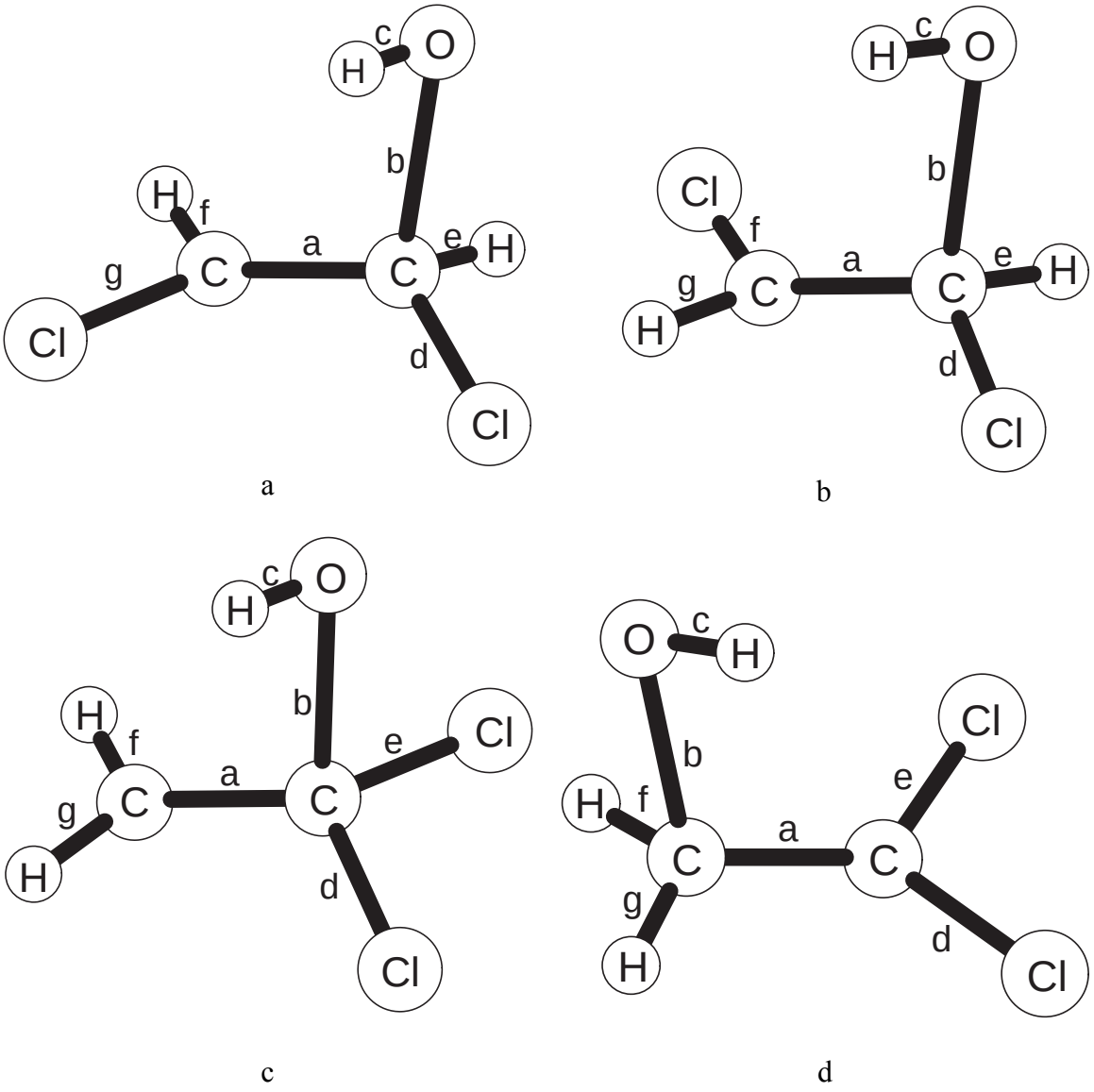

Fig. 6.8. Optimized TS structures of the reaction OH with dichloroethylene at the HF/6-31G(d,p) level: a. cis-1,2-dichloroethylene; b. trans-1,2-dichloroethylene; c. 1,1-dichloroethylene at the CCl_2 end (α site) ; d. 1,1-dichloroethylene at the CH_2 end (β site).

Table 6.4. Optimized geometrical parameters [a] for reactants and transition States of the reaction OH with dichloroethylene at the HF/6-31G(d,p) level.

	a	b	c	d	e	f	g
OH			0.9549				
cis-1,2-$C_2H_2Cl_2$	1.312			1.721	1.072	1.072	1.721
trans-1,2-$C_2H_2Cl_2$	1.310			1.730	1.071	1.730	1.071
1,1-$C_2H_2Cl_2$	1.311			1.728	1.728	1.073	1.073
TS 1 [b]	1.394	1.939	0.9525	1.744	1.071	1.071	1.718
TS 2 [c]	1.390	1.949	0.9523	1.750	1.070	1.720	1.071
TS 3 [d]	1.397	1.932	0.9526	1.744	1.734	1.072	1.073
TS 4 [e]	1.388	1.941	0.9522	1.725	1.718	1.071	1.072

	ba	da	ea	fa	ga	cb
OH						
cis-1,2-$C_2H_2Cl_2$		125.7	120.2	120.2	125.7	
trans-1,2-$C_2H_2Cl_2$		121.7	123.8	121.7	123.8	
1,1-$C_2H_2Cl_2$		122.8	122.8	120.5	120.5	
TS 1 [b]	102.8	120.1	118.0	119.7	124.1	97.47
TS 2 [c]	104.4	115.8	121.6	120.4	123.1	98.64
TS 3 [d]	101.4	117.8	118.5	119.9	119.4	100.5
TS 4 [e]	106.8	121.3	122.0	117.8	117.8	100.1

	dab	eab	fab	gab	cba	daf	eag	dag	eaf
OH									
cis-1,2-$C_2H_2Cl_2$						180.0	180.0	0.0	0.0
trans-1,2-$C_2H_2Cl_2$						180.0	180.0	0.0	0.0
1,1-$C_2H_2Cl_2$						180.0	180.0	0.0	0.0
TS 1 [b]	108.5	-108.5	83.13	-83.13	61.08				
TS 2 [c]	108.1	-108.1	84.77	-84.77	55.19				
TS 3 [d]	110.3	-105.7	80.44	-89.31	60.39				
TS 4 [e]	97.01	-82.77	102.5	-107.4	-44.26				

[a] Refer to Figure 6.8 for definition of parameters: e.g. a = bond length (Å), ba = bond angle (degree), cba = dihedral angle (degree) between the plane containing bonds c, b and the plane containing bonds b, a; [b] TS of the reaction OH with cis-1,2-$C_2H_2Cl_2$; [c] TS of the reaction OH with transs-1,2-$C_2H_2Cl_2$; [d] TS of the reaction OH with 1,1-$C_2H_2Cl_2$, OH added at CCl_2 end (α site); [e] TS of the reaction OH with 1,1-$C_2H_2Cl_2$, OH added at CH_2 end (β site)

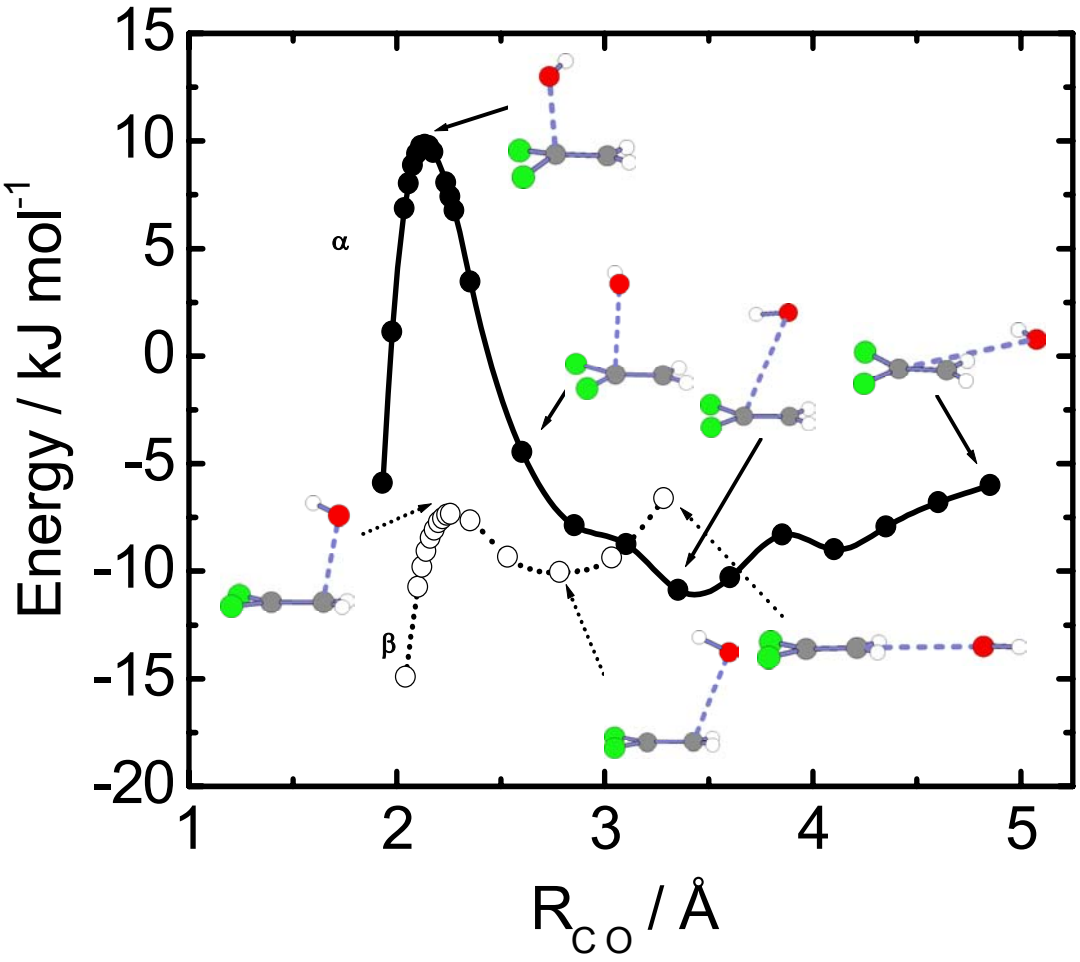

Fig. 6.9. Classical energies (no ZPE) relative to OH + CH_2-CCl_2 for addition of OH at the CH_2 end (β site, open circles) and the CCl_2 end (α site, solid circles), calculated at the PMP4/6-311+G(d,p)//HF/6-31G(d,p) level of theory, together with molecular structures along the reaction path.

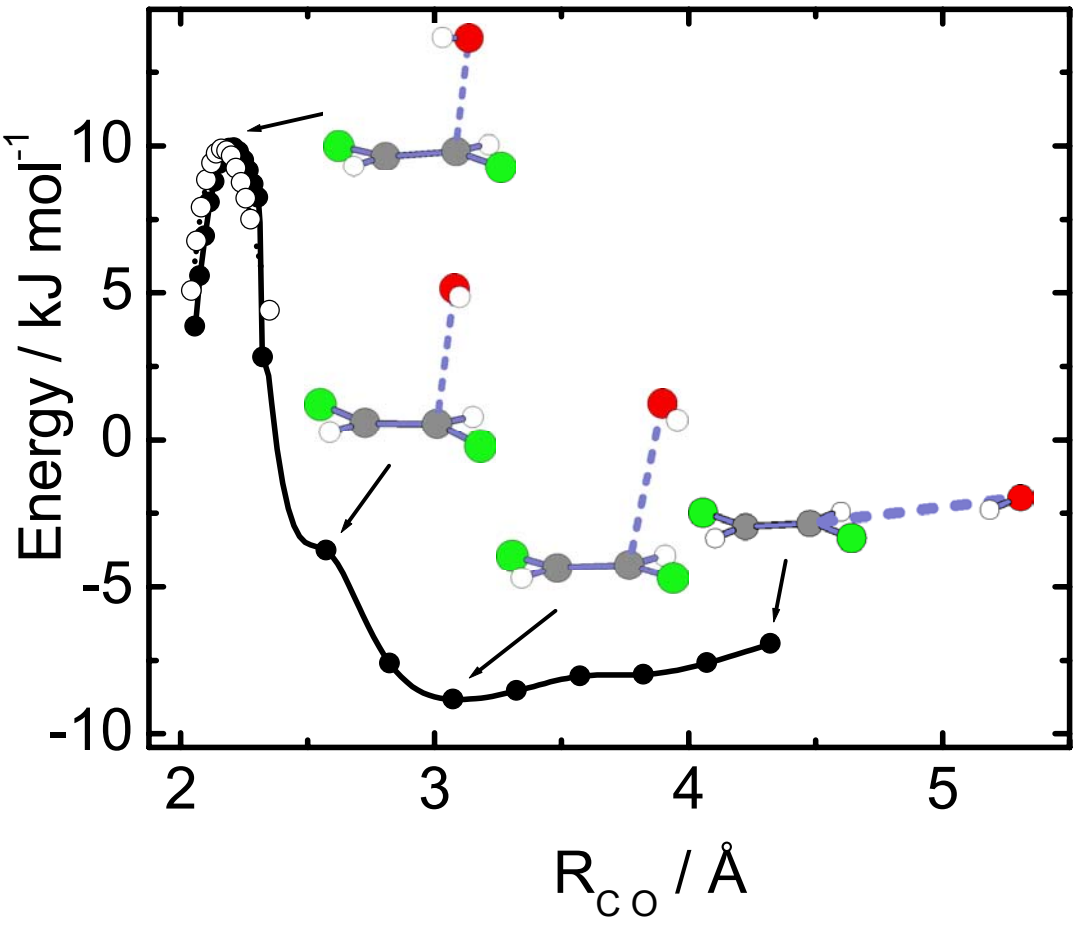

Fig. 6.10. Classical energies (no ZPE) relative to OH + 1,2-CHCLCHCl for addition of OH at the cis- structure (open circles) and the trans- structure (solid circles), calculated at the PMP4/6-311+G(d,p)//HF/6-31G(d,p) level of theory, together with molecular structures along the reaction path.

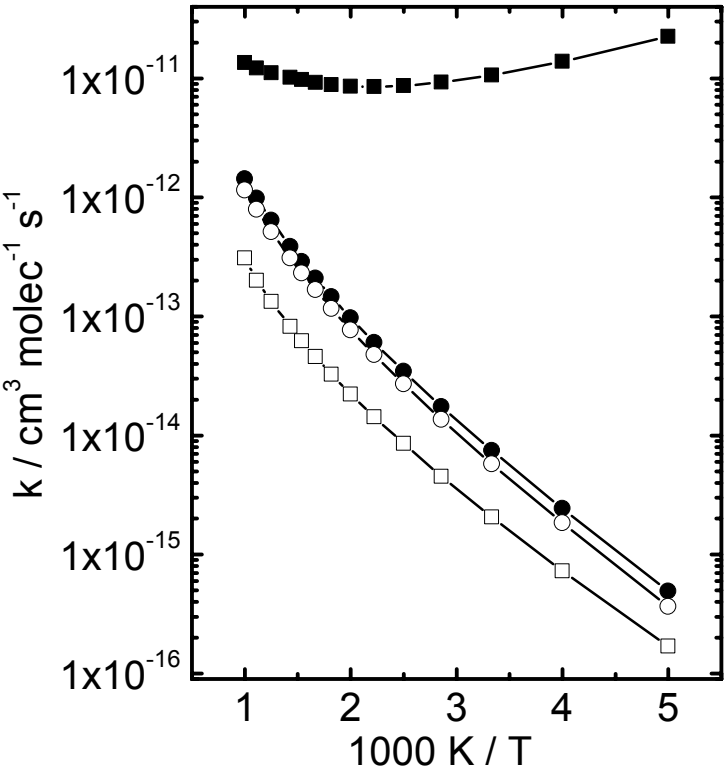

Fig. 6.11. Ab initio high-pressure limit rate constants for OH addition to dichloroethylene: solid square, OH + CH_2CCl_2 (β channel); empty square, OH + CH_2CCl_2 (α channel); solid circle, OH + trans-CHClCHCl; empty circle, OH + cis-CHClCHCl.

Table 6.5. Rate constants for OH addition to dichloroethylene

	$k_{VTST} = B\ T^n\ e^{-E/RT}$ (cm^3 $molecule^{-1}$ s^{-1})
TS 1 [a]	$3.13 \times 10^{-19}\ T^{2.340}\ \exp(-1066/T)$
TS 2 [a]	$3.22 \times 10^{-19}\ T^{2.364}\ \exp(-1034/T)$
TS 3 [a]	$1.42 \times 10^{-20}\ T^{2.543}\ \exp(-783/T)$
TS 4 [a]	$5.28 \times 10^{-18}\ T^{2.004}\ \exp(929/T)$

[a] Refer to Table 6.4

thermodynamic properties, which were used for deeper theoretical computations of energy-dependent rate constants.[30,31]

VTST calculations were performed as previous description in this chapter. The results correspond to the optimized geometries are shown in Figure 6.12 and Table 6.6. Figure 6.13 presents the classical energies curves for the reactions of OH + trichloroethylenes. As may be seen, the barrier for α addition lies around 5 kJ/mol below the reactants' energy, whereas β addition has a positive barrier approximately +5 kJ/mol. Correspond to the derived VTST rate constants (see Figure 6.14), the β channel has a simple positive temperature dependence. The α channel is more important at all temperatures and has a more complex behavior: a negative temperature dependence at low temperature region due to the negative relative TS energy, and a positive temperature dependence at high temperature region as a result of the rapidly increasing of the loose TS's partition function with the temperature increasing. For α addition, all the vibrational modes were treated as harmonic oscillators, except for one at 201cm^{-1}, corresponding to hindered torsion of the hydroxyl group around the forming C – O bond. By using the relationship of Benson,[32] a barrier of 10 kJ/mol was derived and taken into account when determining the overall rate constants.

$OH + C_2Cl_4$

In contrast to the other chloroethenes, there is a distinct barrier presented in the reaction of OH radical with tetrachloroethylene, so that the VTST calculations are not useful to estimate the rate of this reaction. As a replacement, conventional TST

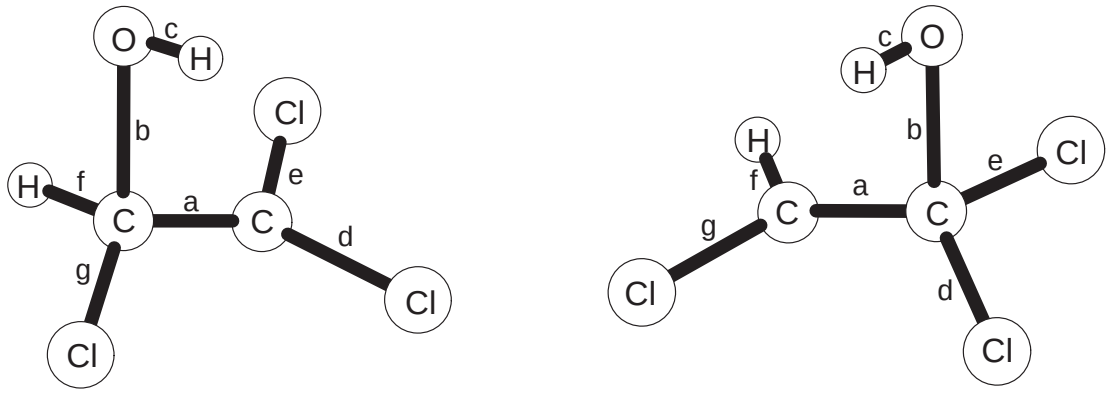

Fig. 6.12. Optimized TS structures of the reaction OH + C_2HCl_3 at the HF/6-31G(d,p) level.

Table 6.6. Optimized geometrical parameters[a] for reactants and transition states of the reaction OH + C_2HCl_3 at the HF/6-31G(d,p) level.

	a	b	c	d	e	f	g
OH			0.9549				
C_2HCl_3	1.314			1.716	1.727	1.071	1.717
TS 1 [b]	1.405	1.939	0.9532	1.733	1.734	1.070	1.714
TS 2 [c]	1.399	1.945	0.9528	1.713	1.716	1.069	1.731

	ba	da	ea	fa	ga	cb
OH						
C_2HCl_3		124.8	120.0	120.6	124.7	
TS 1 [b]	101.1	120.2	115.3	119.7	122.9	99.99
TS 2 [c]	103.7	123.6	118.7	117.4	120.2	99.07

	dab	eab	fab	gab	cba	daf	eag	dag	eaf
OH									
C_2H_3Cl						180.0	180.0	0.0	0.0
TS 1 [b]	111.6	-105.0	80.55	-84.15	65.93				
TS 2 [c]	91.26	-167.5	-145.3	-116.2	-66.15				

[a] Refer to Figure 6.12 for definition of parameters: e.g. a = bond length (Å), ba = bond angle (degree), cba = dihedral angle (degree) between the plane containing bonds c, b and the plane containing bonds b, a; [b] OH added at CHCl end (α site); [c] OH added at CCl_2 end (β site)

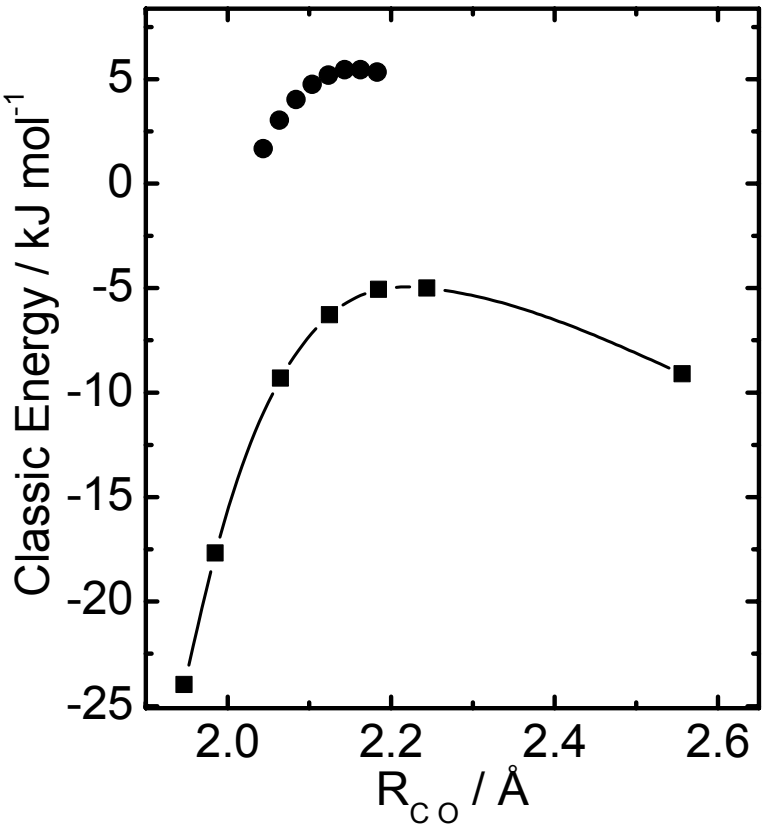

Fig. 6.13. Classical energies (no ZPE) relative to OH + C_2HCl_3 for addition of OH at the CHCl end (α, squares) and the CCl_2 end (β, circles), calculated at the PMP4/6-311+G(d,p)//HF/6-31G(d,p) level of theory

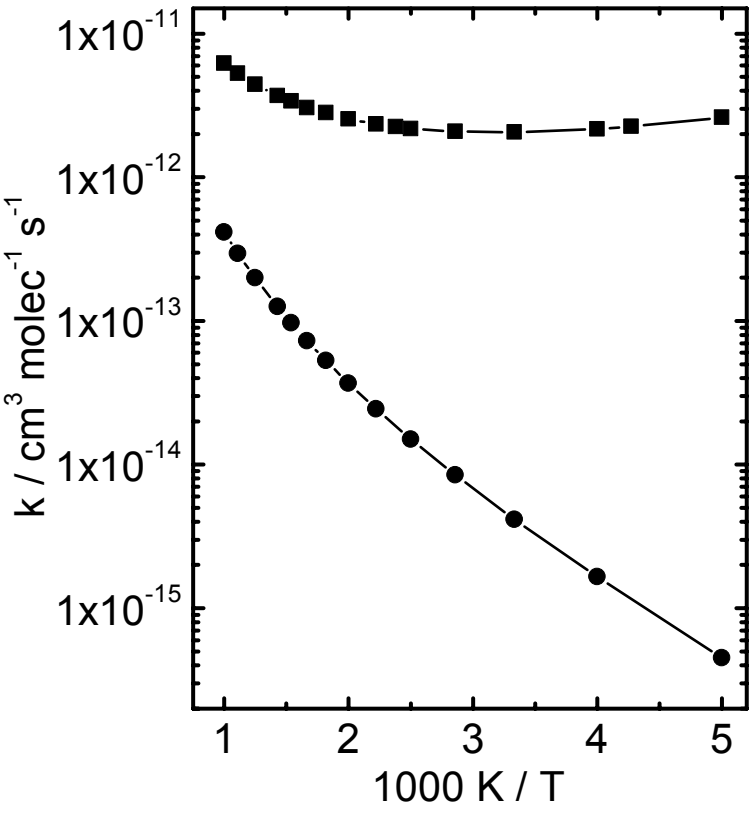

Fig. 6.14. Ab initio high-pressure limit rate constants for OH addition to C_2HCl_3: circle, at the CCl_2 end (β channel); square, at the CHCl end (α channel). The OH rotation was treated as a hindered rotor with a barrier of 10 kJ/mol in the α channel.

Table 6.7. Rate constants for OH addition to trichloroethylene

	$k_{VTST} = B\ T^n\ e^{-E/RT}$ (cm^3 $molecule^{-1}$ s^{-1})
TS 1 (α site)[a]	$1.98 \times 10^{-19}\ T^{2.397}\ \exp(750/T)$
TS 2 (β site)	$4.32 \times 10^{-20}\ T^{2.430}\ \exp(-720/T)$

[a] OH rotation was treated as a hindered rotor

calculations were performed to predict the rate constants in here.

Theoretical approach was described at the beginning of this chapter. High level G3 and G3(mp2) calculations were used to evaluated the activation energy, which are 5.0 kJ/mol and 12.1 kJ/mol, separately. Optimized geometries of reactants and TS at HF/6-31G(d) are presented in Figure 6.15 and Table 6.8. Conventional TST rate constants were derived by POLYRATE 8.0 program package. The lowest vibrational mode at 58 cm^{-1} corresponds to torsion about the C – C bond in the TS. Using the relationship of Benson,[32] a barrier to internal rotation of 53.6 kJ/mol was obtained. This barrier was confirmed by reoptimizing the TS to a second-order saddle point, where the two CCl_2 moieties are close to perpendicular (see Fig. 6.16). At the HF/6-31G(d) level, the zero-point energy corrected geometry was 51.9 kJ/mol above the TS geometry. This value for the barrier to hindered internal rotation was employed with the table of Lewis et al.[33] to derive the partition functions and entropy for this internal mode of the TS. Similarly, the hindered torsion of hydroxyl group around the forming C– O bond, with a frequency of 204 cm^{-1}, has a corresponding[32] barrier of 25.1 kJ/mol and was also taken into account when determining the overall molecular partition function. In fact, both torsional modes had partition functions close to those derived from a purely harmonic oscillator model. The greatest combined deviation was 30%, at 2000K. The results of such ab initio calculations are shown in Figure 6.17, and result in an expression, $k_{TST} = 9.90 \times 10^{-21} T^{2.693} \exp(45/T)$.

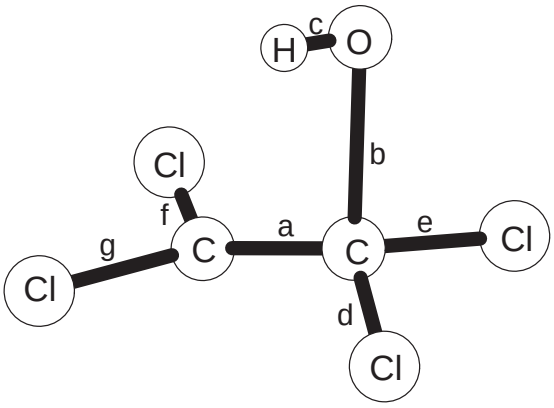

Fig. 6.15. Optimized TS structure of the reaction OH + C_2Cl_4 at the HF/6-31G(d) level.

Table 6.8. Optimized geometrical parameters[a] for reactants and transition state of the reaction OH + C_2Cl_4 at the HF/6-31G(d) level.

	a	b	c	d	e	f	g
OH			0.9585				
C_2Cl_4	1.322			1.718		1.718	
TS	1.418	1.947	0.9573	1.736	1.726	1.709	1.716

	ba	da	ea	fa	ga	cb
OH						
C_2Cl_4				122.8		
TS	100.8	118.0	118.3	121.4	121.1	100.2

	dab	eab	fab	gab	cba	daf
OH						
C_2Cl_4						180.0
TS	100.9	-106.2	79.88	-83.91	69.11	

[a] Refer to Figure 6.15 for definition of parameters: e.g. a = bond length (Å), ba = bond angle (degree), cba = dihedral angle (degree) between the plane containing bonds c, b and the plane containing bonds b, a

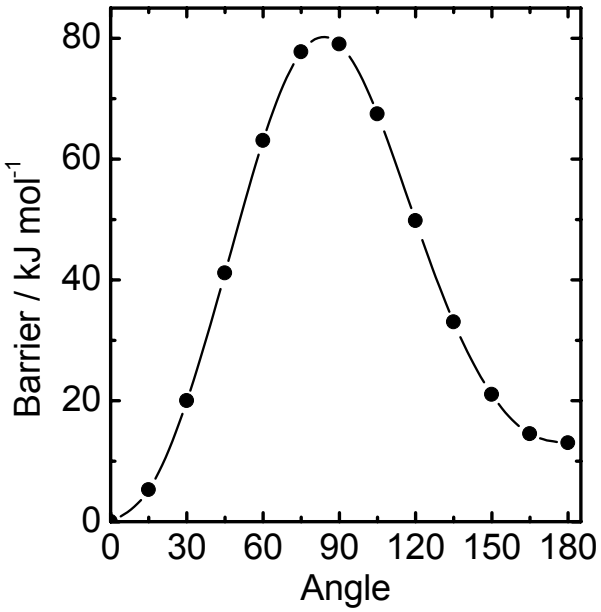

Fig. 6.16. Barrier height for CCl_2 rotation of the TS relative to OH + C_2Cl_4 at the HF/6-31G(d) level of theory.

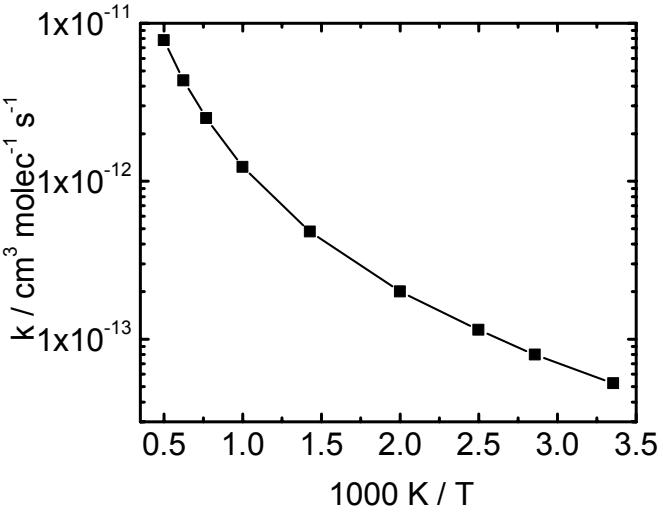

Fig. 6.17. Ab initio rate constants for OH addition to C_2Cl_4, the OH and CCl_2 rotations were treated as hindered rotors.

REFERENCES

(1) Fairchild, P. W.; Smith, G. P.; Crosley, D. R. *Proc. Combust. Inst.* **1982**, *19*, 107.

(2) Warnatz, J.; Bockhorn, H.; Moser, A.; Wenz, H. W. *Proc. Combust. Inst.* **1982**, *19*, 197.

(3) Howard, C. J. *J. Chem. Phys.* **1976**, *65*, 4771.

(4) Perry, P. A.; Atkinson, R.; Pitts, J. N., Jr. *J. Chem. Phys.* **1977**, *67*, 458.

(5) Kirchner, K.; Helf, D.; Ott, P.; Vogt, S. *Ber. Bunsen-Ges. Phys. Chem.* **1990**, *94*, 77.

(6) Edney, E. O.; Kleindienst, T. E.; Corse, E. W. *Int. J. Chem. Kinet.* **1986**, *18*, 1355.

(7) Tuazon, E. C.; Atkinson, R. A.; Aschmann, S. M.; Goodman, M. A.; Winer, A. M. *Int. J.. Chem. Kinet.* **1988**, *20*, 241.

(8) Zhang, Z.; Liu, R.; Huie, R. E.; Kurylo, M. J. *J. Phys. Chem.* **1991**, *95*, 194.

(9) Abbatt, J. P.; Anderson, J. G. *J. Phys. Chem.* **1991**, *95*, 2382.

(10) Davis, D.; Machado, U.; Smith, G.; Wagner, S.; Watson, R. T. *J. Phys. Chem. Ref. Data* **1977**, *6*, 871.

(11) Chang, J. S.; Kaufman, F. *J. Chem. Phys.* **1977**, *66*, 4989.

(12) Donovan, W. H.; Famini, G. R. *J. Phys. Chem.* **1994**, *98*, 7811.

(13) Sekušak, S.; Liedl, K. R.; Sabljic, A. *J. Phys. Chem. A* **1998**, *102*, 1583.

(14) Villà, J.; González-Lafont, A.; Lluch, J. M. *J. chem. Phys.* **1997**, *107*, 7266.

(15) Fulle, D.; Hamann, H. F.; Hippler, H.; Jänsch, C. P. *Ber. Bunsenges. Phys. Chem.* **1997**, *101*, 1433.

(16) Frisch, M. J.; Trucks, G. W.; Schlegel, H. B.; Gill, P. M. W.; Johnson, B. G.; Robb, M. A.; Cheeseman, J. R.; Keith, T. A.; Petersson, G. A.; Montgomery, J. A.; Raghavachari, K.; Al-Laham, M. A.; Zakrzewski, V. G.; Ortiz, J. V.; Foresman, J. B.; Cioslowski, J.; Stefanov, B.; Nanayakkara, A.; Challacombe, M.; Peng, C. Y.; Ayala, P. Y.; Chen, W.; Wong, W.; Andres, J. L.; Replogle, E. S.; Gomperts, R.; Martin, R. L.; Fox, D. J.; Binkley, J. S.; Defree, D. J.; Baker, J.; Stewart, J. P.; Head-Gordon, M.; Gonzalez, C.; Pople, J. A. Gaussian 94 (Revision D.2); Gaussian, Inc.: Pittsburgh, PA, 1995.

(17) Chuang, Y.; Corchado, J. C.; Fast, P. L.; Villà, J.; Coitiño, E. L.; Hu, W.; Liu, Y.; Lynch, G. C.; Nguyen, K. A.; Jackels, C. F.; Gu, M. Z.; Rossi, I.; Clayton, S.; Melissas, V. S.; Steckler, R.; Garrett, B. C.; Issacson, A. D.; Truhlar, D. G. POLYRATE; 8.0 ed.; University of Minnesota: Minneapolis, 1998.

(18) Gonzalez, C.; Schlegel, H. B. *J. Chem. Phys.* **1989**, *90*, 2154.

(19) Gonzalez, C.; Schlegel, H. B. *J. Phys. Chem.* **1990**, *94*, 5523.

(20) *NIST-JANAF Thermochemical Tables*; 4 ed.; Chase, M. W. J., Ed.; the American Chemical Society and the American Institute of Physics: Woodbury, N. Y., 1998.

(21) Frisch, M.; Frisch, Æ.; Foresman, J. B. *Gaussian 94 User's Reference*; Gaussian, Inc.: Pittsburgh, PA, 1995.

(22) Curtiss, L. A.; Raghavachari, K.; Redfern, P. C.; Rassolov, V.; Pople, J. A. *J. Chem. Phys.* **1998**, *109*, 7764.

(23) Curtiss, L. A.; Redfern, P. C.; Raghavachari, K.; Rassolov, V.; Pople, J. A. *J. Chem. Phys.* **1999**, *110*, 4703.

(24) Liu, A.; Mulac, W. A.; Jonah, C. D. *J. Phys. Chem.* **1989**, *93*, 4092.

(25) Atkinson, R. *J. Phys. Chem. Ref. Data* **1989**, Monograph 1.

(26) Yamada, T.; Siraj, M.; Taylor, P. H.; Peng, J.; Hu, X.; Marshall, P. *J. Phys. Chem. A* **2001**, *105*, 9436.

(27) Zhu, L.; Bozzelli, J. W.; Ho, W.-P. *J. Phys. Chem. A* **1999**, *103*, 7800.

(28) *CRC Handbook of Chemistry and Physics*; 71st ed.; Lide, D. R., Ed.; CRC Press: Boston, 1990.

(29) Yamada, T.; El-Sinawi, A.; Siraj, M.; Taylor, P. H.; Peng, J.; Hu, X.; Marshall, P. *J. Phys. Chem. A* **2001**, *105*, 7588.

(30) Tichenor, L. B.; Lozada-Ruiz, A. J.; Yamada, T.; El-Sinawi, A.; Taylor, P. H., Peng, J.; Hu, X.; Marshall, P. *Proc. Combus. Inst.* **2000**, *28*, 1495.

(31) Tichenor, L. B.; El-Sinawi, A.; Yamada, T.; Taylor, P. H.; Peng, J.; Hu, X.; Marshall, P. *Chemosphere* **2001**, *42*, 571.

(32) Benson, S. W. *Thermochemical Kinetics*; John Wiley & Sons: New York, 1976.

(33) Lewis, G. N.; Randall, M.; Pitzer, K. S.; Brewer, L. *Thermodynamics*; McGraw-Hill: New York, 1961.

CHAPTER 7

CONCLUSIONS

In conclusion, the rate constant for the H + H_2S reaction has been measured from 298 to 598 K by the laser photolysis / resonance fluorescence (LP-RF) technique, and the results coupled with a transition state theory (TST) analysis support the suggestion by Yoshimura et al. that the reaction support the suggestion by Yoshimura et al. that the reaction shows significant curvature in the Arrhenius plot.[1] With a 1.6 kJ mol^{-1} lowering of the reaction barrier from the QCISD(T)/6-311+G(3df,2p) value, conventional TST combined with an Eckart tunneling model accounts well for the observed rate constants over 190-1000 K. Above this temperature, nonvariational TST begins to overestimate the rate constant, by up to a factor of 2 at around 2000 K. A possible reason is that variational effects become significant above 1000 K. Future work can be extended to the study of this reaction at high temperature with variational TST (VTST) calculations. Also, a collaboration is underway with the group of Seakins in the UK to extend rate constant measurement down to about 200 K and to explore the isotopic combinations H / D + H_2S / D_2S, in order to define the role of tunneling more carefully.

The LP-RF technique was also used to measure the temperature-dependent rate constants of the H + CH_3Br reaction over the temperature range 400 - 813 K. The results of TST and density functional theory (DFT) calculations show that the dominant reaction channel is Br-abstraction. The kinetic modeling using TST and flexible TST (FTST) has

yielded curves in very good agreement with the experimental data. Combined the literature data as well as the geometry and frequency of the transition state, the FTST calculations with modified G2//QCISD/6-31G(d,p) barrier height $V^{\dagger}$ = 26.8 kJ mol^{-1} is considered to be the most physically realistic. However, only limited experimental information is available in the literature, it is worth investigating this reaction continually, especially at temperature above 1000 K to test whether nonvariational TST analysis will overestimate the rate constant at high temperature, as already be found in the reaction of H + H_2S.

The reaction H + CF_2=CF-CF=CF_2 was first studied by Flash Photolysis / Resonance Fluorescence (FP-RF) Method. The experiments of this work revealed distinctly non-Arrhenius behavior: the rate constant increases up to 620 K, then drop, then increases again above about 700 K, which was interpreted in terms of a change in mechanism. At low temperatures addition of H atoms may create a substituted butenyl radical, a process which reaches equilibrium at higher temperatures so that the thermochemistry can be assessed. At even higher temperatures, it was speculated that an observed increase in the overall rate constant reflected fragmentation of the adduct to further products. Density functional calculations suggest that the adduct is CF_2H-CF•-CF=CF_2. At lower temperatures a mixture of this molecule and CF_2•-CFH-CF=CF_2 is likely. To confirm the assumed reaction mechanism, a further study of F atom migration in activated C_4F_6 radicals is necessary.

As a preliminary investigation for this future work, 1,2-hydrogen atom migration in fluoroethyl radicals was inspected using ab initio quantum mechanics up to MP2/6-

31G(d,p). The calculation results show that H atom migrates in the fluoroethyl radicals through a bridging intermediate, and the barrier height for this process is lower in the less fluorinated ethyl radical. By using similar methods, the further study of F atom migration can be extended.

High level computations were also employed in studies of the rate constants of OH + chloroethylenes reactions. VTST calculations indicate that except the reaction of OH + C_2Cl_4, the other reactions involve a chemically activated system, and present a complex behavior. For OH + C_2Cl_4, conventional TST was used to carry out the rate constant, which shows a simple positive temperature-dependence behavior. The computational results of this work were applied for further investigation of the reaction mechanisms coupled with experimental data by our co-workers.[2-6]

REFERENCE

(1) Yoshimura, M.; Koshi, M.; Matsui, H.; Kamiya, K.; Umeyama, H. *Chem. Phys. Lett.* **1992**, *189*, 199.

(2) Tichenor, L. B.; Lozada-Ruiz, A. J.; Yamada, T.; El-Sinawi, A.; Taylor, P. H., Peng, J.; Hu, X.; Marshall, P. *Proc. Combus. Inst.* **2000**, *28*, 1495.

(3) Tichenor, L. B.; Graham, J. L.; Yamada, T.; Taylor, P. H.; Peng, J.; Hu, X.; Marshall, P. *J. Phys. Chem. A* **2000**, *104*, 1700.

(4) Tichenor, L. B.; El-Sinawi, A.; Yamada, T.; Taylor, P. H.; Peng, J.; Hu, X.; Marshall, P. *Chemosphere* **2001**, *42*, 571.

(5) Yamada, T.; El-Sinawi, A.; Siraj, M.; Taylor, P. H.; Peng, J.; Hu, X.; Marshall, P. *J. Phys. Chem. A* **2001**, *105*, 7588.

(6) Yamada, T.; Siraj, M.; Taylor, P. H.; Peng, J.; Hu, X.; Marshall, P. *J. Phys. Chem. A* **2001**, *105*, 9436.

APPENDIX

SUMMARIES OF OPTIMIZED GEOMETRIES, HARMONIC VIBRATIONAL FREQUENCIES, AND RATE CONSTANTS (k_{TST})

Table 8.1. Optimized geometries (in cartesian coordinates) and harmonic vibrational frequencies of C_4F_6, five C_4F_6 isomers and two transition states for H + C_4F_6 addition at the HF/6-31G(d) levels of theory [a]

cis-C_4F_6

	X	Y	Z
C	-1.557103	-0.370296	0.190813
C	-0.716825	0.580661	-0.132982
C	0.716836	0.580662	0.132978
C	1.557106	-0.370292	-0.190839
F	-1.214451	-1.455483	0.814476
F	-2.820558	-0.351571	-0.087003
F	-1.183857	1.666826	-0.741862
F	1.183878	1.666814	0.741874
F	2.820550	-0.351594	0.087002
F	1.214430	-1.455482	-0.814467

51.4804	105.4243	120.1161
205.8558	228.1561	278.3045
321.4019	407.1096	452.3289
517.5618	588.8472	615.9975
681.1642	692.8889	735.4795
779.3557	1078.1961	1263.5369
1335.7024	1493.8523	1508.0943
1547.3727	2024.9801	2048.8877

CF2H–CF• –CF=CF2

	X	Y	Z
C	1.391353	-0.562255	-0.000354
C	0.718371	0.628534	0.000083
C	-0.661913	0.828168	0.000139
C	-1.762703	-0.182605	0.000279
F	0.802874	-1.720424	-0.000397
F	2.687134	-0.639581	0.000081
F	1.476439	1.714583	0.000197
F	-1.080690	2.085709	-0.000282
F	-1.687472	-0.975122	-1.076980
F	-1.686756	-0.975486	1.077208
H	-2.714406	0.321825	0.000664

35.6182	64.4480	91.5006

132.2270	136.2430	166.2630
221.7707	327.1237	365.3922
426.8006	473.0656	508.8041
556.8697	623.4781	700.3782
798.8195	1082.8103	1247.8429
1251.4853	1315.8321	1387.8851
1513.1072	1528.3108	1553.8619
1610.6609	1718.5987	3351.6356

•CF2–CFH –CF=CF2

	X	Y	Z
C	1.584249	-0.291914	-0.251261
C	0.724000	0.447279	0.398383
C	-0.683418	0.056525	0.731572
C	-1.583707	-0.006785	-0.474616
F	1.291445	-1.460144	-0.734904
F	2.811428	0.040366	-0.490978
F	1.105680	1.639703	0.848837
F	-0.721611	-1.168031	1.321503
F	-2.808971	-0.383854	-0.198562
F	-1.586217	1.107585	-1.174119
H	-1.072528	0.788732	1.429545

10.1953	66.0457	109.1667
151.0913	204.3665	292.4235
308.2943	386.5786	433.2503
470.9142	553.3388	581.3756
635.4366	715.4624	730.3473
870.5226	1116.6212	1227.1403
1294.6510	1332.4614	1379.3402
1403.8680	1498.2513	1526.3773
1570.4015	2043.6127	3263.3990

•CFH–CF2 –CF=CF2

	X	Y	Z
C	1.719787	0.149895	-0.109958
C	0.574053	-0.462995	0.052441
C	-0.791720	0.131896	0.217250
C	-1.727788	-0.317595	-0.857958
F	1.887246	1.430531	-0.164773
F	2.841380	-0.483640	-0.244325
F	0.564562	-1.792984	0.073215
F	-0.700008	1.471275	0.230263

F	-2.994438	-0.025994	-0.622554
H	-1.437812	-0.258408	-1.889499
F	-1.288539	-0.237943	1.403602

37.5186	77.7021	118.4667
188.8849	216.9737	269.7849
301.4615	365.0162	380.9018
435.8900	535.8548	601.0055
619.2169	711.3533	733.3334
784.2865	877.7855	1069.5744
1282.2816	1287.2400	1315.6243
1377.6530	1462.4619	1537.1681
1566.4605	2040.7777	3398.3365

CF2H–CF2–C•=CF2

	X	Y	Z
C	1.828467	-0.174158	-0.174129
C	0.610628	-0.045144	-0.644026
C	-0.632829	0.602046	-0.169402
C	-1.718661	-0.369204	0.266784
F	2.775647	-0.813888	-0.789197
F	2.255386	0.310967	0.953301
F	-0.370600	1.400520	0.874660
F	-2.014068	-1.171687	-0.755822
F	-1.257539	-1.113639	1.271402
H	-2.603789	0.158649	0.582550
F	-1.157920	1.361073	-1.138555

19.5648	79.5152	92.7943
139.1468	227.6567	275.1767
355.5503	386.8646	414.0576
551.4391	589.1106	607.6031
633.6469	687.5135	774.0321
871.9579	1108.3198	1253.8292
1292.6416	1314.8604	1330.8871
1446.6450	1460.4790	1543.2909
1589.5238	1861.5624	3349.9472

CF3–CH• –CF=CF2

	X	Y	Z
C	-1.551755	-0.446937	0.000029
C	-0.909585	0.766205	-0.000007
C	0.447221	1.050635	-0.000020

C	1.547213	0.039283	0.000000
F	-0.934922	-1.589312	-0.000016
F	-2.844094	-0.561594	0.000001
F	-1.731612	1.811888	-0.000003
F	1.512698	-0.744748	-1.064229
F	1.512752	-0.744644	1.064308
H	0.738225	2.081619	-0.000029
F	2.714424	0.657661	-0.000059

58.2515	78.2676	131.3280
151.2597	188.2550	227.4114
349.0481	366.7662	435.0520
450.9202	524.5659	576.3090
586.7880	654.1810	690.2262
765.3987	831.5186	981.3648
1237.6583	1299.5890	1351.7761
1415.4728	1421.1044	1520.8093
1612.1975	1708.8042	3422.8543

H…CF2–CF•–CF=CF2 (alpha-TS)

	X	Y	Z
C	1.593602	-0.405648	-0.139464
C	0.742001	0.603401	0.060160
C	-0.680428	0.595660	-0.154660
C	-1.575482	-0.375496	0.211646
F	1.243051	-1.569521	-0.592948
F	2.859920	-0.334525	0.123194
F	1.255994	1.767740	0.437518
F	-1.199596	1.759165	-0.514419
F	-2.802227	-0.362475	-0.221882
F	-1.182289	-1.572643	0.545511
H	-2.051835	0.302834	2.141142

-682.1364	57.8956	106.7584
122.8957	188.4923	210.8205
277.8152	303.1661	337.5729
367.5639	396.2194	412.1953
470.5775	519.1762	528.2566
600.2869	622.7052	661.2234
740.3146	1041.4200	1222.7237
1349.7638	1481.4376	1504.1395
1536.4891	1672.8996	1806.9389

•CF2–CF(…H)–CF=CF2 (beta-TS)

	X	Y	Z
C	1.867713	-0.072709	-0.054216
C	0.617363	0.394267	0.062301
C	-0.592414	-0.381434	0.169687
C	-1.851850	0.072428	-0.223106
F	2.185171	-1.325915	-0.150156
F	2.904861	0.706689	-0.076341
F	0.470156	1.709437	0.146586
F	-0.431058	-1.694685	0.104246
F	-2.885677	-0.709903	-0.089363
F	-2.172659	1.332116	-0.143707
H	-0.882012	-0.234961	2.150620

-700.4144	38.9026	106.0271
133.9552	165.5872	228.6811
286.5309	305.6805	336.4712
367.2572	393.3403	410.6521
464.2317	519.0342	563.1942
621.7143	629.6646	658.2820
750.5272	998.0073	1270.8820
1343.8919	1463.5988	1500.4175
1547.9148	1660.0673	1778.5980

[a] Cartesian Coordinates in 10^{-10} m, Harmonic Frequencies in cm^{-1}

Table 8.2. Optimized geometries (in cartesian coordinates) and harmonic vibrational frequencies of ethyl radical, fluoroethyl radicals, and transition states for the 1,2-hydrogen atom migration at various levels of theory [a]

CH_3-CH_2•								
		HF/3-21G(d)				HF/6-31G(d)		
Geometry	C	0.703857	0.000003	0.001347	C	-0.034941	0.124402	-0.686853
	C	-0.802891	0.000000	-0.026795	C	0.049096	-0.174807	0.778545
	H	1.104168	-0.878269	-0.492750	H	0.920808	-0.032030	-1.177148
	H	1.104159	0.878559	-0.492244	H	-0.769823	-0.506437	-1.177062
	H	1.081792	-0.000296	1.023304	H	-0.325345	1.159296	-0.872095
	H	-1.347949	-0.920809	0.057188	H	0.928509	0.089041	1.338072
	H	-1.347967	0.920797	0.057190	H	-0.839079	-0.407435	1.338081
Frequency	128.5467	436.1560	894.7281	1046.4275	165.8695	459.8741	870.7531	1083.3319
	1110.0715	1318.9864	1574.8483	1596.5022	1113.2899	1309.2124	1552.5063	1608.7293
	1660.1087	1664.9026	3151.0701	3218.8313	1629.9758	1634.8894	3160.4591	3229.0537
	3251.5372	3292.6948	3397.3224		3263.6671	3314.7486	3412.3827	
		HF/6-31G(d, p)				MP2/6-31G(d, p)		
Geometry	C	0.698330	0.000003	0.002409	C	0.694479	0.000003	0.001772
	C	-0.798275	0.000000	-0.035920	C	-0.793995	0.000000	-0.034825
	H	1.106930	-0.877815	-0.488816	H	1.103935	-0.881499	-0.489602
	H	1.106917	0.878098	-0.488324	H	1.103922	0.881762	-0.489145
	H	1.077231	-0.000288	1.025615	H	1.077355	-0.000269	1.028005
	H	-1.345693	-0.918974	0.076294	H	-1.344048	-0.920805	0.074529
	H	-1.345710	0.918963	0.076297	H	-1.344068	0.920793	0.074533

Frequency	164.3408	459.6904	866.9280	1074.4074	171.8215	470.1910	836.0421	1024.3761
	1110.2818	1300.6468	1536.2695	1596.3259	1108.1312	1245.8778	1461.5086	1537.7391
	1613.2118	1616.8101	3139.9087	3210.1203	1551.1939	1551.2540	3092.2681	3179.9423
	3246.1466	3293.1761	3394.6872		3225.7885	3266.5315	3380.5790	

$(CH_2...H...CH_2)\bullet$ TS

		HF/3-21G(d)				HF/6-31G(d)		
Geometry	C	0.750916	-0.000004	-0.023244	C	0.742357	0.000008	-0.023173
	C	-0.750949	0.000007	-0.023117	C	-0.742392	0.000004	-0.023111
	H	1.266008	-0.922832	-0.196012	H	1.265254	-0.922706	-0.190723
	H	1.265938	0.922911	-0.195788	H	1.265066	0.922861	-0.190343
	H	0.000168	-0.000044	1.062076	H	0.000292	-0.000125	1.039804
	H	-1.265932	-0.922871	-0.195972	H	-1.265111	-0.922842	-0.190401
	H	-1.265985	0.922817	-0.196139	H	-1.265290	0.922742	-0.190628
Frequency	-2486.9578	609.9495	872.7784	884.3808	-2428.9198	602.5773	823.7543	832.9572
	904.9552	1141.8040	1300.7187	1372.0110	856.1830	1214.6998	1304.3088	1392.0403
	1553.8384	1571.5600	2002.1696	3319.2116	1550.3820	1584.3279	2234.8980	3324.9986
	3325.5169	3424.5094	3448.3132		3333.2423	3427.9854	3449.9643	
		HF/6-31G(d, p)				MP2/6-31G(d, p)		
Geometry	C	0.742669	0.000005	-0.022507	C	-0.743011	0.000009	-0.021689
	C	-0.742697	0.000005	-0.022492	C	0.742969	0.000001	-0.022102
	H	1.264938	-0.922835	-0.192001	H	-1.266280	0.927114	-0.187870
	H	1.264764	0.922982	-0.191605	H	-1.266276	-0.927112	-0.187811
	H	0.000302	-0.000104	1.036985	H	-0.000154	-0.000071	1.012473
	H	-1.264835	-0.922971	-0.191560	H	1.266497	0.927189	-0.186954

	H	-1.264998	0.922871	-0.191829	H	1.266469	-0.927176	-0.187094
Frequency	-2386.3665	600.9956	829.2556	836.9604	-2205.2618	573.5972	759.3467	805.4597
	851.1792	1211.302	1298.0828	1387.5185	816.2004	1182.4317	1237.4574	1361.8066
	1540.3850	1573.7847	2254.0359	3303.5459	1477.1593	1505.0851	2441.3362	3260.3483
	3311.9824	3409.3545	3431.2625		3265.6132	3378.4158	3397.1529	

$CH_2F\text{-}CH_2\bullet$

		HF/3-21G(d)				HF/6-31G(d)		
Geometry	C	0.033129	0.537744	0.035561	C	0.051883	0.520915	0.054284
	C	-1.223883	-0.264387	-0.028974	C	-1.218085	-0.250194	-0.044755
	F	1.145550	-0.322699	-0.031412	F	1.124881	-0.326082	-0.047399
	H	0.091509	1.240328	-0.784890	H	0.128841	1.257953	-0.736464
	H	0.101005	1.095554	0.962707	H	0.139654	1.038106	1.006202
	H	-1.193835	-1.303611	0.226808	H	-1.255714	-1.250654	0.343396
	H	-2.164109	0.231876	-0.161443	H	-2.139497	0.265011	-0.243724
Frequency	143.1359	413.5794	444.6467	930.6498	175.8684	428.5671	492.3215	930.7410
	1055.4753	1140.4380	1201.9944	1356.7851	1070.8632	1187.6468	1232.7037	1374.8678
	1552.1091	1572.6644	1684.3336	3193.3228	1554.7210	1597.1285	1664.2435	3199.4508
	3239.7141	3319.7479	3437.0452		3258.2737	3331.2033	3439.4375	

		HF/6-31G(d, p)				MP2/6-31G(d, p)		
Geometry	C	0.051580	0.520474	0.053217	C	0.035194	0.525275	0.056332
	C	-1.217860	-0.250530	-0.043542	C	-1.217257	-0.259225	-0.043753
	F	1.125268	-0.325425	-0.046522	F	1.140849	-0.321935	-0.049634
	H	0.126092	1.257292	-0.739815	H	0.098046	1.274687	-0.735628

	H	0.000302	0.000005	-0.022507	H	0.116683	1.046706	1.016962
	H	-1.252374	-1.255147	0.335028	H	-1.243495	-1.257793	0.359467
	H	-2.139848	0.265678	-0.239413	H	-2.146492	0.237521	-0.269573
Frequency	176.4100	428.7806	491.3425	927.3002	189.0471	417.7095	494.1950	880.7222
	1064.9523	1184.2560	1229.4709	1368.2232	1019.2789	1142.9282	1166.5393	1278.1489
	1542.7923	1586.4741	1644.5213	3171.5786	1457.5553	1521.9983	1564.6217	3087.0383
	3229.8007	3308.5311	3420.5614		3159.8911	3275.5121	3399.4044	

CH_3-CHF•

		HF/3-21G(d)				HF/6-31G(d)		
Geometry	C	-0.106614	0.523832	-0.108085	C	-0.122830	0.519802	-0.120959
	C	1.204893	-0.179580	0.013678	C	1.189443	-0.171181	0.015100
	F	-1.216463	-0.278224	0.018982	F	-1.187394	-0.282182	0.021193
	H	-0.258041	1.516151	0.266585	H	-0.294616	1.495930	0.296674
	H	2.009897	0.498848	-0.236184	H	1.998377	0.518509	-0.196973
	H	1.239561	-1.027972	-0.658967	H	1.253070	-1.003943	-0.677086
	H	1.367071	-0.548524	1.024174	H	1.330037	-0.562581	1.021802
Frequency	180.1484	404.7559	649.0556	958.8463	206.0529	435.1998	717.4046	984.9797
	1151.2891	1200.3878	1277.7128	1500.1589	1145.4594	1218.0619	1291.1290	1498.4273
	1580.8051	1641.8449	1660.4192	3171.1374	1573.5700	1614.8508	1632.8640	3179.5625
	3243.4551	3281.5241	3359.5893		3251.6944	3287.3357	3359.0081	
		HF/6-31G(d, p)				MP2/6-31G(d, p)		
Geometry	C	-0.122326	0.519681	-0.119525	C	-0.109288	0.524457	-0.117977
	C	1.188923	-0.171548	0.014947	C	1.189918	-0.176764	0.014946

	F	-1.187242	-0.282171	0.020992	F	-1.198690	-0.280190	0.020554
	H	-0.293603	1.499311	0.292523	H	-0.275663	1.512840	0.289955
	H	1.997494	0.518568	-0.197790	H	2.006753	0.507825	-0.202878
	H	1.251356	-1.004082	-0.677848	H	1.240085	-1.014169	-0.678933
	H	1.330347	-0.563051	1.021656	H	1.333264	-0.570948	1.025054
Frequency	206.0794	436.0799	708.7189	981.7158	212.4532	413.5635	670.8250	946.1079
	1134.5853	1211.8664	1289.4412	1489.1115	1081.2179	1173.9687	1222.7247	1419.9494
	1559.4971	1597.0542	1615.6896	3159.6653	1479.8673	1528.6355	1550.1388	3106.8527
	3233.8538	3270.0510	3334.5378		3199.4583	3242.4437	3275.2308	

$(CH_2...H...CHF)\bullet$ TS

		HF/3-21G(d)				HF/6-31G(d)		
Geometry	C	0.059878	0.483051	0.058361	C	0.071457	0.480583	0.062933
	C	-1.234080	-0.226875	-0.042144	C	-1.214575	-0.218181	-0.042162
	F	1.217752	-0.259423	-0.042585	F	1.188191	-0.263271	-0.044052
	H	0.139502	1.478125	-0.326133	H	0.176520	1.475530	-0.327242
	H	-0.785410	0.369751	1.075368	H	-0.760528	0.347321	1.059589
	H	-1.214018	-1.289101	0.085588	H	-1.205670	-1.285316	0.069759
	H	-2.054634	0.238977	-0.548861	H	-2.045334	0.257497	-0.530262
Frequency	-2590.9562	355.0574	452.7013	851.4707	-2550.2516	349.1686	473.3096	811.9315
	914.2119	1012.1641	1207.1626	1263.0203	871.4199	1034.7900	1236.4152	1282.7669
	1363.9339	1492.7000	1552.2991	1931.9759	1383.5635	1501.7021	1570.8195	2176.6590
	3327.8942	3377.6711	3451.5285		3330.1985	3374.8206	3450.8159	
		HF/6-31G(d, p)				MP2/6-31G(d, p)		

Geometry	C	0.071400	0.481322	0.061714	C	0.058188	0.475905	0.070557
	C	-1.214939	-0.218390	-0.041035	C	-1.225885	-0.220007	-0.044788
	F	1.187818	-0.263457	-0.043677	F	1.211386	-0.258805	-0.049346
	H	0.176984	1.477768	-0.326392	H	0.146660	1.489921	-0.294550
	H	-0.756264	0.342418	1.058276	H	-0.774735	0.358269	1.029279
	H	-1.202929	-1.286529	0.061641	H	-1.219063	-1.282014	0.135170
	H	-2.046918	0.259865	-0.524499	H	-2.049162	0.227680	-0.580397
Frequency	-2508.1806	349.0578	471.7846	815.8844	-2334.3286	356.6950	459.2475	734.6485
	868.1944	1031.5851	1232.2925	1282.1158	833.1098	969.8184	1164.1792	1229.7602
	1383.3568	1495.3521	1561.3794	2201.5782	1354.7237	1449.5141	1489.1887	2406.6111
	3309.2869	3350.9236	3432.6547		3251.1253	3276.4288	3388.6019	

CH_2F-CHF•

		HF/3-21G(d)			HF/6-31G(d)			
Geometry	C	-0.657717	0.429635	0.374949	C	0.677325	0.497988	-0.310663
	C	0.642666	0.482881	-0.330998	C	-0.663458	0.489334	0.321510
	F	-1.620063	-0.370196	-0.172439	F	1.535192	-0.406208	0.159208
	H	-0.748073	0.572927	1.430119	H	0.813067	0.705003	-1.355730
	H	0.487829	0.315130	-1.384018	H	-0.571850	0.341352	1.388144
	F	1.536722	-0.497569	0.157860	F	-1.440997	-0.526369	-0.183878
	H	1.100619	1.446734	-0.178589	H	-1.172175	1.422904	0.124526
Frequency	107.4955	329.7629	451.6193	655.7186	115.4380	342.0656	505.4611	765.9462
	958.1273	1094.7657	1180.0361	1275.9411	983.9411	1135.3426	1213.4104	1305.3451
	1385.7017	1514.9068	1561.2028	1673.5585	1394.5840	1509.5899	1587.2621	1653.5490
	3269.6555	3319.5229	3396.8030		3266.8778	3321.8985	3385.7485	

		HF/6-31G(d, p)				MP2/6-31G(d, p)			
Geometry	C	0.677035	0.498124	-0.309197	C	0.675923	0.504428	-0.309211	
	C	-0.662985	0.488020	0.322663	C	-0.655261	0.500779	0.324671	
	F	1.534822	-0.407541	0.157889	F	1.544860	-0.420547	0.154443	
	H	0.816992	0.718417	-1.351872	H	0.832009	0.759019	-1.347153	
	H	-0.569840	0.337974	1.390090	H	-0.554565	0.350489	1.398563	
	F	-1.441693	-0.525564	-0.185381	F	-1.460414	-0.533506	-0.184986	
	H	-1.169613	1.424684	0.128418	H	-1.161426	1.445727	0.130719	
Frequency	115.4687	342.1953	504.4395	756.9889	120.6172	320.4455	473.9181	692.2178	
	980.8551	1133.9726	1208.8968	1304.9009	941.6135	1041.1494	1155.0870	1246.9089	
	1388.3461	1500.5257	1579.4454	1634.8579	1304.4692	1419.6995	1494.7826	1553.5416	
	3237.8124	3294.4744	3360.8591		3155.3309	3225.9724	3305.6741		

cis-(CHF...H...CHF)• TS

		HF/3-21G(d)				HF/6-31G(d)			
Geometry	C	0.744943	0.600922	-0.082689	C	0.737390	0.591760	-0.080689	
	C	-0.715743	0.580746	0.101977	C	-0.712398	0.573359	0.108243	
	F	1.379266	-0.612113	0.034896	F	1.336708	-0.599398	0.037028	
	H	1.237774	1.310195	-0.715453	H	1.251230	1.280053	-0.729761	
	H	0.136366	0.917975	1.096521	H	0.139785	0.888811	1.078167	
	F	-1.414701	-0.586483	-0.067950	F	-1.368532	-0.579363	-0.072146	
	H	-1.230417	1.469181	-0.199307	H	-1.254554	1.449264	-0.197666	
Frequency	-2678.7775	146.9232	244.5677	641.0494	-2671.8598	163.7945	274.8332	678.9248	
	808.8539	961.8311	1001.6652	1198.0052	829.5043	939.62882	1063.1396	1226.8259	
	1312.9766	1367.5483	1454.8863	1522.3895	1316.6138	1397.6834	1459.3274	1573.4784	
	1822.9869	3355.2196	3383.3339		2076.7896	3337.4618	3374.9625		

		HF/6-31G(d, p)				MP2/6-31G(d, p)		
Geometry	C	0.737939	0.592909	-0.075658	C	0.732139	0.587970	-0.125487
	C	-0.713835	0.575125	0.104018	C	-0.694233	0.564785	0.145360
	F	1.335400	-0.600302	0.034332	F	1.378090	-0.601139	0.058111
	H	1.253728	1.287989	-0.716487	H	1.241728	1.260143	-0.807810
	H	0.132779	0.885583	1.076332	H	0.196282	0.861906	1.038495
	F	-1.365917	-0.580948	-0.070124	F	-1.427716	-0.568753	-0.091105
	H	-1.256476	1.449478	-0.207875	H	-1.218816	1.490450	-0.052981
Frequency	-2631.2204	161.4158	270.5244	679.9009	-2486.7713	168.2383	333.8732	626.2408
	832.6340	939.9966	1063.0694	1227.7862	786.8807	845.4241	1005.8966	1132.2905
	1317.1727	1400.7168	1453.2343	1569.8015	1240.9506	1364.7986	1390.8793	1505.4621
	2117.8272	3315.5751	3350.7912		2358.4202	3220.2704	3275.4383	

trans-(CHF...H...CHF)• TS

		HF/3-21G(d)				HF/6-31G(d)		
Geometry	C	-0.616849	-0.381847	0.284006	C	0.614288	0.379419	0.277304
	C	0.616912	0.382051	0.283795	C	-0.614499	-0.378787	0.278099
	F	-1.752498	0.138496	-0.294314	F	1.719652	-0.141998	-0.285636
	H	-0.533697	-1.446064	0.226673	H	0.549265	1.447919	0.203555
	H	0.000130	0.000333	1.437892	H	-0.000209	0.001816	1.402572
	H	0.534245	1.446306	0.226055	H	-0.548780	-1.447347	0.205811
	F	1.752381	-0.138695	-0.294289	F	-1.719542	0.141311	-0.285959
Frequency	-2572.0871	249.0566	365.9114	445.1377	-2564.2270	244.0006	389.8406	453.7014
	818.4165	965.1513	1153.7926	1167.8271	800.5632	957.6146	1180.2083	1182.7385
	1295.3737	1318.5050	1479.3147	1566.3678	1306.8158	1327.0988	1489.9453	1604.4207
	1816.1046	3396.3374	3409.6404		2072.5808	3398.0948	3407.6846	

		HF/6-31G(d, p)				MP2/6-31G(d, p)			
Geometry	C	0.613520	0.380971	0.274246	C	0.616717	0.367612	0.292064	
	C	-0.613719	-0.380502	0.274805	C	-0.617055	-0.366445	0.293070	
	F	1.721598	-0.141863	-0.282621	F	1.749807	-0.138571	-0.302982	
	H	0.546702	1.449946	0.198774	H	0.563139	1.447024	0.279261	
	H	-0.000138	0.001442	1.395680	H	-0.000344	0.002397	1.384569	
	H	-0.546240	-1.449544	0.200568	H	-0.562911	-1.445866	0.283458	
	F	-1.721501	0.141345	-0.282860	F	-1.749569	0.137398	-0.303473	
Frequency	-2524.9824	244.7137	388.4327	454.0748	-2334.2143	268.3740	365.2053	436.0967	
	802.7890	953.8610	1180.4903	1181.6445	729.8280	894.7572	1065.7921	1103.5401	
	1304.6224	1328.7285	1483.4200	1600.2847	1271.3563	1280.6696	1483.2827	1505.4433	
	2111.6039	3373.9471	3383.5761		2347.2796	3295.7854	3306.3833		

CH_3-CF_2•

		HF/3-21G(d)				HF/6-31G(d)			
Geometry	C	0.054510	-0.000140	-0.303337	C	0.065567	-0.000092	-0.312546	
	C	-1.392938	-0.000967	0.045535	C	-1.381441	-0.000649	0.045969	
	F	0.736937	1.109843	0.063622	F	0.727830	1.080577	0.065850	
	F	0.738972	-1.108739	0.063664	F	0.729191	-1.079857	0.065883	
	H	-1.863607	-0.883752	-0.360222	H	-1.860349	-0.883486	-0.356264	
	H	-1.865029	0.880233	-0.362189	H	-1.860987	0.881578	-0.356987	
	H	-1.523972	0.000229	1.123649	H	-1.496605	-0.000126	1.127127	
Frequency	197.5574	370.6901	458.6629	548.5940	209.4705	396.5896	496.5329	582.4039	
	896.7909	1110.0164	1219.3499	1369.4378	937.1384	1089.8933	1210.5554	1398.2817	
	1417.7855	1590.1689	1644.2479	1650.5655	1399.9482	1576.3552	1620.0352	1623.3846	
	3199.3498	3283.7046	3320.4960		3205.9926	3288.0313	3321.6922		

		HF/6-31G(d, p)				MP2/6-31G(d, p)			
Geometry	C	0.064955	-0.000097	-0.312352	C	0.058952	-0.000090	-0.320334	
	C	-1.381185	-0.000687	0.046112	C	-1.383177	-0.000681	0.047937	
	F	0.727756	1.080523	0.065748	F	0.730454	1.103081	0.066958	
	F	0.729189	-1.079766	0.065785	F	0.731868	-1.102322	0.066988	
	H	-1.859525	-0.883770	-0.356582	H	-1.864254	-0.887995	-0.352301	
	H	-1.860141	0.881835	-0.357234	H	-1.865083	0.885701	-0.353483	
	H	-1.495458	-0.000173	1.127464	H	-1.486217	0.000087	1.134653	
Frequency	209.0658	397.0066	496.9165	582.3192	219.3280	375.7498	467.8536	542.1267	
	935.3118	1082.9849	1201.7220	1394.0448	893.1416	1018.7949	1144.0601	1301.2690	
	1395.8466	1562.1946	1602.7968	1606.5255	1316.7824	1471.4738	1537.4166	1540.2731	
	3185.7208	3270.1203	3303.9203		3131.9805	3235.6549	3273.8135		

CHF_2-CH_2•

		HF/3-21G(d)				HF/6-31G(d)			
Geometry	C	0.018615	-0.000026	0.344649	C	0.027074	-0.000025	0.337120	
	C	-1.396070	-0.000088	-0.093627	C	-1.392505	-0.000028	-0.098963	
	F	0.664378	-1.116225	-0.142244	F	0.660322	-1.086501	-0.141200	
	F	0.664192	1.116328	-0.142101	F	0.660258	1.086540	-0.141047	
	H	0.131090	-0.000104	1.414818	H	0.155444	-0.000120	1.410836	
	H	-1.911892	-0.932093	-0.180284	H	-1.924226	-0.929858	-0.149122	
	H	-1.911601	0.931957	-0.181560	H	-1.923851	0.929942	-0.150442	
Frequency	150.1110	401.9222	444.8643	494.7466	144.3428	410.5201	420.7866	525.9740	
	661.4273	1019.0507	1034.7458	1235.8679	688.5553	1017.6675	1071.5034	1278.7284	
	1293.2598	1523.9912	1550.5960	1575.8166	1290.1791	1533.6963	1557.3153	1598.0509	
	3284.0440	3344.8419	3467.9112		3278.9097	3351.1346	3466.9701		

		HF/6-31G(d, p)				MP2/6-31G(d, p)			
Geometry	C	0.026302	-0.000027	0.337750	C	0.018670	-0.000022	0.342370	
	C	-1.392103	-0.000047	-0.098869	C	-1.392276	-0.000069	-0.101631	
	F	0.660372	-1.086135	-0.141381	F	0.663604	-1.112699	-0.142385	
	F	0.660269	1.086193	-0.141219	F	0.663465	1.112776	-0.142237	
	H	0.152995	-0.000117	1.413970	H	0.149545	-0.000109	1.428112	
	H	-1.922162	-0.931001	-0.151224	H	-1.925925	-0.932887	-0.154813	
	H	-1.921791	0.931033	-0.152634	H	-1.925606	0.932852	-0.156132	
Frequency		140.4324	413.3244	419.9953	526.8814	155.7240	396.1766	431.6059	491.4370
		688.5099	1011.6152	1069.2203	1276.3969	654.2608	953.8885	1023.8541	1195.5161
		1286.6663	1522.0444	1547.0044	1588.0247	1198.6591	1431.6672	1445.1493	1520.0379
		3242.1276	3328.8603	3448.6757		3130.5756	3290.5151	3420.7831	

$(CH_2...H...CF_2)\bullet$ TS

		HF/3-21G(d)				HF/6-31G(d)			
Geometry	C	-0.016354	0.000134	0.222273	C	0.024854	-0.000136	0.222426	
	C	1.414550	-0.000584	-0.087724	C	-1.399089	-0.001362	-0.084474	
	F	-0.723410	1.118854	-0.073297	F	0.715675	-1.091723	-0.073866	
	F	-0.724472	-1.118353	-0.073272	F	0.713019	1.093108	-0.073804	
	H	0.907098	-0.000329	1.191774	H	-0.887199	0.000066	1.169471	
	H	1.867658	0.934003	-0.339980	H	-1.862417	-0.936129	-0.333295	
	H	1.867006	-0.935485	-0.339961	H	-1.863211	0.932587	-0.334862	
Frequency		-2661.9373	271.4450	409.7865	483.2204	-2640.4738	283.5269	427.6874	514.3204
		617.8519	918.0630	972.6147	1020.9072	647.7289	828.9608	1017.5656	1026.2595
		1291.4375	1404.5838	1435.0063	1541.1883	1309.1477	1438.7801	1443.1554	1573.5664
		1851.2009	3350.9166	3481.1535		2093.5202	3349.2115	3475.0181	

		HF/6-31G(d, p)				MP2/6-31G(d, p)			
Geometry	C	0.023986	-0.000230	0.221305	C	0.017178	0.000181	0.218692	
	C	-1.400397	-0.001922	-0.083126	C	-1.408296	-0.001882	-0.084530	
	F	0.716842	-1.091113	-0.073608	F	0.722486	-1.117949	-0.072412	
	F	0.713094	1.093071	-0.073517	F	0.718925	1.119745	-0.072365	
	H	-0.886324	0.000190	1.166340	H	-0.874752	-0.000453	1.135384	
	H	-1.861872	-0.937095	-0.334508	H	-1.874334	-0.944059	-0.317757	
	H	-1.862762	0.932197	-0.336781	H	-1.876904	0.938560	-0.319604	
Frequency	-2606.4130	282.9838	426.0154	514.4156	-2512.0092	242.9633	404.2734	468.8546	
	647.5450	832.93431	1016.8343	1019.5061	617.7437	737.89831	948.9237	952.5699	
	1312.6500	1435.0372	1443.0391	1565.6106	1258.1216	1363.5085	1386.9589	1476.7871	
	2128.4430	3326.7868	3455.5149		2379.3500	3273.4314	3416.3222		

$CH_2F\text{-}CF_2\bullet$

		HF/3-21G(d)				HF/6-31G(d)			
Geometry	C	-0.550649	-0.000032	0.378809	C	-0.557486	-0.000007	0.398403	
	C	0.909956	-0.001206	0.632828	C	0.916181	-0.000400	0.619462	
	F	-1.063500	1.110758	-0.180590	F	-1.037502	1.080331	-0.178258	
	F	-1.064837	-1.109846	-0.181716	F	-1.037702	-1.080144	-0.178678	
	H	1.169036	0.879860	1.192289	H	1.200203	0.884512	1.168779	
	F	1.629138	0.000423	-0.576752	F	1.569386	0.000262	-0.581248	
	H	1.167908	-0.884436	1.189408	H	1.199986	-0.886114	1.167693	
Frequency	95.8008	205.4600	360.4293	526.9793	94.9551	227.2807	389.7133	562.5845	
	735.8868	868.8681	1093.4320	1119.6390	802.5246	929.12391	1087.7984	1172.9895	
	1333.7914	1417.6964	1504.8663	1556.8854	1349.1838	1444.8727	1470.6375	1587.4373	
	1675.8338	3297.9881	3350.6885		1654.1574	3285.7842	3344.6983		

		HF/6-31G(d, p)				MP2/6-31G(d, p)			
Geometry	C	-0.556974	-0.000018	0.398108	C	-0.560273	-0.000038	0.406489	
	C	0.916120	-0.000490	0.619097	C	0.910593	-0.001188	0.634113	
	F	-1.037748	1.080276	-0.178273	F	-1.040761	1.102587	-0.184282	
	F	-1.038113	-1.079993	-0.178769	F	-1.042102	-1.101687	-0.185413	
	H	1.198366	0.885053	1.170664	H	1.190230	0.889767	1.192038	
	F	1.570157	0.000267	-0.581103	F	1.584925	0.000427	-0.588612	
	H	1.198099	-0.886952	1.169416	H	1.189284	-0.894348	1.189107	
Frequency		94.7264	227.3307	389.6110	562.7012	96.3105	208.2160	370.0038	521.1019
		802.4586	928.0408	1081.6532	1173.1233	753.9038	878.2984	1017.3581	1077.1461
		1345.7118	1441.3178	1465.3288	1579.2628	1254.7988	1358.5635	1372.0165	1477.3168
		1635.2488	3256.1958	3316.4270		1554.3540	3172.2997	3245.5998	

CF_2H-CHF•

		HF/3-21G(d)				HF/6-31G(d)			
Geometry	C	-0.566132	-0.044655	0.432086	C	-0.564222	-0.043995	0.428446	
	C	0.883248	-0.293090	0.585655	C	0.905458	-0.163218	0.618563	
	F	-0.772896	1.213004	-0.071318	F	-0.861640	1.141793	-0.113573	
	F	-1.138559	-0.941973	-0.447056	F	-1.014974	-0.992555	-0.414118	
	H	-1.062640	-0.139708	1.377539	H	-1.092429	-0.146810	1.363153	
	F	1.680605	0.094395	-0.441657	F	1.624229	0.109459	-0.459254	
	H	1.237596	-1.122654	1.156299	H	1.316483	-0.938185	1.237303	
Frequency		82.5871	233.0706	355.2779	526.6035	90.6962	246.1734	390.2725	562.0895
		678.5183	801.9170	949.9575	1186.0151	777.4527	841.0943	984.3717	1224.5873
		1237.8158	1330.6572	1523.1430	1539.3600	1260.3219	1344.8181	1526.5354	1549.5809
		1579.3615	3346.2456	3411.2950		1596.8958	3327.5441	3393.6325	

		HF/6-31G(d, p)				MP2/6-31G(d, p)			
Geometry	C	-0.563902	-0.044098	0.428794	C	-0.562292	-0.041411	0.440868	
	C	0.905479	-0.161876	0.618174	C	0.901584	-0.180588	0.625072	
	F	-0.862876	1.141008	-0.114331	F	-0.842611	1.173965	-0.116022	
	F	-1.014062	-0.993078	-0.413777	F	-1.039701	-1.004031	-0.421433	
	H	-1.090848	-0.147418	1.366534	H	-1.098229	-0.136651	1.385047	
	F	1.623833	0.108934	-0.460233	F	1.631473	0.098119	-0.467553	
	H	1.319332	-0.928522	1.246728	H	1.320020	-0.943825	1.264385	
Frequency		90.6373	246.3047	389.8436	562.4931	89.6448	230.8624	364.1095	514.9091
		766.4239	840.7887	982.7400	1223.7901	704.5746	790.5257	947.6419	1112.2867
		1259.8504	1343.9404	1517.7338	1541.5858	1166.5765	1268.5731	1419.8554	1457.5378
		1590.7265	3291.7376	3368.8044		1496.8768	3185.9770	3306.9233	

$(CF_2...H...CHF)\bullet$ TS

		HF/3-21G(d)				HF/6-31G(d)			
Geometry	C	-0.525829	-0.041748	0.278018	C	-0.521774	-0.039373	0.277204	
	C	0.824223	-0.577660	0.300250	C	0.820095	-0.588918	0.279942	
	F	-0.634736	1.279904	0.020120	F	-0.613053	1.249762	0.021300	
	F	-1.533612	-0.737619	-0.299018	F	-1.516402	-0.709913	-0.287908	
	H	0.135073	-0.249969	1.474914	H	0.140150	-0.273364	1.432676	
	F	1.855426	0.081069	-0.305311	F	1.813953	0.093537	-0.290061	
	H	0.890861	-1.643766	0.313357	H	0.909444	-1.657362	0.234468	
Frequency		-2622.3514	164.9146	230.0177	389.1623	-2662.3575	156.2433	246.2135	407.4071
		540.8378	709.07151	874.0571	928.2277	570.7227	731.2211	867.6871	977.7162
		1202.4030	1260.8588	1382.7646	1428.8594	1223.7643	1269.3181	1389.0749	1441.8153
		1562.2087	1705.7754	3413.1075		1623.4211	1958.4646	3403.9471	

		HF/6-31G(d, p)				MP2/6-31G(d, p)			
Geometry	C	-0.520730	-0.039480	0.275237	C	-0.519427	-0.048265	0.271739	
	C	0.819769	-0.592051	0.275415	C	0.828277	-0.558580	0.320310	
	F	-0.612250	1.250284	0.021350	F	-0.636514	1.269745	0.027995	
	F	-1.519745	-0.708037	-0.285173	F	-1.540053	-0.735384	-0.303481	
	H	0.141810	-0.278214	1.424336	H	0.127468	-0.208441	1.403420	
	F	1.816057	0.094254	-0.286589	F	1.853551	0.074617	0.320676	
	H	0.907398	-1.661112	0.225465	H	0.926582	-1.631289	0.409744	
Frequency	-2633.1260	157.3018	245.9846	407.8352	-2556.7602	168.4857	243.8996	373.6846	
	571.2127	728.2321	867.8895	977.5386	534.0379	671.1052	804.0621	910.6117	
	1223.9770	1273.8532	1391.1327	1441.0703	1104.1297	1196.7347	1350.9688	1401.4384	
	1622.9399	2015.2020	3379.8847		1523.3595	2308.6734	3300.6734		

CF_2-CF_2•

		HF/3-21G(d)				HF/6-31G(d)			
Geometry	C	0.682479	-0.000004	-0.255877	C	-0.692157	-0.000012	-0.268669	
	C	-0.693621	-0.000005	0.325709	C	0.693969	-0.000022	0.313722	
	F	1.383698	-1.109582	0.018684	F	-1.374749	1.080982	0.023576	
	F	1.383682	1.109592	0.018658	F	-1.374791	-1.080965	0.023645	
	H	-0.681419	-0.000017	1.399847	H	0.684167	-0.000067	1.393787	
	F	-1.342120	-1.115690	-0.119732	F	1.336143	1.086280	-0.116020	
	F	-1.342119	1.115688	-0.119704	F	1.336170	-1.086267	-0.116102	
Frequency	69.3263	197.2965	363.6376	403.0099	78.7359	216.8367	386.1255	438.9825	
	511.1129	551.1212	651.4352	1055.3756	532.8349	586.1466	690.6458	1121.8893	
	1219.0292	1299.7951	1367.1297	1422.2332	1260.9996	1303.7032	1388.9279	1413.2538	
	1535.2256	1559.2837	3320.9041		1544.1720	1605.4928	3311.0597		

		HF/6-31G(d, p)				MP2/6-31G(d, p)			
Geometry	C	-0.691883	-0.000013	-0.268626	C	-0.691702	-0.000002	-0.272048	
	C	0.693833	-0.000022	0.314239	C	0.693961	-0.000010	0.318671	
	F	-1.374661	1.080963	0.023413	F	-1.384149	1.104479	0.023301	
	F	-1.374702	-1.080946	0.023483	F	-1.384168	-1.104470	0.023319	
	H	0.681902	-0.000068	1.396276	H	0.683180	-0.000022	1.410694	
	F	1.336134	1.086022	-0.116181	F	1.345448	1.112322	-0.117212	
	F	1.336162	-1.086008	-0.116265	F	1.345454	-1.112320	-0.117234	
Frequency		78.9345	216.9817	386.1491	439.3408	75.5458	201.6885	358.5157	405.1087
		532.8666	586.3685	690.6012	1120.6170	495.1319	536.2250	642.5455	1046.3521
		1260.8840	1303.0365	1384.1574	1412.9247	1166.6397	1198.3350	1296.0285	1305.4396
		1535.2807	1600.2022	3276.6197		1432.4143	1484.7850	3161.4557	

$(CF_2...H...CF_2)$• TS

		HF/3-21G(d)				HF/6-31G(d)			
Geometry	C	0.732565	0.023239	0.278232	C	-0.731676	-0.020880	0.276992	
	C	-0.732568	-0.023366	0.278257	C	0.731672	0.020771	0.276927	
	F	1.360420	-1.113787	-0.071822	F	-1.347876	1.084653	-0.077137	
	F	1.335100	1.126187	-0.197325	F	-1.320639	-1.099519	-0.189027	
	H	0.000017	-0.000130	1.505524	H	0.000041	-0.000148	1.467479	
	F	-1.335397	-1.126130	-0.197342	F	1.320357	1.099572	-0.189002	
	F	-1.360123	1.113829	-0.071785	F	1.348156	-1.084617	-0.077166	
Frequency		-2650.4601	24.8572	189.9656	300.5277	-2719.5676	25.5050	220.9667	324.2422
		478.1955	519.3211	533.2173	721.5931	508.2718	549.6814	567.4731	745.1414
		872.4067	1108.9238	1183.7304	1399.9899	930.5832	1164.3482	1210.1346	1423.8499
		1432.4085	1480.1628	1618.7668		1440.6384	1639.2670	1828.3032	

		HF/6-31G(d, p)				MP2/6-31G(d, p)		
Geometry	C	-0.731869	0.008425	0.275644	C	0.728080	0.048652	0.263693
	C	0.731856	-0.008458	0.275612	C	-0.728086	-0.048647	0.263703
	F	-1.330793	1.096367	-0.155550	F	1.377410	-1.103452	0.027071
	F	-1.341478	-1.090764	-0.109284	F	1.338861	1.117601	-0.280397
	H	-0.000054	-0.000124	1.459269	H	0.000015	-0.000067	1.395554
	F	1.341390	1.090779	-0.109258	F	-1.338843	-1.117599	-0.280405
	F	1.330896	-1.096345	-0.155552	F	-1.377426	1.103453	0.027072
Frequency	-2709.8323	10.8025	220.5337	325.3092	-2830.2340	65.8085	192.3124	294.8069
	510.8808	547.9418	567.0815	738.3877	457.8389	512.7727	531.3308	649.6044
	932.1457	1185.2486	1209.1896	1423.7982	869.3042	1090.5695	1229.7582	1289.8161
	1442.2967	1656.6430	1893.8035		1353.0662	1560.8724	2247.5763	

[a] Cartesian Coordinates in 10^{-10} m, Harmonic Frequencies in cm^{-1}

Table 8.3. Optimized geometries (in cartesian coordinates) and harmonic vibrational frequencies of the transition state for the addition reaction of hydroxyl radical with ethylene at Various Levels of Theory [a]

HF/3-21G(d)

	X	Y	Z
C	0.000000	0.000000	0.000000
C	0.000000	0.000000	1.393402
O	1.826247	0.000000	-0.508744
H	-0.238079	-0.904959	-0.521370
H	-0.238079	0.904959	-0.521370
H	0.035875	0.917489	1.949387
H	0.035875	-0.917489	1.949387
H	2.257820	0.000000	0.371357

-556.9777	97.2824	303.8793
473.8102	820.0502	894.6449
982.1910	1042.4911	1091.5151
1271.4181	1361.3785	1620.1230
1672.9710	3303.3420	3337.1397
3387.5097	3425.5082	3689.6692

HF/6-31G(d,p)

	X	Y	Z
C	0.000000	0.000000	0.000000
C	0.000000	0.000000	1.392656
O	1.849570	0.000000	-0.530636
H	-0.241990	-0.905960	-0.522238
H	-0.225379	0.909809	-0.522547
H	0.063142	0.918560	1.948465
H	0.038696	-0.919913	1.948926
H	2.275299	-0.103619	0.313058

-603.4289	29.1328	291.6334
457.7068	803.7238	863.9639
956.4109	1019.2056	1068.9416
1270.1789	1333.9788	1589.1711
1666.4010	3302.0618	3331.6003
3393.2475	3427.4235	4101.4750

HF/6-311G(d,p)

	X	Y	Z
C	0.000000	0.000000	0.000000
C	0.000000	0.000000	1.391784
O	1.848775	0.000000	-0.524408
H	-0.257864	-0.902501	-0.521050
H	-0.209500	0.913519	-0.522159
H	0.091757	0.917108	1.946081
H	0.020779	-0.921312	1.947663
H	2.259960	-0.306944	0.271932

-622.0502	89.9147	289.2661
454.6897	803.7444	859.9492
941.1051	1018.4797	1064.5063
1260.1850	1325.8044	1575.9404
1651.3707	3273.3299	3305.7802
3363.8175	3400.4892	4097.5035

MP2/6-31G(d,p)

	X	Y	Z
C	0.000000	0.000000	0.000000
C	0.000000	0.000000	1.338274
O	2.026396	0.000000	-0.328138
H	-0.149102	-0.911260	-0.556989
H	-0.073929	0.920208	-0.556679
H	0.065928	0.919406	1.899757
H	-0.025166	-0.921194	1.901395
H	2.354026	-0.304986	0.534311

-538.3097	84.2334	238.6226
412.3790	795.9837	857.2300
962.0575	1061.0043	1121.0950
1282.5384	1392.5872	1531.8946
1694.6815	3259.3626	3279.7225
3360.1745	3387.6415	3828.4769

MP2/6-311G(d,p)

	X	Y	Z
C	0.000000	0.000000	0.000000
C	0.000000	0.000000	1.339822
O	2.021139	0.000000	-0.289777
H	-0.168666	-0.912824	-0.556511
H	-0.059386	0.926689	-0.555266
H	0.093468	0.922706	1.899627

H	-0.040570	-0.925744	1.902983
H	2.315655	-0.474920	0.498999

-574.0987	144.6504	245.0922
421.9960	776.2456	842.6180
941.9395	1053.4058	1113.2027
1256.3491	1369.9311	1493.6855
1657.2925	3200.6911	3222.8827
3298.9072	3328.8345	3836.7464

QCISD/6-31G(d,p)

	X	Y	Z
C	0.000000	0.000000	0.000000
C	0.000000	0.000000	1.361049
O	2.064582	0.000000	-0.358357
H	-0.186070	-0.907329	-0.556252
H	-0.060724	0.923826	-0.555170
H	0.105881	0.917687	1.922429
H	-0.045667	-0.922003	1.925721
H	2.322840	-0.569458	0.387182

-415.3498	130.8534	227.8474
378.0775	771.4177	844.0484
871.4434	982.8027	1024.7709
1268.0165	1343.6767	1522.1538
1647.4654	3222.9664	3246.2391
3316.7820	3345.4286	3793.8072

[a] Cartesian Coordinates in 10^{-10} m, Harmonic Frequencies in cm^{-1}

Table 8.4. Optimized geometries (in cartesian coordinates) and harmonic vibrational frequencies of OH, chloroethylenes and transition states for the reaction of hydroxyl radical with chloroethylenes at the HF/6-31G(d,p) level of theory [a]

OH

	X	Y	Z
O	0.000000	0.000000	-0.106100
H	0.000000	0.000000	0.848796

4053.8155

CH_2=CHCl

	X	Y	Z
C	-0.743494	0.000000	0.159464
C	-0.749678	0.000000	1.470579
Cl	0.713121	0.000000	-0.787249
H	-1.630628	0.000000	-0.442281
H	-1.687909	0.000000	1.995072
H	0.154514	0.000000	2.050187

430.8999	696.8834	772.9946
1076.7576	1089.1716	1138.6917
1422.5750	1532.2360	1839.1748
3329.8962	3403.9023	3425.4379

OH...CH_2-CHCl (TS, OH at CH_2 end)

	X	Y	Z
C	0.000000	0.000000	0.000000
C	0.000000	0.000000	1.386603
O	1.853124	0.000000	-0.542377
Cl	0.131270	1.473023	2.289961
H	0.079017	-0.886673	1.982207
H	-0.244118	-0.920202	-0.494252
H	-0.240103	0.905068	-0.523132
H	2.196635	0.637499	0.074533

-604.2038	122.9456	181.1035
298.4630	414.8053	644.8802
760.8739	912.3398	1002.6652
1041.3675	1141.6965	1299.8225
1446.4321	1626.2804	3339.4519
3404.7850	3440.0432	4099.0541

CH_2-CHCl... OH (TS, OH at CHCl end)

	X	Y	Z
C	0.000000	0.000000	0.000000
C	0.000000	0.000000	1.389843
O	1.884912	0.000000	-0.451999
Cl	-0.475684	-1.481599	-0.812692
H	-0.277934	0.865672	-0.564035
H	0.073892	0.934670	1.914088
H	0.072326	-0.914861	1.946922
H	2.152245	-0.745586	0.075651

-614.4397	164.0625	246.9105
305.9095	428.6509	515.7482
743.0279	788.5476	946.3676
1050.5988	1119.0089	1295.8642
1433.5056	1608.3160	3320.7598
3419.2613	3433.5975	4093.8556

CH_2=CCl_2

	X	Y	Z
C	0.000000	0.000000	0.000000
C	0.000000	0.000000	1.310750
Cl	1.452799	0.000000	-0.936160
Cl	-1.452849	0.000000	-0.936120
H	-0.923972	0.000000	1.855867
H	0.923972	0.000000	1.855868

324.4828	410.6174	522.0643
654.0985	777.7882	877.1737
1067.8313	1219.1428	1536.2544
1847.3524	3348.7277	3445.9101

OH...CH_2-CCl_2 (TS, OH at CH_2 end)

	X	Y	Z
C	0.000000	0.000000	0.000000
C	0.000000	0.000000	1.387545
O	1.858192	0.000000	-0.561727
Cl	0.076827	1.471733	2.284958
Cl	0.183564	-1.445965	2.296925
H	-0.283778	0.904969	-0.500143
H	-0.205206	-0.924875	-0.499676
H	2.212982	0.654186	0.032338

-586.0828	101.8126	137.7371
185.7027	319.3287	387.2939
413.2539	630.9007	840.7231
916.5835	972.1696	1028.0289
1229.0238	1360.8394	1613.5493
3349.8063	3455.6917	4087.3563

CH_2-CCl_2...OH (TS, OH at CCl_2 end)

	X	Y	Z
C	0.000000	0.000000	0.000000
C	0.000000	0.000000	1.397216
O	1.893755	0.000000	-0.380404
Cl	-0.534983	-1.446696	-0.813505
Cl	-0.411530	1.467493	-0.827868
H	0.011280	-0.930020	1.932118
H	0.155226	0.921302	1.922970
H	2.155856	-0.814136	0.038955

-623.9848	210.8697	218.7997
235.2036	337.8205	372.9218
388.4292	518.0459	627.5600
762.9727	854.3151	988.4949
1210.9135	1334.3125	1594.4518
3333.7929	3449.3133	4083.1499

cis-CHCl=CHCl

	X	Y	Z
C	0.000000	0.000000	0.000000
C	0.000000	0.000000	1.312019
Cl	1.398332	0.000000	-1.003887
H	-0.926271	0.000000	-0.539003
Cl	1.398332	0.000000	2.315907
H	-0.926271	0.000000	1.851022

183.5235	463.3618	619.9044
769.8197	813.8892	931.8506
1060.5788	1334.3411	1452.6427
1841.0851	3396.2503	3419.9867

cis-CHCl-CHCl...OH (TS)

	X	Y	Z
C	0.000000	0.000000	0.000000
C	0.000000	0.000000	1.394244
O	1.890352	0.000000	-0.430462

Cl	-0.479393	-1.431270	-0.873399
H	-0.300175	0.896198	-0.502838
Cl	0.169976	-1.411392	2.358267
H	0.111304	0.924211	1.924780
H	2.112439	-0.826665	-0.012694

-618.4592	112.5229	187.1232
222.4625	254.3161	356.9918
595.1717	656.6438	732.7976
889.6617	972.6341	1041.7550
1248.7383	1429.7366	1475.8287
3399.1819	3422.2302	4085.9532

trans-CHCl=CHCl

	X	Y	Z
C	0.000000	0.000000	0.000000
C	0.000000	0.000000	1.310216
Cl	1.471547	0.000000	-0.909580
H	-0.889950	0.000000	-0.595934
Cl	-1.471552	0.000000	2.219796
H	0.889946	0.000000	1.906155

237.0797	260.6687	380.2673
888.1855	922.3176	930.1357
1059.9669	1345.0172	1428.0867
1836.6932	3417.4633	3423.3671

trans-CHCl-CHCl...OH (TS)

	X	Y	Z
C	0.000000	0.000000	0.000000
C	0.000000	0.000000	1.390495
O	1.888120	0.000000	-0.484319
Cl	-0.489565	-1.496817	-0.762614
H	-0.283263	0.866061	-0.560062
Cl	0.135103	1.477321	2.260062
H	0.081720	-0.893588	1.975147
H	2.160153	-0.773005	0.000736

-593.7771	121.7907	144.6498
231.9202	262.1264	328.2918
374.4993	647.3967	846.2345
896.3971	966.1895	1031.3189
1300.6875	1329.1638	1510.1659
3408.8034	3433.8754	4087.7895

CCl_2=CHCl

	X	Y	Z
H	0.000000	0.000000	0.000000
C	0.000000	0.000000	1.070516
C	1.131303	0.000000	1.739534
Cl	2.636283	0.000000	0.891484
Cl	1.258190	0.000000	3.450433
Cl	-1.560300	0.000000	1.787633

189.2423	230.3148	301.8843
420.2909	536.0136	685.9917
915.0593	957.5517	1042.4109
1409.2905	1842.5256	3423.4619

OH...CCl_2-CHCl (TS, OH at CCl_2 end)

	X	Y	Z
C	0.000000	0.000000	0.000000
C	0.000000	0.000000	1.404845
O	1.902438	0.000000	-0.374465
Cl	-0.552556	-1.392674	-0.870399
Cl	-0.406228	1.513488	-0.741236
Cl	0.146747	-1.431444	2.336854
H	0.152568	0.917058	1.934774
H	2.138596	-0.857160	-0.030802

-613.5972	110.2144	173.3470
224.5121	237.6503	254.9267
306.7913	367.3506	420.0111
638.4431	656.9806	888.7641
956.8754	1057.9035	1320.3419
1460.7206	3420.2971	4077.0105

CCl_2-CHCl...OH (TS, OH at CHCl end)

	X	Y	Z
C	0.000000	0.000000	0.000000
C	0.000000	0.000000	1.398738
O	1.891290	0.000000	-0.462269
Cl	-0.031431	1.426269	2.347674
Cl	0.356846	-1.461602	2.223636
Cl	-0.660246	1.342558	-0.870823
H	-0.140256	-0.938904	-0.491946
H	2.127483	0.860486	-0.128317

-598.4447	82.1834	141.5296

189.2674	201.2402	230.9963
304.6253	398.6876	425.0870
657.6113	865.0965	961.0236
1007.6275	1056.0935	1338.1560
1468.9723	3431.3783	4083.4440

[a] Cartesian Coordinates in 10^{-10} m, Harmonic Frequencies in cm^{-1}

Table 8.5. Optimized geometries (in cartesian coordinates) and harmonic vibrational frequencies of OH, tetrachloroethylene and transition state for the reaction of OH with tetrachloroethylene at the HF/6-31G(d) level of theory [a]

OH

	X	Y	Z
H	0.000000	0.000000	-0.851973
O	0.000000	0.000000	0.106497

3996.9028

CCl_2=CCl_2

	X	Y	Z
Cl	0.000000	0.000000	0.000000
C	0.000000	0.000000	1.717531
C	1.111195	0.000000	2.433686
Cl	2.675357	0.000000	1.724243
Cl	1.111195	0.000000	4.151217
Cl	-1.564163	0.000000	2.426974

110.1237	198.0931	262.9232
334.9504	344.5973	378.9579
487.9528	643.2111	850.2853
999.6350	1116.9385	1824.1380

OH...CCl_2-CCl_2 (TS)

	X	Y	Z
C	-0.071074	0.007984	-0.633649
C	-0.112144	0.012372	0.784163
O	1.850958	0.001765	-0.941990
Cl	-0.596902	-1.424696	-1.460419

Cl	-0.467188	1.465596	-1.468829
Cl	0.122104	1.449491	1.677889
Cl	0.013937	-1.446741	1.678844
H	2.068476	-0.878298	-0.634402

-595.5711	65.0221	139.8073
184.0388	217.3923	228.2274
253.8878	291.8522	356.1286
363.1569	426.8795	477.2412
824.0940	929.8777	1022.1888
1105.4111	1366.8666	4011.5541

[a] Cartesian Coordinates in 10^{-10} m, Harmonic Frequencies in cm^{-1}.

Table 8.6. Sum of rate constants (k_{TST}) at each point along with the reaction path at various temperatures for the reaction OH + CH_2=CHCl → adduct (OH at CH_2 end) [a]

T / K	$R_{c\text{-}o}$ / Å									
	2.064	2.083	2.103	2.123	2.143	2.163	2.182	2.202	2.221	2.241
200	31.955	19.249	10.654	7.9340	5.8507	5.1555	4.6594	5.1596	**4.6573**	5.5379
250	14.481	10.028	6.1927	5.0366	3.9577	3.6527	**3.4014**	3.8198	3.4626	4.1156
300	9.0072	6.8530	4.5510	3.9293	3.2217	3.0688	**2.9164**	3.3094	3.0074	3.5778
350	6.7103	5.4638	3.8220	3.4451	2.9121	2.8383	**2.7374**	3.1315	2.8503	3.3952
400	5.5861	4.7877	3.4817	3.2427	2.8045	2.7816	**2.7129**	3.1233	2.8460	3.3945
450	4.9974	4.4585	3.3417	3.1930	2.8112	2.8268	**2.7812**	3.2186	2.9350	3.5051
500	4.6927	4.3248	3.3199	3.2383	**2.8922**	2.9406	2.9136	3.3862	3.0896	3.6938
550	4.5570	4.3117	3.3764	3.3496	**3.0268**	3.1056	3.0950	3.6099	3.2950	3.9434
600	4.5314	4.3834	3.4893	3.5111	**3.2039**	3.3124	3.3171	3.8806	3.5432	4.2443
650	4.5831	4.5176	3.6463	3.7135	**3.4166**	3.5553	3.5750	4.1931	3.8295	4.5908
700	4.6929	4.7012	3.8398	3.9512	**3.6610**	3.8309	3.8657	4.5443	4.1509	4.9797
800	5.0429	5.1864	4.3185	4.5193	**4.2357**	4.4726	4.5391	5.3557	4.8933	5.8774
900	5.5266	5.8016	**4.0936**	5.1994	4.9168	5.2287	5.3300	6.3072	5.7636	6.9294
1000	6.1189	6.5299	**5.5854**	5.9850	5.7002	6.0962	6.2365	7.3973	6.7603	8.1343

[a] k_{TST} in 10^{-12} cm^3 $molecule^{-1}$ s^{-1}; bold number is the minimum at each temperature.

Table 8.7. Sum of rate constants (k_{TST}) at each point along with the reaction path at various temperatures for the reaction OH + CH_2=CHCl → adduct (OH at CHCl end) [a]

T / K	$R_{c\text{-}o}$ / Å									
	2.069	2.089	2.108	2.128	2.148	2.167	2.187	2.206	2.225	2.245
200	69.223	23.857	11.918	8.2572	6.3926	5.9279	**5.9200**	7.2534	8.6377	11.891
250	277.23	110.03	61.514	45.416	36.847	34.841	**34.744**	41.330	47.779	62.418
300	740.89	322.87	194.50	149.79	125.38	120.12	**119.68**	139.63	158.30	199.78
350	1568.9	730.70	464.21	368.40	315.32	304.92	**303.67**	349.45	390.75	481.21
400	2865.8	1402.6	927.20	752.54	654.96	637.79	**634.97**	723.22	800.41	967.84
450	4731.2	2406.4	1640.7	1355.0	1194.7	1169.6	**1164.2**	1315.4	1444.2	1721.7
500	7261.3	3808.4	2661.3	2228.5	1985.3	1952.0	**1942.6**	2180.9	2379.2	2804.3
550	10548	5672.5	4044.4	3425.2	3077.3	3036.0	**3021.0**	3373.8	3661.4	4275.7
600	14680	8060.7	5844.1	4996.0	4520.1	4472.1	**4449.5**	4947.2	5345.5	6194.0
650	19742	11032	8112.3	6990.1	6361.9	6309.2	**6276.7**	6952.6	7484.5	8615.7
700	25815	14645	10900	9455.3	8649.2	8594.8	**8549.7**	9439.8	10130	11595
800	41303	24009	18222	15982	14739	14694	**14614**	16050	17134	19432
900	61729	36567	28179	24923	23132	23117	**22988**	25142	26730	30100
1000	87635	52701	41108	36604	34145	34188	**33993**	37054	39265	43961

[a] k_{TST} in 10^{-17} cm^3 $molecule^{-1}$ s^{-1}; bold number is the minimum at each temperature.

Table 8.8. Sum of rate constants (k_{TST}) at each point along with the reaction path at various temperatures for the reaction OH + CH_2=CCl_2 → adduct (OH at CH_2 end) [a]

T / K	$R_{c\text{-}o}$ / Å									
	2.043	2.083	2.103	2.123	2.143	2.163	2.182	2.202	2.221	2.241
200	494.29	136.86	62.953	44.078	32.189	30.211	22.515	23.938	**22.429**	24.871
250	143.93	53.749	29.193	22.626	17.895	17.819	**13.856**	15.229	14.540	16.306
300	66.931	35.549	18.543	15.390	12.842	13.315	**10.649**	11.977	11.582	13.096
350	40.526	21.396	14.847	12.249	10.624	11.345	**9.2560**	10.591	10.336	11.762
400	28.857	16.968	11.844	10.722	9.5749	10.457	**8.6610**	10.042	9.8999	11.288
450	22.840	14.626	10.699	9.9740	9.1130	10.131	**8.4895**	9.9471	9.8315	11.290
500	19.429	13.326	10.121	9.6610	8.9911	10.140	**8.5771**	10.137	10.064	11.599
550	17.388	12.618	9.8842	9.6200	9.0896	10.374	**8.8422**	10.525	10.488	12.120
600	16.143	12.281	9.8716	9.7654	9.3448	10.772	**9.2405**	11.065	11.062	12.813
650	15.398	12.193	10.018	10.049	**9.7199**	11.300	9.7462	11.731	11.756	13.649
700	14.989	12.286	10.286	10.440	**10.193**	11.937	10.344	12.506	12.564	14.611
800	14.823	12.852	**11.094**	11.483	11.381	13.489	11.777	14.344	14.465	16.872
900	15.217	13.786	**12.188**	12.808	12.845	15.369	13.498	16.534	16.722	19.551
1000	15.981	14.998	**13.516**	14.378	14.557	17.550	15.486	19.058	19.320	22.632

[a] k_{TST} in 10^{-12} cm^3 $molecule^{-1}$ s^{-1}; bold number is the minimum at each temperature.

Table 8.9. Sum of rate constants (k_{TST}) at each point along with the reaction path at various temperatures for the reaction OH + CH_2=CCl_2 → adduct (OH at CCl_2 end) [a]

T / K	$R_{c\text{-}o}$ / Å						
	2.057	2.077	2.097	2.117	2.137	2.157	2.177
200	4.1558	2.6858	1.9296	1.8592	**1.6903**	1.9714	2.2996
250	4.315	10.246	7.8538	7.8810	**7.2527**	8.3907	9.5174
300	34.859	26.716	21.378	22.062	**20.461**	23.558	26.227
350	69.379	55.841	46.069	48.529	**45.248**	51.932	57.047
400	121.28	101.28	**85.480**	91.467	85.610	98.041	106.62
450	193.82	166.56	**143.09**	155.01	145.51	166.36	179.49
500	290.13	255.13	**222.27**	243.22	228.81	261.27	280.10
550	413.24	370.28	**326.31**	360.02	339.28	387.03	412.76
600	566.04	515.22	**458.38**	509.24	480.58	547.76	581.60
650	751.32	693.00	**621.52**	694.54	656.22	747.44	790.64
700	971.76	906.60	**818.67**	919.50	869.60	989.88	1043.7
800	1528.3	1452.4	**1326.2**	1501.9	1422.5	1617.7	1696.7
900	2255.1	2174.1	**2002.3**	2282.2	2164.0	2459.1	2568.4
1000	3169.9	3091.5	**2866.8**	3284.4	3117.0	3539.8	3684.8

[a] k_{TST} in 10^{-16} cm^3 $molecule^{-1}$ s^{-1}; bold number is the minimum at each temperature.

Table 8.10. Sum of rate constants (k_{TST}) at each point along with the reaction path at various temperatures for the reaction OH + cis-CHCl=CHCl → adduct [a]

T / K	$R_{c\text{-}o}$ / Å				
	2.123	2.122	2.162	2.181	2.201
200	4.9650	3.9505	**3.6470**	3.9217	4.5543
250	23.480	19.544	**18.413**	19.707	22.453
300	70.205	60.206	**57.490**	61.342	69.009
350	161.09	141.12	**136.05**	144.85	161.48
400	312.35	278.01	**269.96**	286.95	317.74
450	539.93	486.55	**475.11**	504.37	555.53
500	859.30	782.02	**767.04**	813.45	892.16
550	1285.4	1179.2	**1160.8**	1230.0	1344.4
600	1832.5	1692.5	**1671.1**	1769.4	1928.3
650	2514.5	2335.4	**2311.9**	2446.4	2659.3
700	3344.5	3121.4	**3096.6**	3275.0	3552.5
800	5498.8	5172.2	**5149.2**	5440.9	5881.2
900	8390.8	7940.2	**7926.3**	8369.4	9021.7
1000	12108	**11513**	11518	12155	13073

[a] k_{TST} in 10^{-16} cm^3 $molecule^{-1}$ s^{-1}; bold number is the minimum at each temperature.

Table 8.11. Sum of rate constants (k_{TST}) at each point along with the reaction path at various temperatures for the reaction OH + trans-CHCl=CHCl → adduct [a]

T / K	$R_{c\text{-}o}$ / Å				
	2.173	2.192	2.211	2.230	2.249
200	5.6589	5.3719	**4.9057**	6.8131	7.4567
250	27.369	26.530	**24.254**	33.024	34.906
300	82.962	81.587	**74.627**	100.40	103.68
350	192.18	191.00	**174.76**	233.24	236.90
400	375.34	376.06	**344.13**	456.73	458.12
450	652.55	657.97	**602.13**	795.88	790.56
500	1043.4	1057.5	**967.78**	1275.2	1256.8
550	1567.0	1594.9	**1459.5**	1918.3	1878.5
600	2241.6	2289.6	**2095.1**	2748.2	2676.8
650	3084.9	3160.5	**2891.8**	3786.9	3671.7
700	4113.7	4225.5	**3865.9**	5055.6	4882.5
800	6792.8	7006.8	**6409.4**	8363.4	8025.6
900	10401	10764	**9844.9**	12825	12245
1000	15052	15619	**14283**	18581	17670

[a] k_{TST} in 10^{-16} cm^3 $molecule^{-1}$ s^{-1}; bold number is the minimum at each temperature.

Table 8.12. Sum of rate constants (k_{TST}) at each point along with the reaction path at various temperatures for the reaction OH + CCl_2=CHCl → adduct (OH at CCl_2 end) [a]

T / K	$R_{c\text{-}o}$ / Å					
	2.044	2.064	2.084	2.104	2.124	2.144
200	152.33	76.887	45.384	**4.5229**	25.684	25.778
250	262.67	154.98	102.62	**16.454**	66.148	68.126
300	402.21	263.52	188.46	**41.511**	132.56	139.04
350	573.44	405.06	306.14	**84.690**	292.26	243.80
400	779.22	582.52	458.94	**150.47**	360.33	387.30
450	1022.5	798.97	650.22	**243.46**	529.71	574.24
500	1306.1	1057.5	883.28	**367.84**	741.20	809.15
550	1632.8	1361.1	1161.4	**527.65**	998.51	1096.4
600	2005.2	1712.7	1487.6	**726.76**	1305.2	1440.3
650	2425.2	2115.2	1865.1	**968.91**	1664.7	1844.7
700	2896.8	2571.1	2296.6	**1257.6**	2080.4	2313.7
800	3999.4	3653.7	3333.0	**1988.4**	3092.5	3460.0
900	5329.8	4979.8	4617.7	**2944.8**	4365.4	4907.3
1000	6903.6	6567.5	6170.4	**4150.6**	5921.1	6681.4

[a] k_{TST} in 10^{-16} cm^3 $molecule^{-1}$ s^{-1}; bold number is the minimum at each temperature.

Table 8.13. Sum of rate constants (k_{TST}) at each point along with the reaction path at various temperatures for the reaction OH + CCl_2=CHCl → adduct (OH at CHCl end) [a]

T / K	$R_{c\text{-}o}$ / Å				
	2.145	2.165	2.185	2.205	2.224
200	3.6385	**2.4850**	2.8470	2.5964	3.0186
250	2.8324	**2.0231**	2.3649	2.1835	2.5313
300	2.5511	**1.8764**	2.2259	2.0722	2.3995
350	2.4865	**1.8673**	2.2401	2.0980	2.4284
400	2.5472	**1.9352**	2.3422	2.2036	2.5508
450	2.6615	**2.0546**	2.5048	2.3651	2.7381
500	2.8400	**2.2136**	2.7147	2.5707	2.9770
550	3.0624	**2.4057**	2.9652	2.8146	3.2604
600	3.3231	**2.6270**	3.2527	3.0937	3.5847
650	3.6190	**2.8774**	3.5750	3.4061	3.9478
700	3.9481	**3.1540**	3.9312	3.7510	4.3457
800	4.7025	**3.7856**	4.7436	4.5370	5.2625
900	5.5830	**4.5213**	5.6890	5.4517	6.3260
1000	6.5900	**5.3622**	6.7705	6.4974	7.5425

[a] k_{TST} in 10^{-12} cm^3 $molecule^{-1}$ s^{-1}; bold number is the minimum at each temperature.

BIBLIOGRAPHY

Abbatt, J. P. D. and Anderson, J. G. (1991). J. Phys. Chem. **95**: 2382.

Aders, W.-K., Pangritz, D., et al. (1975). Ber. Bunsenges. Phys. Chem. **79**: 90.

Afeefy, H. Y., Liebman, J. F., et al. (2000). Neutral Thermochemical Dara. NIST Chemistry WebBook, NIST Standard Reference Datrabase Number 69. W. G. Mallard and P. J. Linstrom. Gaithersburg, MD, NIST.

Allen, H. C. and Plyler, E. K. (1956). J. Chem. Phys. **25**: 1132.

Anderson, J. B. (1973). J. Chem. Phys. **58**: 4684.

Anderson, J. B. (1975). J. Chem. Phys. **62**: 2446.

Andreae, M. O. and Raemdonck, H. (1983). Science **211**: 744.

Astholz, D. C., Glänzer, K., et al. (1979). J. Chem. Phys. **70**: 2409.

Atkinson, R. (1985). Chem. Rev. **85**: 69.

Atkinson, R. (1989). J. Phys. Chem. Ref. Data, Monogr. **1**.

Atkinson, R. and Carter, W. P. L. (1984). Chem. Rev. **84**: 437.

Aubanel, E. E. and Wardlaw, D. M. (1989). J. Phys. Chem. **93**: 3117.

Baulch, D. L., Cobos, C. J., et al. (1992). J. Phys. Chem. Ref. Data **21**: 411.

Baulch, D. L., Drysdale, D. D., et al. (1976). Evaluated Kinetic Data for High-Temperature Reactions. London, Butterworth.

Baulch, D. L., Duxbury, J., et al. (1981). J. Phys. Chem. Ref. Data **10**.

Benson, S. W. (1976). Thermochemical Kinetics. New York, John Wiley & Sons.

Benson, S. W. and Haugen, G. R. (1967). J. Phys. Chem. **71**: 1735.

Berry, R. J., Ehlers, C. J., et al. (1997). Chem. Phys. Lett. **269**: 107.

Bishop, D. M. and Laidler, K. J. (1970). Trans. Faraday Soc. **66**: 1685.

Bradley, J. N., Trueman, S. P., et al. (1973). J. Chem. Soc., Faraday Trans. 1 **69**: 416.

Brasseur, G. P., Orlando, J. J., et al., Eds. (1999). Atmospheric Chemistry and Global Change. New York, Oxford University Press.

Braun, W., Herron, J. T., et al. (1988). Int. J. Chem. Kinet. **22**: 51.

Braun, W. and Lenzi, M. (1967). Faraday Soc. **44**: 252.

Brouard, M., Lightfoot, P. D., et al. (1986). J. Phys. Chem. **90**: 445.

Chadwell, H. M. and Titani, T. (1933). J. Am. Chem. Soc. **55**: 1363.

Chang, J. S. and Kaufman, F. (1977). J. Chem. Phys. **66**: 4989.

Charlson, R. J., Lovelock, J. E., et al. (1987). Nature **326**: 655.

Chase, M. W. J., Ed. (1998). NIST-JANAF Thermochemical Tables. Woodbury, N. Y., the American Chemical Society and the American Institute of Physics.

Chase, M. W. J., Davies, C. A., et al. (1985). J. Phys. Chem. Ref. Data **14**: Suppl. 1.

Chen, K. S., Elson, I. H., et al. (1973). J. Am. Chem. Soc. **95**: 5341.

Chen, Y., Rauk, A., et al. (1990). J. Chem. Phys. **93**: 6620.

Chesnavich, W. J., Su, T., et al. (1980). J. Chem. Phys. **72**: 2641.

Chuang, Y., Corchado, J. C., et al. (1998). POLYRATE 8.0. Minneapolis, University of Minnesota.

Clyne, M. A. A. and Ono, Y. (1983). Chem. Phys. Lett. **94**: 597.

Cupitt, L. T. and Glass, G. P. (1970). Trans. Faraday Soc. **66**: 3007.

Curtiss, L. A., Raghavachari, K., et al. (1997). J. Chem. Phys. **106**: 1063.

Curtiss, L. A., Raghavachari, K., et al. (1998). J. Chem. Phys. **109**: 7764.

Curtiss, L. A., Redfern, P. C., et al. (1999). J. Chem. Phys. **110**: 4703.

Davenport, J. E., Ridley, B. A., et al. (1972). J. Chem. Phys. **57**: 520.

Davis, D., Machado, U., et al. (1977). J. Phys. Chem. Ref. Data **6**: 871.

Ding, L. and Marshall, P. (1992). J. Phys. Chem. **96**: 2197.

Ding, L. and Marshall, P. (1993). J. Chem. Soc. Faraday Trans. **89**: 419.

Donovan, W. H. and Famini, G. R. (1994). J. Phys. Chem. **98**: 7811.

Edge, D. J. and Kochi, J. K. (1972). J. Am. Chem. Soc. **94**: 6485.

Edney, E. O., Kleindienst, T. E., et al. (1986). Int. J. Chem. Kinet. **18**: 1355.

Engel, B. and Peyerimhoff, D. D. (1989). J. Phys. Chem. **93**: 4462.

EPA (1990). Clean Air Act of 1990, 42USC.7412, Title I, Part A, Sec. 112, 53, U. S. Environmental Protection Agency.

Evans, M. G. and Polyani, M. (1935). Trans. Faraday Soc. **31**: 875.

Eyring, H. (1935). J. Chem. Phys. **3**: 107.

Fairchild, P. W., Smith, G. P., et al. (1982). Proc. Combust. Inst. **19**: 107.

Fairchild, P. W., Smith, G. P., et al. (1982). 19th Symposium (Int.) on Combustion, The Combustion Institute.

Farrar, J. M. and Lee, Y. T. (1976). J. Chem. Phys. **65**: 1414.

Finlayson-Potts, B. J. and Pitts, J. N., Jr. (1986). Atmospheric Chemistry: Fundamentals and Experimental Techniques. New York, John Wiley & Sons, Inc.

Finlayson-Potts, B. J. and Pitts, J. N., Jr. (2000). Chemistry of the Upper and Lower Atmosphere. San Diego, Academic Press.

Frisch, M., Frisch, Æ., et al. (1995). Gaussian 94 User's Reference. Pittsburgh, PA, Gaussian, Inc.

Frisch, M. J., Trucks, G. W., et al. (1995). Gaussian 94 (Revision D.2). Pittsburgh, PA, Gaussian, Inc.

Fulle, D., Hamann, H. F., et al. (1997). Ber. Bunsenges. Phys. Chem. **101**: 1433.

Gardiner, W. C., Jr., Ed. (2000). Gas-Phase Combustion Chemistry. New York, Springer-Verlag.

GaussView (1998). . Pittsburgh, PA, Gaussian, Inc.

Gillbert, D., Goyer, M., et al. (1980). An Exposure and Risk Assessment for Tetrachloroethylene, EPA-440/4-85-015.

Glassman, I. (1996). Combustion. San Diego, Academic Press.

Gonzalez, C. and Schlegel, H. B. (1989). J. Chem. Phys. **90**: 2154.

Gonzalez, C. and Schlegel, H. B. (1990). J. Phys. Chem. **94**: 5523.

Goumri, A., Yuan, W.-J., et al. (1993). Chem. Phys. **177**: 233.

Greiner, N. R. (1970). J. Chem. Phys. **53**: 1284.

Guerra, M. (1992). J. Am. Chem. Soc. **114**: 2077.

Gurvich, L. V., Veyts, I. V., et al., Eds. (1992). Thermodynamic Properties of Individual Substances. New York, Hemisphere.

Haworth, N. L., Smith, M. H., et al. (2000). J. Phys. Chem. A **104**: 7600.

Hoffmann, R., Radom, L., et al. (1972). J. Am. Chem. Soc. **94**: 6221.

Howard, C. J. (1976). J. Chem. Phys. **65**: 4771.

Hoz, T., Sprecher, M., et al. (1985). J. Phys. Chem. **89**: 1664.

Hu, X., Goumri, A., et al. (2001). J. Phys. Chem. **in press**.

Huber, K. P. and Herzberg, G. (1979). Constants of Diatomic Molecules. New York, Van Nostrand Reinhold.

Husain, D. and Slater, N. K. H. (1980). J. Chem. Soc., Faraday Trans. 2 **76**: 276.

Hynes, A. J. and Wine, P. H. (Chapter 3, in press). Combustion Chemistry. W. C. Gardiner, Jr.

IARC (1979). Monographs on the Evaluation of the Carcinogenic Risk of Chemicals to Humans. Lyon, France, International Agency for Research on Cancer, World Health Organization. **19**.

Ihee, H., Zewail, A. H., et al. (1999). J. Phys. Chem. A **103**: 6638.

Jacox, M. E. (1981). Chem. Phys. **58**: 289.

Johnston, H. S. (1966). Gas-Phase Reaction Rate Theory. New York, Ronald.

Jursic, B. S. (1997). J. Chem. Soc. Perkin Trans. **2**: 637.

Kato, S. and Morokuma, K. (1980). J. Chem. Phys. **72**: 206.

Kawamura, T., Edge, D. J., et al. (1972). J. Am. Chem. Soc. **94**: 1752.

Keck, J. C. (1960). J. Chem. Phys. **32**: 1035.

Keck, J. C. (1967). Adv. Chem. Phys. **13**: 85.

Kellogg, W. W., Cadle, R. D., et al. (1972). Science **175**: 587.

Kiefer, J. H. (1975). J. Chem. Phys. **62**: 1354.

Kielhorn, J., Melber, C., et al. (2000). Environ. Health Perspect **108**: 579.

Kirchner, K., Helf, D., et al. (1990). Ber. Bunsen-Ges. Phys. Chem. **94**: 77.

Kleinbaum, D. G., Kupper, L. L., et al. (1998). Applied Regression Analysis and Other Multivariable Methods. Pacific Grove, Duxbury Press.

Klemm, R. B. and Stief, L. J. (1974). J. Chem. Phys. **61**: 4900.

Klippenstein, S. J. (1990). Chem. Phys. Lett. **170**: 71.

Klippenstein, S. J. (1991). J. Chem. Phys. **94**: 6469.

Klippenstein, S. J. (1992). J. Chem. Phys. **96**: 367.

Klippenstein, S. J. (1993). Chem. Phys. Lett. **214**: 418.

Klippenstein, S. J. (1994). J. Phys. Chem. **98**: 11459.

Klippenstein, S. J. and Marcus, R. A. (1987). J. Chem. Phys. **87**: 3410.

Klippenstein, S. J. and Marcus, R. A. (1988). J. Phys. Chem. **92**: 3105.

Kohida, T., Kotaka, M., et al. (1987). Bull. Chem. Soc. Jpn. **60**: 3131.

Kotaka, M. S., S. Shimokoshi, K. (1987). J. Fluorine Chem. **37**: 387.

Kurylo, M. J., Peterson, N. C., et al. (1970). J. Chem. Phys. **54**: 943.

Kurylo, M. J., Peterson, N. C., et al. (1970). J. Chem. Phys. **53**: 2776.

Lewis, G. N., Randall, M., et al. (1961). Thermodynamics. New York, McGraw-Hill.

Lide, D. R., Ed. (1990). CRC Handbook of Chemistry and Physics. Boston, CRC Press.

Liu, A., Mulac, W. A., et al. (1989). J. Phys. Chem. **93**: 4092.

Lovelock, J. E., Maggs, R. J., et al. (1972). Nature **237**: 452.

MacPherson, M. T., Pilling, M. J., et al. (1985). J. Phys. Chem. **89**: 2268.

Manning, R. G. and Kurylo, M. J. (1977). J. Phys. Chem. **81**: 291.

Massey, B. S. (1986). Measures in Science and Engineering: Their Expression, Relation and Interpretation. New York, John Wiley.

McCulloch, A., Aucott, M. L., et al. (1999). J. Geophys. Res. **104**: 8417.

McCulloch, A. and Midgley, P. M. (1996). Atmos. Environ. **30**: 601.

Mihelcic, D. and Schindler, R. N. (1970). Ber. Bunsen-Ges. Phys. Chem. **74**: 1280.

Misra, A. (1997). Kinetics and Thermochemistry of Halogenated Species. Denton, University of North Texas.

Nicholas, J. E., Amodio, C. A., et al. (1979). J. Chem. Soc., Faraday Trans. 1 **75**: 1868.

Nicovich, J. M., Kreutter, K. D., et al. (1992). J. Phys. Chem. **96**: 2518.

Okabe, H. (1978). Photochemistry of Small Molecules. New York, John Wiley.

Perner, D. and Franken, T. (1969). Ber. Bunsen-Ges. Phys. Chem. **73**: 897.

Perry, P. A., Atkinson, R., et al. (1977). J. Chem. Phys. **67**: 458.

Perry, R. A., Atkinson, R., et al. (1977). J. Phys. Chem. **81**: 296.

Perry, R. A., Atkinson, R. A., et al. (1977). J. Chem. Phys. **67**: 458.

Pesa, M., Pilling, M. J., et al. (1998). J. Phys. Chem. **102**: 8526.

Pilling, M. J. and Seakins, P. W. (1995). Reaction Kinetics. New York, Oxford University Press Inc.

Pratt, G. and Rogers, D. (1977). J. Chem. Soc., Faraday Trans. 1 **73**: 54.

Pugh, E. M., Jr. and Winslow, G. H. (1966). The Analysis of Physical Measurements. Reading, Addison-Wesley.

Ramamoorthy, S. (1997). Chlorinated Organic Compounds in the Environment. New York, Lewis Publishers.

Robertson, S. H., Wagner, A. F., et al. (1995). J. Chem. Phys. **103**: 2917.

Rommel, H. and Schiff, H. I. (1972). Int. J. Chem. Kinet. **4**: 547.

Roth, P., Lohr, R., et al. (1982). Combust. Flame **45**: 273.

Samson, J. A. R. (1967). Techniques of Vacuum Ultraviolet Spectroscopy. New York, John Wiley & Sons.

Schlegel, H. B. (1982). J. Phys. Chem. **86**: 4678.

Schlegel, H. B. and Sosa, C. (1984). J. Phys. Chem. **88**: 1141.

Schwarz, S. E. (1988). Nature **336**: 441.

Seakins, P. W. and Pilling, M. J. (1991). J. Phys. Chem. **95**: 9878.

Sekušak, S., Liedl, K. R., et al. (1998). J. Phys. Chem. A **102**: 1583.

Shi, Y. and Marshall, P. (1991). J. Phys. Chem. **95**: 1654.

Smith, S. C. (1991). J. Chem. Phys. **95**: 3404.

Smith, S. C. (1992). J. Chem. Phys. **97**: 2406.

Smith, S. C. (1993). J. Phys. Chem. **97**: 7034.

Sosa, C. and Schlegel, H. B. (1987). J. Am. Chem. Soc. **109**: 7007.

Sosa, C. and Schlegel, H. B. (1987). J. Am. Chem. Soc. **109**: 4193.

Stachnik, R. A. and Molina, M. J. (1987). J. Phys. Chem. **91**: 4603.

Steinfeld, J. I., Francisco, J. S., et al. (1989). Chemical Kinetics and Dynamics. Englewood Cliffs, NJ, Prentice Hall.

Stuhl, F. and Niki, H. (1972). J. Chem. Phys. **57**: 3671.

Tichenor, L. B., El-Sinawi, A., et al. (2001). Chemosphere **42**: 571.

Tichenor, L. B., Graham, J. L., et al. (2000). J. Phys. Chem. A **104**: 1700.

Tichenor, L. B., Lozada-Ruiz, A. J., et al. (2000). Proc. Combus. Inst. **28**: 1495.

Townes, C. H. and Schawlow, A. L. (1955). Microwave Spectroscopy. New York, McGraw-Hill.

Tsang, W., Burgess, D. R., Jr., et al. (1998). Combust. Sci. Tech **139**: 385.

Tuazon, E. C., Atkinson, R. A., et al. (1988). Int. J.. Chem. Kinet. **20**: 241.

Villà, J., González-Lafont, A., et al. (1997). J. chem. Phys. **107**: 7266.

Wardlaw, D. M. and Marcus, R. A. (1984). Chem. Phys. Lett. **110**: 230.

Wardlaw, D. M. and Marcus, R. A. (1985). J. Chem. Phys. **83**: 3462.

Warnatz, J., Bockhorn, H., et al. (1982). Proc. Combust. Inst. **19**: 197.

Warnatz, J., Bockhorn, H., et al. (1982). . 19th Symposium (Int.) on Combustion, The Combustion Institute.

Watson, R. T., Machado, G., et al. (1976). J. Chem. Phys. **65**: 2126.

Wayne, R. P. (2000). Chemistry of Atmospheres. New York, Oxford University Press Inc.

Westenberg, A. A. and de Haas, N. N. (1973). J. chem. Phys. **59**: 6685.

Westenberg, A. A. and deHaas, N. (1975). J. Chem. Phys. **62**: 3321.

Wong, M. and Radom, L. (1995). J. Phys. Chem. **99**: 8582.

Yamada, T., El-Sinawi, A., et al. (2001). J. Phys. Chem. A **105**: 7588.

Yamada, T., Siraj, M., et al. (2001). J. Phys. Chem. A **105**: 9436.

Yoshimura, M., Koshi, M., et al. (1992). Chem. Phys. Lett. **189**: 199.

Zellner, R. (1979). J. Phys. Chem. **83**: 18.

Zellner, R. (1984). Bimolecular Reaction Rate Coefficients. Combustion Chemistry, Chapter 3. W. C. Gardiner, Jr. New York, Springer-Verlag.

Zhang, Z., Liu, R., et al. (1991). J. Phys. Chem. **95**: 194.

Zhu, L., Bozzelli, J. W., et al. (1999). J. Phys. Chem. A **103**: 7800.